

Carbon Nanotubes in Cancer Therapy

“CNTs: King of nanomaterials”

Banu Abdallah

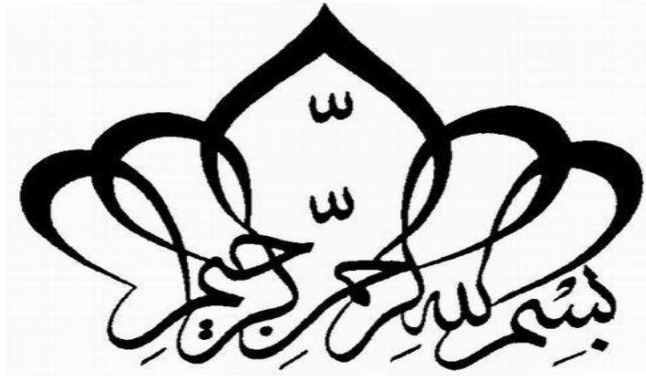
Ph.D. Thesis

2013



A thesis submitted in partial fulfilment for the requirements of the degree of Doctor of

Philosophy at the University of Central Lancashire



To my wonderful parents

Mohamed and Kurda

&

My beloved brother Aram and beautiful sisters, Roobar and Juan.

Thank you for your unconditional love

“The ink of the scholar is more holy than the blood of the martyr”

Prophet Muhammad (SWA)

DECLARATION

I declare that whilst registered as a candidate for the research degree, I have not been a registered candidate or enrolled student for another award of the University or other academic or professional institution. No material contained in this thesis has been used in any other submission for an academic award and is solely my own work.

Banu Abdallah

19 June 2013

ABSTRACT

Carbon Nanotubes (CNTs) are highly attractive vehicles for the delivery of biomolecules into living systems specifically for applications in cancer therapy. Two main types of CNTs; single-walled (SWNT) and multi-walled (MWNT) have been investigated. Pristine CNTs are poorly soluble in aqueous solvents, and therefore need to be functionalized (*f*-CNT) to enhance their solubility and biocompatibility. The *f*-CNTs possess the ability to cross cell membranes and enter cells consequently having the potential as vehicles for drug delivery. Polyethylene glycol (PEG400) and Pluronic®F127 (PF127) functionalized SWNTs and MWNTs have been investigated in this study for *in vitro* cancer therapy. Both have demonstrated high tumour suppression efficacy with respect to an anti-cancer drug Paclitaxel, when utilised solely. However, *f*-CNTs for the delivery of anti-cancer agents for brain tumours, in particular the most common tumour Glioblastoma, have not been researched. The toxicity of these materials is another issue that requires further investigation. Cytotoxicity of CNTs is thought to be dependent on several characteristics such as length, purity and type of functionalization.

The aim of this study was to characterize, functionalize and investigate *in vitro* cell cytotoxicity of *f*-CNTs with and without Paclitaxel (PTX). As dispersing and stabilization agents two polymeric systems were used; PEG400 and PF127. CNTs characteristics have been investigated by using various techniques and two stabilization and dispersing agents have been used for functionalization.

Raman spectra have been recorded using two laser lines at 325 nm and 488 nm. Scanning Electron Microscopy (SEM) and Transmission Electron Microscopy (TEM) were used to analyse their structure and morphology. All samples were functionalized,

homogenised, centrifuged and their ζ -potentials were measured. CNTs were found to be in a size range of 100 nm to several microns long, with diameter values ranging from 07 ± 1.0 nm for SWNT and inner diameter I.D. 10-20 nm and 30-40 nm Outer Diameter values (O.D.) with 6-12 concentric walls for MWNT. Both SWNT and MWNT exhibited stability in both polymeric systems implemented even after a 10 day period. Particularly PEG400 based formulations showed superior performance in terms of greater ζ -potential values. Notable shifts in G-band were examined confirming the presence of *f*-CNTs. Higher entrapment efficiency was accomplished with *f*-CNTs reaching a maximum efficiency at 200 $\mu\text{g/ml}$.

Cell lines SVGp12 and U87-MG were exploited for cytotoxicity evaluations. SWNT and MWNT demonstrated insignificant cytotoxic effects on SVGp12 (normal astrocytes) cell lines even at elevated concentrations of up to 15 mg/ml. Nevertheless, *f*-CNTs showed significant reduction in the cell viability at low Paclitaxel concentrations on U87-MG grade IV Glioblastoma. As a selection of CNTs have been investigated by various researchers, it is exceptionally challenging to conclusively state whether or not they are indeed toxic.

This research into CNTs has successfully examined the effects of co-formulation with various components and the potential effects on drug delivery for cancer cells. Conceptually, CNTs are rightfully labelled as the king of nanomaterials due to their elusive chemical and physical properties; ensure that they are likely to receive much attention in the not too distant future.

TABLE OF CONTENTS

ABSTRACT	i
ACKNOWLEDGEMENTS	vi
LIST OF ABBREVIATIONS	viii
LIST OF FIGURES	x
LIST OF TABLES	xviii

CHAPTER 1

1.1 Introduction	1
1.2 Aims and objectives	4
1.3 Outline of the thesis	5

CHAPTER 2

2.1 Carbon based materials	7
2.2 Allotropes of carbon	8
2.3 CNTs and their properties	13
2.3.1 Single walled CNTs	14
2.3.2 Multi walled CNTs	17
2.4 Synthesis of CNTs	21
2.4.1 Solid sources	21
2.4.2 Laser ablation	22
2.4.3 Arc discharge	24
2.4.4 Solar furnace	26
2.4.5 Vapour phase deposition	27
2.5 Biomedical applications of CNTs	34
2.6 Cancer	36
2.6.1 Glioma	44
2.7 Cancer treatments	46
2.7.1 Radiation therapy	46
2.7.2 Surgery	47
2.7.3 Chemotherapy	47
2.7.4 CNTs as carriers for cancer treatment	51
2.8 Toxicity of CNTs	54
2.9 Conclusions	56

CHAPTER 3

3.1 Materials and methods	58
3.2 Materials	59
3.2.1 Carbon Nanotubes	59
3.2.2 Surfactant and Paclitaxel	59
3.2.3 Cell and MTT assay	59
3.3 Characterization	60
3.3.1 Scanning Electron Microscopy	60
3.3.2 Transmission Electronic Microscopy	61
3.3.3 Raman Spectroscopy	63
3.3.4 ζ -potential measurements	65
3.4 Non-covalent functionalization	66
3.4.1 Functionalization of CNTs with Pluronic	67
3.4.2 Functionalization of CNTs with PEG400	69
3.4.3 Paclitaxel	71
3.5 Techniques	73
3.5.1 Probe-and Ultrasonication	73
3.5.2 Centrifugation technique	73
3.5.3 High performance liquid chromatography – loading efficacy of PTX	73
3.6 Cell culture: Materials and Methods	75
3.6.1 Glioma cell lines tissue culture to study glioma growth	75
3.6.2 Media importance in tissue culture	75
3.6.3 Eagle’s Minimal Essential Medium and Dulbecco’s Modified Eagle Medium used for the proliferation of cells	76
3.7 Equipment and materials used for cell culture	79
3.7.1 Chemicals and Reagents in cell culture	80
3.7.2 Composition of medium and supplements required for cell culture	81
3.8 Cell culture passaging	82
3.8.1 Cell culture and passaging of the Primary Glial Cells (U87-MG and SVGP12)	82
3.8.2 Haemocytometer and cell quantification	83
3.8.3 Cryopreservation of cells	85
3.8.4 Growth curve	85
3.9 Plating of cell lines	86
3.9.1 Plating of cells with PTX-f -CNTs	86
3.10 MTT assay	92
3.10.1 MTT assay protocol	92
3.11 Statistical analysis	93

CHAPTER 4

4.1 Characterization and functionalization	94
4.2 Raman Spectroscopy visible 488 nm - Ultra violet 325 nm	95
4.2.1 Raman spectra SWNT	96
4.2.2 Raman Spectra of MWNT	101

4.2.3 Raman comparison of SWNT and MWNT	104
4.2.4 Raman spectra of pristine and <i>f</i> -CNTs	106
4.3 X-ray diffraction for sample purity	108
4.4 Functionalization and comparison of aqueous stability of CNTs with Polyethylene glycol 400 and Pluronic 127	110
4.5 ζ-potential	117
4.6 Paclitaxel <i>f</i>-CNTs	122
4.6.1 Calibration Curve	122
4.6.2 Entrapment efficiency of <i>f</i> -CNTs	123
4.6.3 Saturation effect	130
4.7 Conclusions	131
CHAPTER 5	
5.1 In Vitro Cytotoxicity	132
5.2 Growth curve of cell lines	133
5.2.1 Growth curve of SVGp12	133
5.2.2 U87-MG growth curve	134
5.3 Effects of PTX on SVGp12 and U87-MG	136
5.3.1 Effect of PTX concentrations of SVGp12	136
5.3.2 Effects of PTX concentration on U87-MG	140
5.4 Effect of pristine CNTs on SVGp12 and U87-MG	144
5.4.1 Effect of p-CNTs on SVGp12	144
5.4.2 Effect of p-CNTs on U87-MG	146
5.5 PTX and p-CNTs cytotoxic effect on SVGp12 and U87-MG	148
5.5.1 Effect of PTX and p-CNTs on SVGp12	148
5.5.2 Effect of PTX and p-CNTs on U87-MG	150
5.6 Effect of PTX-<i>f</i>-CNT in comparison with PTX alone and PTX-CNT on SVGp12 and U87-MG	152
5.6.1 Cytotoxic effect of CNT-PTX conjugate functionalized with PF127 and PEG400 on SVGp12	152
5.6.2 Cytotoxic effect of PF127 and PEG400 functionalized SWNT/MWNT and PTX conjugates on U87-MG	156
5.7 Conclusions	159
CHAPTER 6	
6.1 Conclusions and future work	160
CHAPTER 7	
References	162

ACKNOWLEDGEMENTS

On the outset, I feel it is necessary to clarify that the acknowledgements in this section are by no means chronological. However I would like to acknowledge the help and support of so many kind people around me, only some are given particular mention here but all are of great importance to me.

First of all, I would like to express my deepest appreciation of my director of studies, Professor Waqar Ahmed for his invaluable and constructive suggestions during the planning and development of this research work. His willingness to give his time so generously has been very much appreciated. I would also like to express my gratitude to my supervisor Dr Abdelbary Elhissi for his support and encouragement.

Extended acknowledgments go to Professor Gracio and his research group at the University of Aveiro for being most accommodating and helpful in allowing me to use their facilities. Not least for their encouragement during my visit. Dr Vinod Dhanak (University of Liverpool) is acknowledged for access to Daresbury Laboratories. I would also like to thank Dr Sim K Singhrao at UCLan for her kindness in aiding me to carry out *in vitro* studies.

I have been blessed to come across many great friends, in particular Iftikhar Khan and Sakib Yousaf to whom I will be eternally grateful for their kindness, loyalty, unerring friendship and motivation. Countless colleagues and friends that have advised and encouraged me during my PhD to whom I will always be grateful; Dr Basel Arafat, Dr Mohamed Albed Alhnan, Dr Alicia D'Souza, Kanar Hidayat and Aisha Ahmed for their

advice, encouragement support and love. My earnest gratitude and appreciation goes to Karla, Aseel and Bilal for their transcending friendship and support but importantly for always being there for me through my most difficult times.

By no means, in anyway least, I am indebted to my extremely loving and supporting parents Mohamed and Kurda, without whom I would most certainly not have made it this far in life. I can only offer heartfelt gratitude and appreciation to my lovely brother Aram and my beautiful sisters Roobar and Juan for motivating me in my darkest hour's often by unorthodox means, but most of all having the faith in me.

Finally, I would like to thank the favourite people in my life, Uncle Rebwar and Aunt Viyan for their unconditional love, support and encouragement for as long as I can remember.

Banu Abdallah

LIST OF ABBREVIATIONS

Abbreviation	Meaning
ANOVA	Analysis of variance
CCD	Charge-Coupled Device
CNH	Carbon Nanohorn
CNS	Central Nervous System
CNT	Carbon Nanotubes
C60	Fullerene
CCVD	Catalytic Chemical Vapour Deposition
CVD	Chemical Vapour Deposition
DMSO	Dimethyl Sulphoxide
DOX	Doxorubicin
DWNT	Double Walled Carbon Nanotubes
DEM	Dulbecco's Modified Eagle Medium
EMEM	Eagle's Minimal Essential Medium
FBS	Fetal Bovine Serum
<i>f</i> -CNT	Functionalized carbon nanotubes
<i>f</i> -MWNT	Functionalized Multi Walled Nanotubes
<i>f</i> -SWNT	Functionalized Single Walled Nanotubes
HPLC	High Performance Liquid Chromatography
HipCo	High pressure Carbon monoxide
kDA	kilo Dalton
MG	Microglia
mg	Milligram
ml	Millilitre
MWNT	Multi Walled Nanotubes
NIR	Near Infra-Red
nm	Nanometre

Abbreviation	Meaning
p-	Pristine
PBS	Phosphate Buffer Saline
PECVD	Plasma Enhanced Chemical Vapour Deposition
PEG	Polyethylene Glycol
PF127	Pluronic® PF127
PTX	Paclitaxel
RBM	Radial Breathing Mode
rpm	Revolutions per minute
SD	Standard Deviation
SEM	Scanning Electron Microscopy
SVGp12	Human astrocyte cell line
SWNT	Single Walled Nanotubes
TEM	Transmission Electron Microscopy
µg	Micrograms
UV	Ultra Violet
U87-MG	Grade IV Glioblastoma cell line
XRD	X-Ray Diffraction
ζ-	Zeta

LIST OF FIGURES

CHAPTER 1

Figure 1.1 Damascus sword	2
---------------------------------	---

CHAPTER 2

Figure 2.1 Electronic structure and states of carbon	7
--	---

Figure 2.2 Allotropes of carbon	8
---------------------------------------	---

Figure 2.3 TEM micrographs of carbon nanohorns (a and b), with schematic diagram (c) for illustration.....	11
--	----

Figure 2.4 (a) Nanocoils, (b) nanofibres, (c) nanocapsules and (d) nanobuds.....	12
--	----

Figure 2.5 Graphene sheet rolled up to obtain a SWNT	16
--	----

Figure 2.6 Typical MWNTs adapted from	17
---	----

Figure 2.7 Herringbone structure	18
--	----

Figure 2.8 Bamboo textured CNTs	19
---------------------------------------	----

Figure 2.9 Schematic diagram of a laser ablation system used for the growth of CNTs	23
---	----

Figure 2.10 Schematic diagram of an Arc discharge system	25
--	----

Figure 2.11 Solar method for large scale CNT synthesis.....	27
---	----

Figure 2.12 Base growth model	31
-------------------------------------	----

Figure 2.13 Schematic view of widely accepted growth mechanism; tip-growth model	31
Figure 2.14 Schematic representation of functionalization of SWNTs; adapted from (a) with quantum dots, EDC and Cisplatin; (b) SWNT bio-conjugated with Cisplatin and EGF, targeting cancer cell surface receptor EGFR; (c-e) TEM images showing the various functional groups, with Cisplatin shown as bright spots.....	35
Figure 2.15 World cancer incidence in 2008 (adapted from (Boyle and Levin 2008) ...	36
Figure 2.16 Typical growth of normal cells and cancerous growth in uncontrolled manner	39
Figure 2.17 Twenty Most Commonly Diagnosed Cancers	41
Figure 2.18 Microglia cells showing the Glioma in the brain	44
Figure 2.19 Various forms of PTX from natural and synthetic sources.	50
Figure 2.20 Paclitaxel mechanism of action	50
Figure 2.21 Phagocytosis process of long and short CNTs	52

CHAPTER 3

Figure 3.1 Picture and schematic view of Scanning Electronic Microscopy.....	61
Figure 3.2 (a) Transmission Electronic Microscopy (b) TEM grid where the sample is to be viewed on (c) Schematic view of TEM.....	62
Figure 3.3 Schematic overview of Raman scattering.....	63
Figure 3.4 Raman Spectra showing the characteristic features of CNTs.....	64
Figure 3.5 Schematic overview of zeta potential curette that has been used for measurements.....	65
Figure 3.6 Chemical formula of Pluronic F127 with hydrophilic chains of polyoxyethylene, hydrophobic chain of polyoxypropylene and Hydrophilic chains of polyoxyethylene	68
Figure 3.7 Non-covalent functionalization; surfactant chains onto the CNT	70
Figure 3.8 Neubauer Haemocytometer: each large square gives an area of 1 mm ² (1 mm x 1 mm) with a depth of 0.1 mm.....	83
Figure 3.9 Schematic view of a 96 well plate with recorded samples (a) without PTX and (b) with PTX, where; C is CONTROL, S is SAMPLE, MT is no cells and CELL is untreated seeded cells.....	87

CHAPTER 4

Figure 4.1 (a) Raman Spectra of SWNT with Ar + laser (488 nm) the peak marked with * is Hg calibration peak (b) expanded spectra of D-band (c) Expanded spectra of second order G'-band.	96
Figure 4.2 Room temperature Raman spectrum of SWNT on the expanded scale show the details of RBM and tube diameter (nm).....	97
Figure 4.3 RBM frequencies vs tube diameter (nm).....	98
Figure 4.4 TEM micrograph of SWNT at x 245000 magnification.....	99
Figure 4.5 TEM micrographs of SWNT x 65000 magnification	100
Figure 4.6 SEM micrographs at various magnifications.....	100
Figure 4.7 Raman Spectra of MWNT with 488 nm, the peak marked with * is Hg calibration peak	101
Figure 4.8 TEM micrograph of MWNT x33000 magnification	103
Figure 4.9 TEM micrograph of MWNT at x180 000 magnification	103
Figure 4.10 SEM micrograph of MWNTs with various magnifications	104
Figure 4.11 Raman Spectra of MWNT and SWNT with 325 nm.....	105
Figure 4.12 Raman Spectra of functionalized CNTs	106
Figure 4.13 XRD spectra of MWNTs	108
Figure 4.14 XRD spectrum of SWNTs (left) and Graphite (right) in red line.....	109

Figure 4.15 SWNT and MWNT in PEG400 and PF127 (a) SWNT (left) and MWNT (right) in PEG400, (b) dispersion of SWNT (left) and MWNT (right) in PF127 prior homogenising and sonication.....	110
Figure 4.16 Dispersions of SNWTs after 10 minutes ultrasonication	111
Figure 4.17 MWNT (left) and SWNT (right) in PEG.....	111
Figure 4.18 TEM Micrographs of <i>f</i> -SWNT in PEG400.....	112
Figure 4.19 Raman spectra showing a shift and decrease in intensity of <i>f</i> -SWNT.....	113
Figure 4.20 Raman spectra of <i>f</i> -MWNT in PEG.....	114
Figure 4.21 MWNT (left) and SWNT (right) in PF127.....	114
Figure 4.22 Raman spectra of p-SWNT and <i>f</i> -SWNT-PF127	115
Figure 4.23 SEM micrograph of <i>f</i> -SWNT-PF127	115
Figure 4.24 Raman spectra of p-MWNT and <i>f</i> -MWNT-PF127.....	116
Figure 4.25 ζ -potential of pristine CNTs (p-CNT), CNT-PEG and CNT-PF127 were demonstrated. The error bars represent the standard deviation (SD) of three samples.	118
Figure 4.26 ζ -potential of SWNT in PEG and PF127 on preparation day and after 10 days. The error bars represent the standard deviation (SD) of three samples.....	119
Figure 4.27 ζ -potential of MWNT in PEG400 and PF127 on the preparation day and 10 days after. The error bars represent the standard deviation (SD) of three samples	120
Figure 4.28 ζ -potential of SWNT and MWNT in PEG and PF127 1% on preparation day and 10 days after. The error bars represent the standard deviation (SD) of three samples.....	121

Figure 4.29 Phase plot that shows the quality of the samples used for ζ -potential measurement	121
Figure 4.30 Paclitaxel calibration curve.....	122
Figure 4.31 Entrapment efficiency of p-MWNT and p-SWNT.....	125
Figure 4.32 Entrapment efficiency of <i>f</i> -SWNT.....	126
Figure 4.33 Entrapment efficiency of <i>f</i> -MWNT	127
Figure 4.34 Paclitaxel <i>f</i> -CNTs and their entrapment efficiency	128
Figure 4.35 Entrapment efficiency achieved with all formulations at 200 $\mu\text{g/ml}$; the bar represent with * is anomalous and not calculated with other formulations	129
Figure 4.36 Correlation of both SWNTs and MWNTs against PTX concentrations ...	130

CHAPTER 5

Figure 5.1 (a) Growth percentage of SVGP12 from three densities and (b) shows the microscopic picture of 10^5 cell/well (x100).....	134
Figure 5.2 (a) Growth percentage of U87-MG from three densities and (b) shows the microscopic picture of 10^5 cell/well density (x100)	135
Figure 5.3 The effect of different PTX concentrations on SVGP12 cell line. The error bars represent the standard deviation (SD) of three samples	136
Figure 5.4 Microscopic pictures of SVGP12 treated with Paclitaxel for 24 hours (x100)	138
Figure 5.5 Microscopic pictures of SVGP12 treated with Paclitaxel for 48 hours (x100)	139
Figure 5.6 The effect of different PTX concentrations on U87-MG cell lines. The error bars represent the standard deviation (SD) of three samples	140
Figure 5.7 Microscopic pictures of U87-MG different treated with four different concentrations for 24 hours (x100)	141
Figure 5.8 Microscopic pictures of U87-MG treated with four different concentrations for period of 48 hours (x100)	143
Figure 5.9 SVGP12 cell lines treated with pristine CNTs for 24 and 48hours. The error bars represent the standard deviation (SD) of three samples	144
Figure 5.10 Microscope pictures of p-MWNT and p-SWNT of SVGP12 treated for 24 hours (x200)	145
Figure 5.11 Different concentrations of pristine (p) CNTs (CNTs) on U87-MG cell line. The error bars represent the standard deviation (SD) of three samples	146

Figure 5.12 Microscope pictures of p-MWNT and p-SWNT of U87-MG (x200)	147
Figure 5.13 Cell viability of SVGP12 treated with PTX alone and p-CNT-PTX for 24 hours. The error bars represent the standard deviation (SD) of three samples	148
Figure 5.14 Cell viability of SVGP12 treated with PTX alone and p-CNT-PTX for 48 hours. The error bars represent the standard deviation (SD) of three samples	149
Figure 5.15 Cell viability of U87-MG treated with PTX alone and p-CNT-PTX for 24 hours The error bars represent the standard deviation (SD) of three samples	150
Figure 5.16 Cell viability of U87-MG treated with PTX alone and p-CNT-PTX for 48 hours. The error bars represent the standard deviation (SD) of three samples	151
Figure 5.17 SVGP12 cell lines treated with different f-CNTs formulations. The error bars represent the standard deviation (SD) of three samples	153
Figure 5.18 Cytotoxicity effect of formulations in viability percentage of SVGP12. The error bars represent the standard deviation (SD) of three samples	154
Figure 5.19 U87-MG cell lines treated with f-CNTs for 24 and 48 hours. The error bars represent the standard deviation (SD) of three samples.....	156
Figure 5.20 Microscopic picture of U87-MG cell lines treated with various CNTs formulations (x200).....	157
Figure 5.21 Cytotoxicity effect of formulations in viability percentage of SVGP12 ...	158

LIST OF TABLES

CHAPTER 2

Table 2.1 Carbon nanomaterial discovery	20
Table 2.2 Most common types of brain tumours	43
Table 2.3 Anticancer drugs that have been used in the past decades.....	48

CHAPTER 3

Table 3.1 Concentrations of CNTs in PF127	69
Table 3.2 Concentrations of CNTs in PEG400.....	71
Table 3.3 Dilutions of stock solution for calibration curve	72
Table 3.4 HPLC gradient phase used for Paclitaxel	74
Table 3.5 List of essential and non-essential amino acids in EMEM.....	77
Table 3.6 Materials and equipment used for cell culture	79
Table 3.7 Samples and controls description used for plating of SVGp12 and U87-MG on the 96 well plates with PTX.....	88
Table 3.8 Control labels have been described for each sample with and without PTX..	89

CHAPTER 4

Table 4.1 Tube diameters calculated from radial breathing mode (RBM) frequencies using the relation $\omega_{\text{RBM}} = 234/dt - 10$	98
Table 4.2 ζ -potential Mean \pm SD of Pristine and <i>f</i> -CNTs.....	117
Table 4.3 Entrapment efficiency of pristine (p) and functionalized (f) CNTs.....	124

CHAPTER 5

Table 5.1 IC ₅₀ Values of the formulations in mg for SVGP12 cells	150
Table 5.2 IC ₅₀ Values of the formulations in mg for U87-MG cells	151
Table 5.3 IC ₅₀ Values of the formulations in mg for SVGP12 cells	155
Table 5.4 IC ₅₀ Values of the formulations in mg for U87-MG cells	158

CHAPTER 1

INTRODUCTION

*"He who asks is a fool for five minutes, but he who does not ask is a fool
for ever."*

-Chinese proverb-

CHAPTER 1

1.1 Introduction

‘Plenty room at the bottom’ (Richard P. Feynman, 1959)

Richard Feynman, infamously proposed a new field in 1959 in ‘which little has been done, but in which an enormous amount can be done, in principle’. However, the actual term nanotechnology was never used. Subsequently in 1974 Taniguchi coined the term ‘Nanotechnology’ to describe this field as having innumerate potential applications (Taniguchi 1974). However, the manipulation of matter on an atomic level was popularised by the work of Drexler during the 1980’s (Drexler 1981). For mankind, nanotechnology has been documented as early as 500BC, surrounding claims of an ancient existence with the incorporation of 1.5% Carbon into Indian steel, exponentially increasing material strength. Records following, describe the use of this steel in the production of swords (Figure 1.1) in Damascus during the times of Alexander the Great (Srinivasan 2007).

Whilst nanotechnology is an exceptionally vast field, it has a considerable number of sub-disciplines, notably; nanoengineering, nanophysics, and nanomedicine. A significant role is played in many applications such as catalysis and drug delivery systems exploiting the large surface area generated from the miniscule size of nanoparticles.



Figure 1.1 Damascus sword (Srinivasan, 2007)

Carbon Nanotubes (CNTs) utilised in nanomedicine have attracted considerable interest since their first introduction by Iijima (Iijima 1991) using High Resolution Transmission Electron Microscopy (HR-TEM). The relationship between CNTs and fullerenes was discovered by Nobel Laureate winner, H. Kroto, (Kroto, Heath et al. 1985). CNTs are conjoined and concentrically nested graphene cylinders of varied lengths possessing an ultra-high aspect ratio of greater than 10,000. Extensive research has been conducted into the synthesis, properties, functionalization and the immense range of potential applications of CNTs.

The potential of CNTs in the delivery of bio-molecules for a range of applications has received significant interest as of late. Particularly transport of drugs into cancerous cells for the purpose of diagnostics and therapeutics. Pristine CNTs have inherent limitations, namely poor solubility, which inhibits their utilization in medical

applications. Pluralities of approaches to enhance their solubility have been investigated.

Prior research has entailed polyethylene glycol (PEG) SWNTs (Zhuang et al. 2008) and Pluronic®F108 functionalized MWNTs (*f*-MWNT) (Kateb et al. 2007) investigated *in vitro* and *in vivo* applications. Both aforementioned studies demonstrated SWNT and MWNT achieving higher tumour suppression efficacy than an anti-cancer drug alone. Functionalized CNTs (*f*-CNTs) possess the ability to penetrate cells and have the potential for use as vehicles for drug delivery. However, *f*-CNTs for the delivery of anticancer agents in Glioma have yet to be explored offering scope for further research. Glioma is defined as a primary brain tumour arising from the Microglia (MG) and is considered as an immune effector in cells of the Central Nervous System (CNS) capable of phagocytosis. The process of phagocytosis entails the engulfment of particles to remove pathogens using specialised cells known as phagocytes. Precise selection of size and functionalization of CNTs may enable them to be eliminated by phagocytosis. The unique properties of CNTs reduce the limitations of anticancer drugs e.g. Paclitaxel (PTX), a drug which has known problems in bypassing the Blood Brain Barrier (BBB). Consequently, CNTs have a higher tumour reduction efficacy.

Conversely toxicity of these materials is an issue which should receive due consideration. This may be evaluated through cytotoxicity assays. Cytotoxicity itself may be dependent on multiple characteristics, including the structure, length, purity and the type of functionalization. One *in vitro* study utilising primary mouse microglia cells (MG-BV2) showed insignificant signs of cytotoxicity by evaluating the efficacy of MWNTs as potential nanoscale delivery vehicles (Bong J. et al 2011).

Studies using a multitude of CNTs purchased or synthesised from various sources are inconclusive with respect to toxicity (Lacerda L et al 2006). Therefore, preparation methods and conditions employed are influential on characteristics and purity. In this study, polyethylene glycol (PEG400) and Pluronic®F127 (PF127) have been affixed to SWNTs and MWNTs in order to increase their solubility.

1.2 Aims and objectives

The aim of this study was to characterize, functionalize and investigate *in vitro* cell cytotoxicity of *f*-CNTs. Two polymeric systems were utilized as dispersing and stabilization agents; PEG400 and PF127. An anti-cancer drug, PTX has been non-covalently attached to *f*-CNTs. For cytotoxicity and cell entrapment investigation cell lines including U87-MG and normal astrocytes SVGp12 were utilised.

Chemotherapy is an integral component in the treatment of most cancers. Sadly it is associated with low success rates due to the acquired resistance developed in cancer cells to chemotherapeutic agents. This study investigated the use of functionalized CNTs for drug delivery in anti-cancer applications, particularly in Glioma.

Specific objectives identified were as follows:

- Characterization of SWNTs, MWNTs and *f*-CNTs using an array of techniques including; ZetaSizer, Scanning Electron Microscopy (SEM), Transmission Electron Microscopy (TEM), X-ray Diffraction (XRD) and Raman spectroscopy for size, structure, surface area and charge analysis
- Non-covalent functionalization of pristine SWNTs and MWNTs with PF127
- Non-covalent functionalization of pristine SWNTs and MWNTs with PEG
- Attachment of PTX onto SWNTs, MWNTs and *f*-CNTs

- Utilization of p-SWNTs, p-MWNTs and *f*-CNTs on cell lines, U87-MG and SVGp12
- Cytotoxicity assay of p-SWNTs, p-MWNTs, *f*-CNTs and PTX-CNTs

1.3 Outline of the thesis

Chapter 1 provides an introduction summarising the aims and objective of the study, outlining the chapters contained in this thesis.

Chapter 2 gives a detailed literature review of carbon materials and CNTs, their structure and properties and discusses their synthesis and applications.

Chapter 3 entails a detailed experimental work pertaining to characterization and functionalization of SWNTs and MWNTs. Moreover, procedures used for studying their use in drug delivery systems and cytotoxicity are investigated.

Chapter 4 contains results and discussions relating to the characterization and functionalization of SWNTs and MWNTs.

Chapter 5 offers a description of the results and discussion from cytotoxicity studies for cell and tissue culture (*in vitro*) studies on Glioma and SVGp12 cell lines.

Chapter 6 derives overall conclusions from the work conducted and proposed future work that may be carried out to deepen the comprehensions of this field.

CHAPTER 2

CARBON BASED MATERIALS:

APPLICATIONS & TOXICITY

"Do not worry if others do not understand you. Instead worry if you do not understand others."

(Confucius, 551-479 BC)

2.1 Carbon based materials

Carbon is a remarkable element and materials based upon it have gained significant momentum in the field of nanotechnology in the previous quarter of a century. Scientists have developed several forms of carbon in addition to the two naturally existing allotropes; diamond and graphite. Carbon is categorised as a Group 4 element consisting of 6 protons and neutrons in the nucleus, with electrons in the surrounding shells (Figure 2.1).

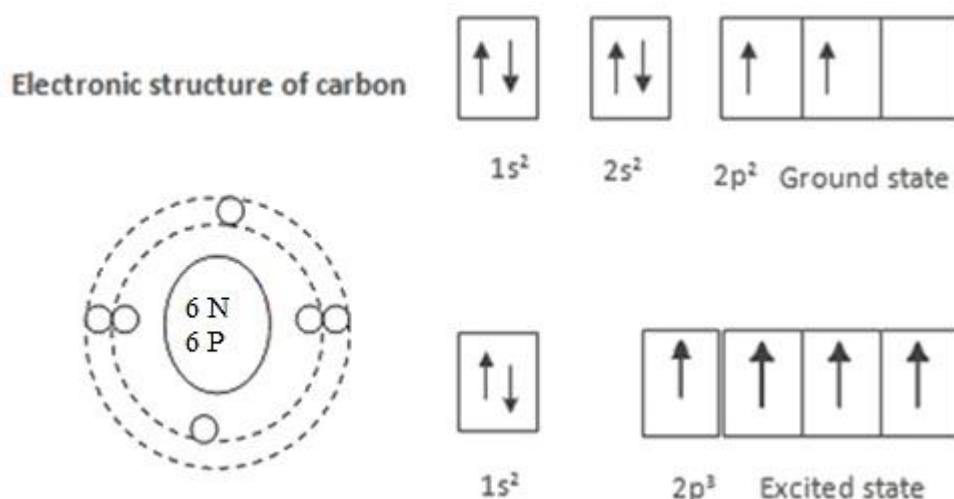


Figure 2.1 Electronic structure and states of carbon

A number of carbon isotopes exist which possess identical chemical properties due to their outer 4 electrons.

In the ground state carbon has an electronic configuration of $1s^2 2s^2 2p^2$. In contrast in an excited state leading to bonding the one $2s$ and the two $2p$ orbitals hybridise forming sp orbital. This facilitates carbon in forming four covalent bonds with carbon or alternative elements.

2.2 Allotropes of carbon

Diamond is considered one of the most attractive and useful allotropes (Figure 2.2) each atom tetrahedrally bonded to four other carbon atoms in a 3-dimensional network via covalent bonds. This gigantic structure imbues diamond with a unique set of properties such as unparalleled hardness and an exceptionally high melting point (Asmann, Heberlein et al. 1999).

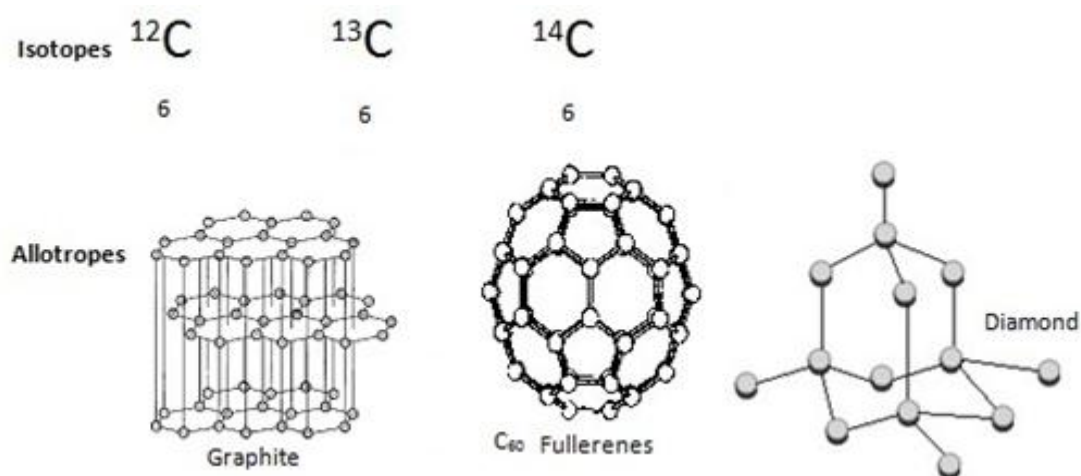


Figure 2.2 Allotropes of carbon

Graphite a second allotrope of carbon essentially comprises hexagonal layers which are structured through strong covalent bonding between carbon atoms in the arrangement of layers. The subsequent layers are held in place by weaker forces known as stacking interactions (van der Waals) however possess enough mobility to slide over one another.

Planar graphene in graphite possess π electrons resulting in agglomeration, allowing van der Waals forces to develop within the layers. Fullerenes gather in a similar way and form fullerite crystals (Sengupta, Bhattacharya et al. 2011).

Recently graphene has attracted considerable interest as a wonder material. The 2010 Nobel Prize was awarded to physicists Andre Geim and Konstantin Novoselov from the University of Manchester, UK “*for ground breaking experiments regarding the 2-dimensional material graphene*”. Graphene offers interesting electrical, mechanical and optical properties. The application of graphene in the field of drug delivery is opening new avenues particularly in cancer treatment. In order to appreciate its grand potential the fundamental material characteristics require further understanding. Graphene is composed of a single layer of hexagonal carbon packed carbon structure with carbon atoms being sp^2 hybridised. Strong covalent bonds within the planes contrast to weak attraction between the graphene sheets. The anti-cancer drugs can be entrapped or added to functionalized components and delivered to target cells (Yang 2011). Graphene additionally absorbs light strongly between the Ultra-Violet (UV) and Near Infra-Red (NIR) hence may be employed via photo thermal cancer therapy (Yang, Zhang et al. 2010). Moreover, the fluorescent properties of graphene oxide can be utilised in optical based detection of biological molecules. As a single sheet graphene has a large surface area, a resultant large quantity of anticancer drugs may be loaded onto it.

Studies have focused on the delivery of anticancer drugs to target tumour cells. The large surface area, thermal conductivity, the biocompatibility of graphene and the ability to functionalize this material makes it a promising candidate for the delivery of drug molecules, such as PTX, Doxorubicin (DOX) and Amphotericin B, as well as genes (Shen, Zhang et al. 2012).

C_{60} commonly known as fullerene, an allotrope of carbon possesses an anatomical arrangement representing a ‘‘cage’’, which is hollow sphere, ellipsoid or a tube. The spherical form consists of 60 carbon atoms organized in a series of interlocking hexagons and pentagons. However, less spherical fullerenes are also formed such as C_{20} , C_{36} , C_{70} and C_{76} (Kroto, Heath et al. 1985).

Another recently discovered structure of carbon is known as a Carbon Nanohorn (CNH) (Ge and Sattler 1994), which is composed of a single layered graphite sheet of 2-3 nanometres (nm) in diameter. These sheets cluster into aggregates having a diameter of approximately 80 nm. Individual CNHs are cone shaped graphite structures with their tips capped with 5 member rings as may be observed in Figure 2.3. The diameter of CNHs increases as their length increases. Potential applications include artificial organs, molecular electronics, fuel cells and hydrogen storage.

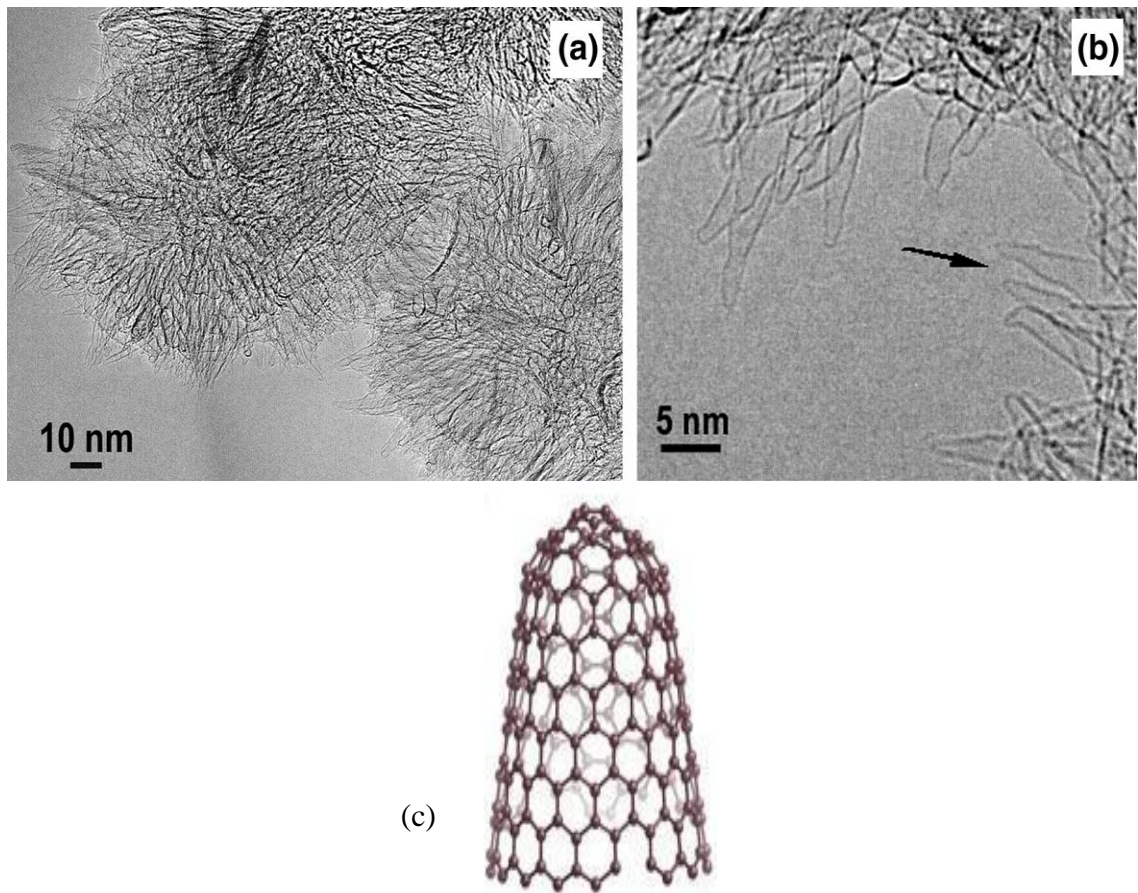


Figure 2.3 TEM micrographs of carbon nanohorns (a and b), with schematic diagram (c) for illustration (Bekyarova, Hanzawa et al. 2002)

Alternative carbon based structures encompass nanobuds, nanocapsules, nanocoils and nanofibres (Figure 2.4). Having said this, detailed discussion of this structure exceeds the scope of this project.

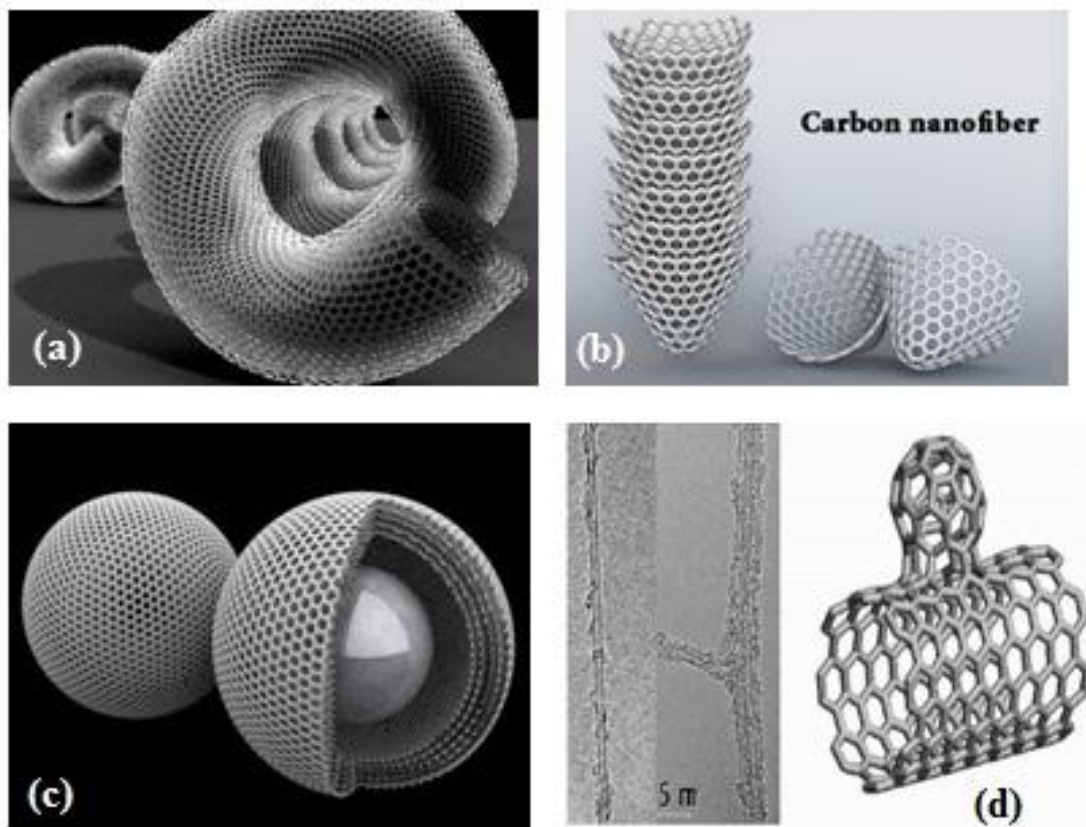


Figure 2.4 (a) Nanocoils, (b) nanofibres, (c) nanocapsules and (d) nanobuds (Nasibulin, Pikhitsa et al. 2007)

2.3 CNTs and their properties

CNTs are essentially ‘‘rolled’’ up layers of graphene sheets in a tubular structure. Though discovered 60 years ago by Radushkevich and Lukyanovich (Radushkevich and Lukyanovich 1952), it only became apparent to the nanotechnology world through a rediscovery by the Japanese scientist Iijima (Iijima 1991). As previously mentioned there are various types of CNTs including: SWNTs, MWNTs and Double Walled CNTs (DWCTs) (Iijima and Ichihashi 1993). All exhibit unique physical and chemical properties which are highly dependent on the various fabrication methods discussed further on. The chemical bonding of CNTs are based upon the sp^2 orbital bond, making them the strongest and hardest material documented in terms of tensile strength and elastic modulus respectively (Peng, Locascio et al. 2008). Depending on the chirality of the tubes the electrical properties can vary from being either metallic or semiconducting. The morphology of CNTs differ depending on the exact process conditions and preparation methods (Qian, Wagner et al. 2002).

The reasons for functionalizing CNTs are multifarious including, improvement in their solubility, biodegradation and for the attachment of various molecules or drugs. They may be functionalized by the addition of a wide range of chemical groups to the ends and sidewalls. Additionally, chemical groups and drugs can be added to the inner of the tubes depending on the CNTs diameter and the size of the drug molecule (Bianco, Kostarelos et al. 2005).

The high strength of the sp^2 carbon-carbon bonds imparts CNTs with greater mechanical properties, which can supply *in vivo* stability. Their high aspect ratio,

tendency towards functional modification and their ability to cross biological barriers are deemed as excellent nanocarriers for drug delivery (Kostarelos, Lacerda et al. 2007). Furthermore, they are advantageous in terms of being utilized as potential nanofluidic device for controlled drug delivery (Foldvari and Bagonluri 2008).

2.3.1 Single walled CNTs

A SWNT is composed of a rolled up single sheet of graphene in a cylindrical shape as illustrated in Figure 2.5 (Iijima and Ichihashi 1993). The cylindrical ends may be sealed by using two caps; each cap being composed of a hemi fullerene. All the carbon atoms are in equivalent positions in hexagonal aromatic rings, with the exception of atoms at the tips of the nanotubes. Pentagonal rings are also present at the tips of the tubes as these favour chemical reactivity (Baughman, 2002).

The carbon atoms involved in the rings have alkene bonds (C=C) however are not planar due to hybridisation with some sp^3 character which increases as the tubular diameter decreases. This effect is similar to that observed for C_{60} which has approximately 30% of sp^3 bonding, with a radius of 0.35 nm. The surface of SWNTs is thus more reactive than the planar graphene. Variable overlapping of bonds of density states imparts onto SWNTs a unique and versatile electronic behaviour.

A graphene sheet is composed of sp^2 hybridised carbon atoms in a hexagonal shape. The joints between the caps and ends of the sheet are seamless. Whilst there is no restriction in the diameter, it appears that collapsing a single-walled tube into a flattened two-layered ribbon is energetically more favourable than the larger diameter tubular structure, particularly when the diameter supersedes ≈ 2.5 nm. Energetic and stresses

become unfavourable on lowering of the diameter beneath 0.4 nm. Figure 2.5(a) provides a description of a rolled up SWNT.

Figure 2.5(b,c,d) shows the potential chiral configurations of assorted SWNTs i.e. Armchair, Zigzag and Chiral arrangements. A compromise may be reached with the most commonly occurring diameter ≈ 1.5 nm (which is in the mid-range). The lengths of CNTs however are variable ranging from nm to μm . The longest CNT length observed was reported to be 18.5 cm (Wang, Li et al. 2009). Features covering small diameters and long lengths give SWNT a very high aspect ratio. In contrast, short SWNTs are highly desirable for biomedical utilization, particularly for *in vitro* and *in vivo*, due to phagocytosis and cytotoxicity. There are three distinct ways into which a graphene sheet may be ‘rolled’ into a tube. These structures give SWNTs well defined metallic, semi-conducting or semi-metallic properties, depending on the tube diameter and the chirality.

Chirality of SWNTs is obtained from its chiral vector C which is defined by integers (n,m) obtained from the arrangement of hexagons with respect to the SWNTs axis. Arm-chair configuration is characterised by chiral vectors (n,n) with a perpendicular shape of the chair to the tube axis. Zigzag configuration is characterised by vectors $(n,0)$ and has a V-shape perpendicular to the axis (Figure 2.5). All other vector configurations may be classified as chiral or helical. The chirality determines the electronic properties of the SWNTs allowing potential applications in a wide range of applications in the electronic industry.

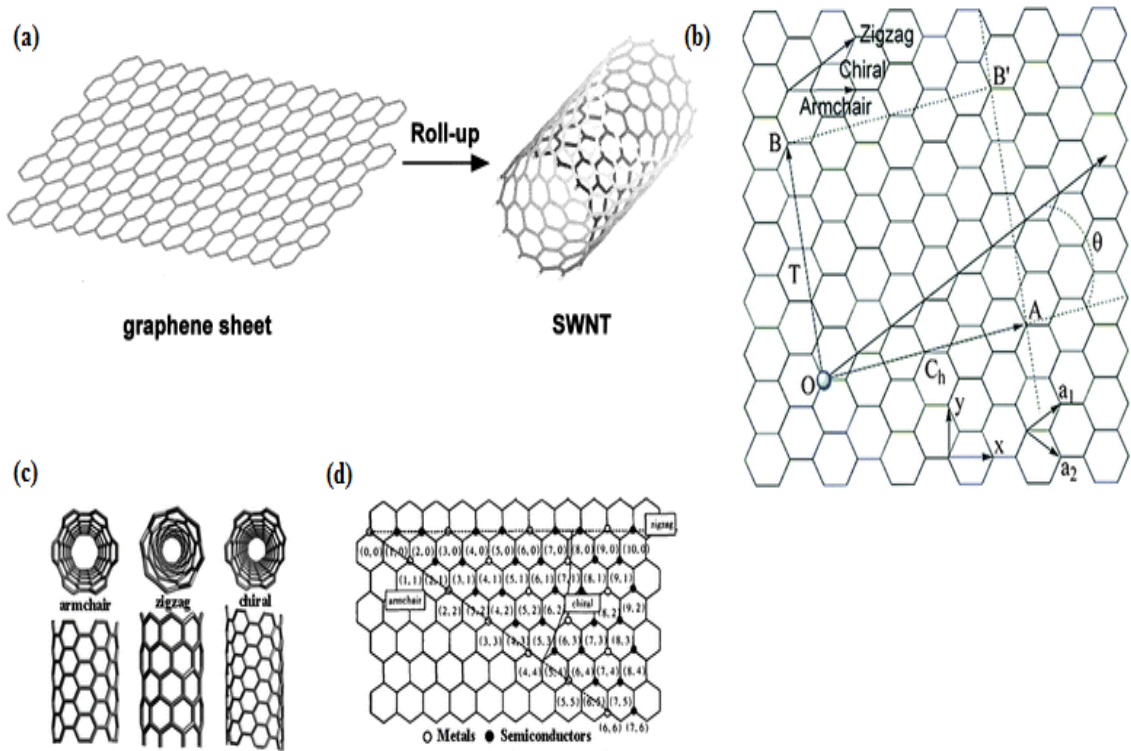


Figure 2.5 Graphene sheet rolled up to obtain a SWNT adapted (a) from (Odom, Huang et al. 2000) and (b,c,d) from (Zhang, Wu et al. 2011)

2.3.2 Multi walled CNTs

In many ways MWNTs (Iijima 1991) are inherently more complex than SWNTs. There are innumerate configurations from the basic graphene building block (Figure 2.6). The simplest arrangement involves a concentric arrangement in which successive tubes increase in diameter. Smaller tubes are contained within in turn into larger ones. MWNT have a number of walls, which may vary from two to an unlimited upper limit.



Figure 2.6 Typical MWNTs adapted from (Sanchez, Jachak et al. 2012)

The diameter between tube walls within the MWNT is approximately 0.34 nm (Xie, Gan et al. 2008). The carbon atoms of graphene are positioned either opposite to one another or opposite carbon atoms from the neighbouring graphene. These enable the carbon nanotube to have a 3-D structure of graphite (Qian, Wagner et al. 2002). The MWNT do not possess as high or varied properties however are easier to process because of their larger diameter ranging from 10-50 nm with a length of 1-20 μm . As

grown by CVD their diameter may vary from 20-40 nm and 1-50 μm in length (Li, Wen et al. 2003).

The herringbone is another common structure of MWNTs (Figure 2.7). Structurally, two graphene sheets are arranged at an angle with respect to the nanotube axis. The size of this angle is dependent upon the exact processing conditions employed for the synthesis, such as composition, catalyst used etc. The size of the angle varies from 0° to 90° considerably. The latter are often called nanofibres as opposed to nanotubes. The mechanism by which the herringbone structure is formed is yet to be concretely confirmed.

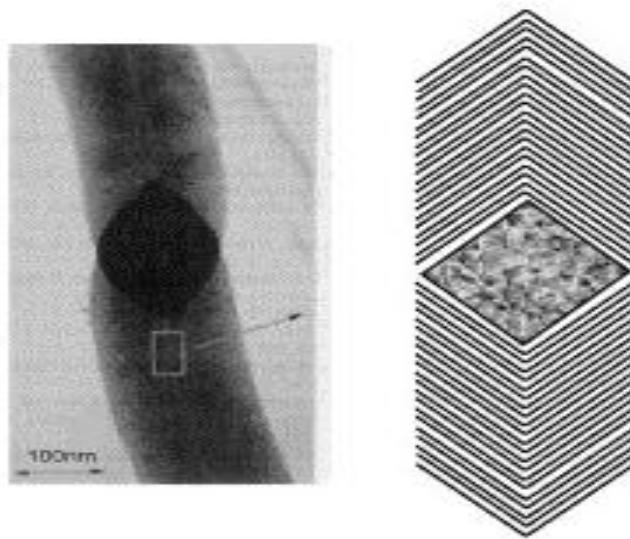


Figure 2.7 Herringbone structure adapted from right (Strobel, Garche et al. 2006) and left from (Serp, Corrias et al. 2003)

‘‘Bamboo’’ textured graphenes, are also frequently encountered and may be viewed as a combination of the textures described above (Figure 2.8). It does not arise independently but contains a variable amount of herringbone and graphite textures.

These structures are hollow, but do not have an open inner cavity throughout the full length. They are often referred to as nanofibres rather than nanotubes. Nanofilaments are built from graphenes orientated perpendicular to the filaments axis and began as piled- up plates.

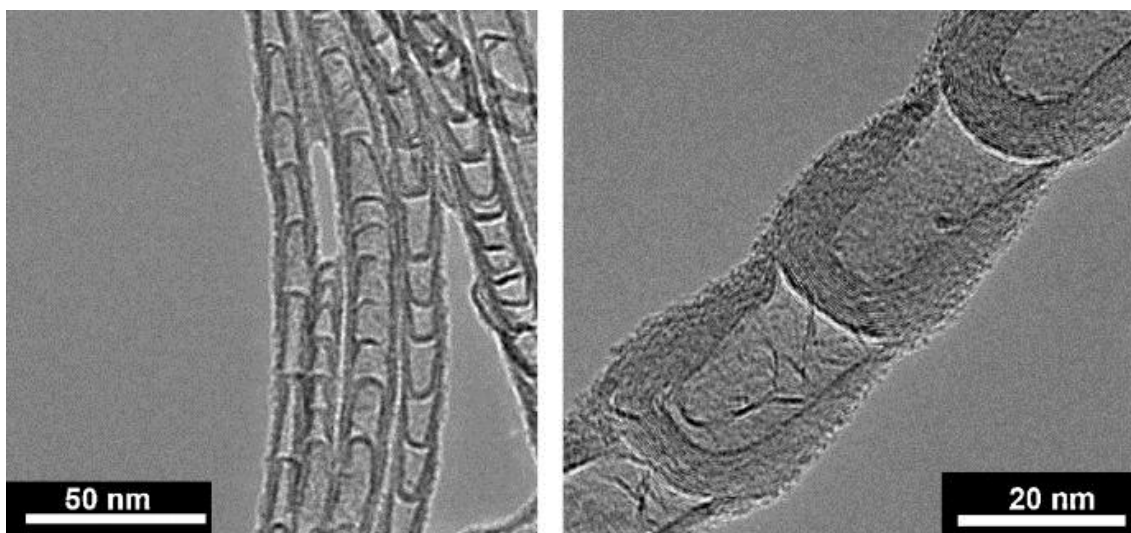


Figure 2.8 Bamboo textured CNTs (Chizari, Janowska et al. 2010)

MWNTs have an aspect ratio much lower than the SWNTs and the ends can often be viewed with a TEM and are shown to frequently contain a catalyst. The properties of MWNTs are highly dependent on the perfection and orientations of graphenes in the tubes, they are influenced by processing conditions and subsequent thermal or chemical treatments. The structures of CNTs may have an effect on their application in the area of drug delivery. They may also impact the functionalization and transport across membranes. However, no work to date has been carried out on the impact of the structure on drug delivery efficiency and mechanisms involved.

Carbon nanomaterials have had a profound and defying influence in all disciplines. In recent times each discovery has led to a greater one as may be seen in table 2.1. Dating early as 1952, when Radushkevich and Lukyanovich intruduced the Carbon filament.

Table 2.1 Carbon nanomaterial discovery

Year	Event
1952	Carbon filament (Radushkevich and Lukyanovich 1952)
1960	Production of carbon tubes with graphite layer structure (Bacon 1960)
1985	C60 (Kroto, Heath et al. 1985)
1991	Multi-walled carbon (Iijima 1991)
1993	Single –walled CNTs (Iijima and Ichihashi 1993)

2.4 Synthesis of CNTs

CNTs have been synthesised using a wide range of techniques including laser vaporisation, Arc-discharge, high-pressure carbon monoxide, CVD and plasma enhanced chemical vapour deposition (PECVD). Moreover, on the syntheses of CNT they require purification in order to be utilised for specific application. Functionalization of particular interest as the addition of chemical groups can facilitate transport and recognition of drug molecules.

2.4.1 Solid sources

This process requires high temperatures in excess of 800 °C and a solid source of carbon i.e. graphite is a pre-requisite. The types and properties of CNTs produced by solid methods are variable. Laser vaporisation of graphite was identified as the first to demonstrate the existence of a number of fullerenes many years ago with C₆₀ being the most abundant and stable. The electric arc technique enables C₆₀ to be produced in large quantities. However, in order to produce CNTs with these methods a catalyst is an essential requirement. In general, a catalyst speeds up the formation and growth of CNTs and metal catalysts are employed for CNT synthesis. In these methods energy is transferred from an external radiator (laser beam, solar energy or electric arc) to the target material. This causes the removal of material from the target source resulting in the formation of complex plasma containing a ‘soup’ composed of free radicals, ion and neutral species. The extent of ionisation depends on various factors such as composition of the target, pressure, temperature and energy stored. The characteristics of the plasma such as density, composition and energy determine the characteristics of the CNTs synthesised.

The major advantage of these techniques is the possibility of varying a large number of parameters and enabling the formation of a range of CNTs. The optimum conditions can thus be defined for general CNT characteristics. Conversely, a pitfall would be that CNTs produced contain impurities such as other undesirable carbon phases and metal catalyst particles. Consequently, the use of acids and thermal treatments are necessitated to obtain high quality purer CNTs (Djordjevic, Djustebek et al. 2006).

2.4.2 Laser ablation

In the laser ablation process a graphite pellet containing a catalyst is used. It is heated in a furnace containing an inert gas, such as argon, at a temperature of about 1200 °C (Figure 2.9). The Laser beam focused onto the target causes the material to vaporise. The carbon species is transported to another region in the reactor where it is deposited onto water cooled copper collector on the quartz reactor tube walls and the backside of the pellet. This method was the first used to synthesise fullerenes (Popov 2004).

As of late modifications and considerable improvements to this method have been made. A second pulsed laser has also been employed which allows the carbon aggregates to follow the first ablation for CNTs growth. Researchers have also utilized second quartz tubes placed inside the larger tube coaxially to enable more carbon containing species to deposit. In addition, researchers have also employed two pellets, one made entirely of graphite and another made of a mixture of graphite and catalyst. Both of these are irradiated simultaneously.

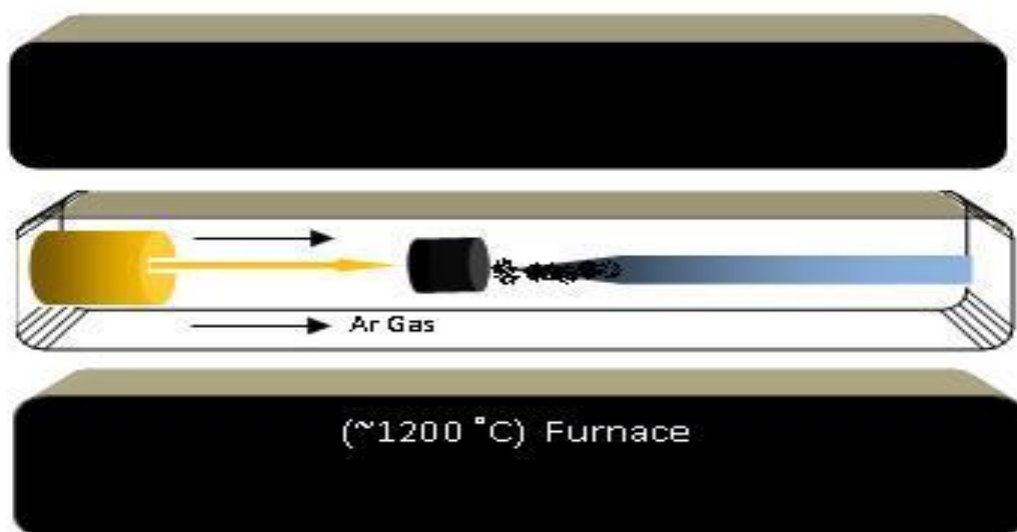


Figure 2.9 Schematic diagram of a laser ablation system used for the growth of CNTs

In this system a continuous CO₂ laser beam ($\lambda = 10.6 \mu\text{m}$) is commonly utilized to ablate the graphite material. The laser power can be accurately controlled between 100 W to 1600 W in order for the evaporation rate to be controlled. On increasing power, the evaporation rate also increases resulting in a higher growth rate of CNTs. Importantly control over the temperature in the reactor is a highly influential factor. An optical pyrometer is used to determine and control the temperature in the reactor. The solid products are transported away by the gas and collected at the filter. The yield is controlled by several factors such as the catalyst, cooling rate, residence time and the temperature.

In the absence of a catalyst that is used in this method, the “soot” collected is composed mainly of MWNTs. Typically the lengths of the MWNTs are of the order $\approx 300 \text{ nm}$. CNTs obtained at 1200 °C deteriorate as temperature is reduced. In addition of catalysts, such as Ni or Co, the growth mechanism changes and SWNTs are formed. The type and the quantity of the catalyst used, determine the yield of SWNTs along with the furnace

temperature gradient. They have a uniform diameter and organise themselves into “rope-like” structures known to have varying lengths between 5-20 nm diameter and 10-100 μm in length. The ends of the CNTs have closed caps on them. This technique has been used to prepare SWNTs commercially, with its ability to produce clean CNTs. As the technology advances this method may be replaced by alternative CNT methods with better control and output.

2.4.3 Arc discharge

In this technique the carbon is vaporised between two electrodes, the anode and cathode. Graphite is implemented in the form of rods, producing a cathode and the anode arranged horizontally and vertically (Figure 2.10). This is done in the presence of iron (Fe), nickel (Ni), cobalt (Co) and barium (B) etc. catalysts under reduced pressure in the presence of an inert gas such as argon. Once the arc is triggered plasma is formed, consisting of a carbon vapour, gas and catalyst particles. Energy is transformed between the arc and the anode made out of graphite. The anode is eroded with the rate dependent on the power of the arc and the details of the experimental conditions. On completion CNTs are deposited in various regions of the reactor, including the cathode, reactor walls and bottom of the reactor.

The electrode diameters are also variable. Two types of anodes are present, each contains holes which are drilled; allowing the graphite powder and catalyst to be introduced and mixed together in correct proportions. The graphite anode with the catalyst is homogeneously dispersed.

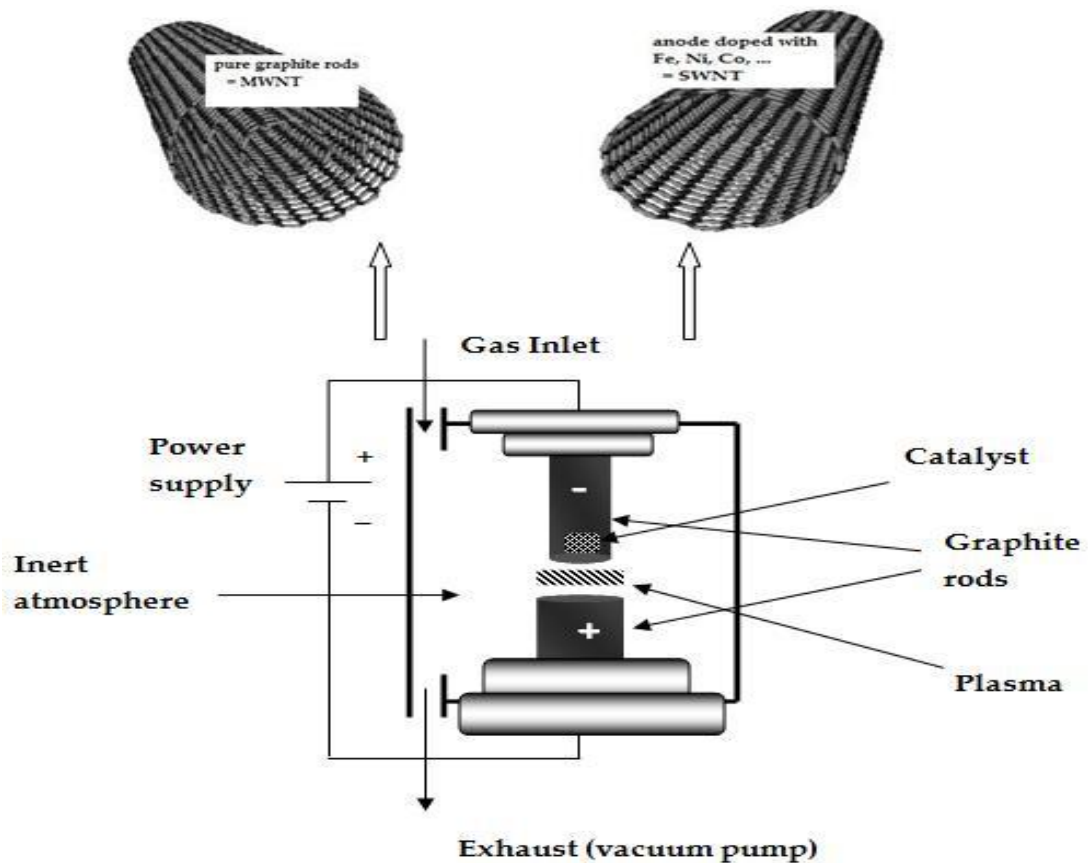


Figure 2.10 Schematic diagram of an Arc discharge system

Researchers have also investigated the use of electric arc within a liquid media such as water or liquid nitrogen. Greater ease in processing and the lack of requirement for a vacuum means this process can be set up to be continuous and therefore highly suitable for mass production.

This method results in a variety of products such as CNTs, nanoparticles, fullerenes, nanofibres, MW Shells, single walled nanocapsules, and amorphous carbon. By altering the conditions such the anode, pressure etc. the type of product obtained varies. Anode is consumed and a “cigar like” deposit is formed. Outer parts of the deposit is MWNTs, polyhedral particles and amorphous carbon. SWNTs can be obtained by adding a catalyst such as Ni:Yttrium (Y), Fe:Co instead onto the anode. When a Fe catalyst is

used with H₂ (Hydrogen) and inert gas, SWNTs are found with the length as high as 20-30 cm and replacing He (Helium) with H₂ gives MWNTs.

2.4.4 Solar furnace

The solar furnace technique also implements the principle of using sublimation of graphite powder and catalysts placed in a crucible (Figure 2.11). The solar energy is collected by a plane mirror and reflected towards a parabolic mirror which focuses onto the graphite pellet. Elevated temperatures results in vaporization of the pellet and catalyst simultaneously. The vapour then condenses onto a water cooled surface. The reactor consists of a support assembly cooled by water circulation, onto which a Pyrex® chamber is mounted. The target is mounted onto a Cu (Copper) rod which is surrounded by a graphite tube acting as a thermal screen and reduces losses of free radicals. The graphite crucible is filled with graphite powder for fullerenes and graphite plus catalyst for CNTs.

On utilization of a Ni/Co catalyst at low pressure, MWNTs are the primary products. At high pressures smaller SWNTs are obtained. Ni/Y at high pressures, relatively long SWNT are obtained with diameters ranging from 1 to 2 nm.

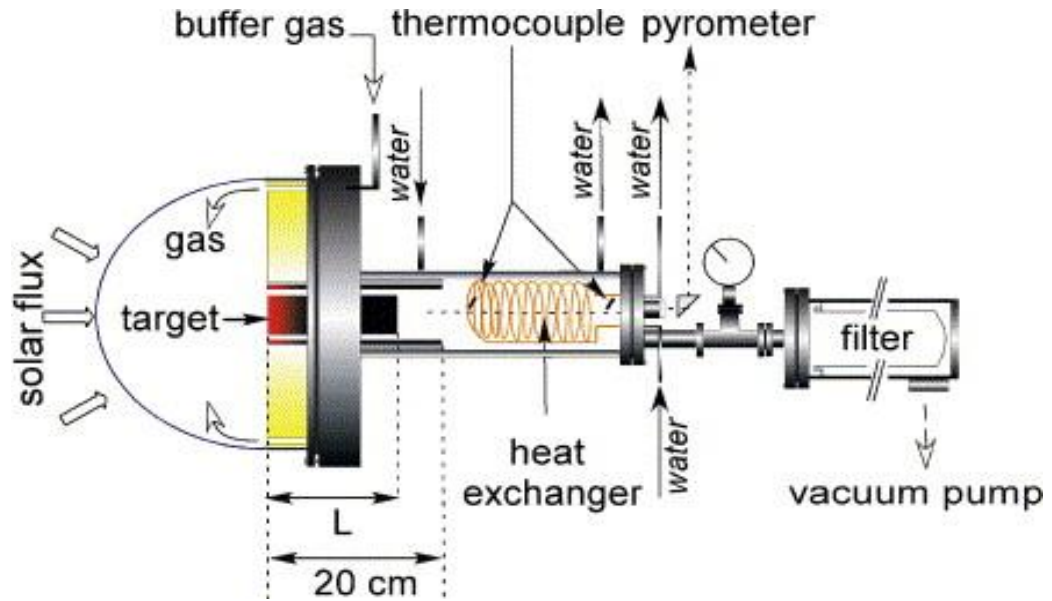


Figure 2.11 Solar method for large scale CNT synthesis (adapted from Luxembourg, Flamant et al. 2004)

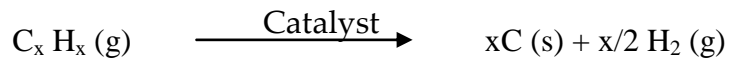
2.4.5 Vapour phase deposition

Catalytic decomposition of hydrocarbon has been known for over a century now. In the 1980's Endo developed a floating catalyst reactor containing metallic catalyst particles with a diameter of 10 nm (Endo 1988; Belin and Epron 2005). CNTs are now widely produced using Catalytic Chemical Vapour Deposition (CCVD) technique (Kumar and Ando 2010). This method involves the decomposition of hydrocarbons in the presence of catalysts, which are normally transition metals such as Fe, Ni, Co etc. producing MWNTs and SWNTs. On usage of lower temperatures between 300-800 °C MWNTs are produced in an inert atmosphere of He or Ar (Argon). In contrast, at higher temperatures typically 600-1150 °C and in the presence of H₂ and Ar SWNTs are produced. Plasma enhanced CVD (PECVD) using acetylene and H₂ gas mixtures have been used to grow MWNTs onto steel plates. CVD has also been used to grow aligned

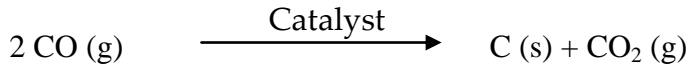
MWNTs and SWNTs substrates such as Ni, Si (Silicon), SiO₂ (Silicon Dioxide), Cu/Ti (Titanium)/Si, stainless steel and glass (Bell, Teo et al. 2006).

CNTs produced by this method differ from those produced by arc discharge particularly in that they have a lower degree of crystallinity and have more defects. CCVD is a versatile method for growing doped CNTs with B, N (Nitrogen) or both and can be centimeters in length with a diameter up to 10 nm. MWNT the number of walls can vary from 3 to more than 100. Diameters may potentially range up to 100 nm (Ionescu, Zhang et al. 2012). They tend to grow perpendicular to the substrate allowing ease in determination of their length using cross sectional SEM or TEM.

The CVD process is simple in concept and consists of a furnace, which can be heated in a controlled manner to the required temperature. A mixture of hydrocarbon (CH₄, C₂H₂, C₂H₄ or C₆H₆) an H₂ or inert gas (He, Ar) is passed over small transition metal particles (Ni, Co, Fe) or a flat substrate with a thinly deposited layer of the transition metal onto the substrate (Si, Steel etc.) A catalytic chemical reaction occurs on the surface of the particle or flat substrate with the reaction rate being accelerated by the catalyst. Cracking of the hydrocarbon occurs onto the surface giving carbon. The below diagram offers a summary of the process:



The carbon containing processor transfer other gases such as CO or CO₂



The growth characteristic of CNTs is dependent upon the process parameters entailing the pressure, catalyst, (type and size) of reactor, temperature, gas composition and flow rate. The stages involved in the CCVD process are as follows:

- Transport of gas mixture to the surface where the catalyst is present (particle or flat substrate)
- Adsorption of the gases onto the surface

Chemical reaction (decomposition) on the surface and subsequent growth of CNT (

- Figure 2.12Figure 2.12-Figure 2.13)
- Desorption of unwanted byproducts such as H₂ and unreacted species
- Transport of products away from the surface and eventually out of the reactor

A critical parameter in growing CNTs is the size and distribution of the catalytic nanoparticles. Control over the size is crucial and condensing in large clusters is highly undesirable. Condensation into large clusters is prevented by using support materials, such as Al₂O₃ (Aluminium Oxide), SiO₂, MgAl₂O₄, MgO (Magnesium Oxide) and occasionally graphite. Generally, a low concentration of catalyst is required to limit the coalescence of the metal particles.

As the catalyst is a critical component in the CVD process it is informative to look at the myriad of ways in which this can be produced. Several methods are documented including impregnation which involves:

- The salt solution (nitrate, chloride) containing the metal impregnates, the support material
- Dry and calcinate the supported catalyst to obtain the oxide
- Reduction in a H_2 atmosphere to make metal nanoparticles

Decomposition of carbon containing gas over freshly prepared metal particles to form CNTs. For example, C_2H_2 in H_2 can be decomposed on a well dispersed metal particle such as Fe, Co, Ni, Cu that is supported on graphite or Co-SiO₂ for MWNTs formation.

The usage of zeolite support medium is implemented to support Co catalysis, with particle sizes of 1-50 nm in diameter only allow for the formation of two to three walls. CO (Carbon Monoxide) disproportionation has also been used to form CNTs onto nano-sized Mo particles. The diameter is related to original particle size and ranges from 1 to 50 nm.

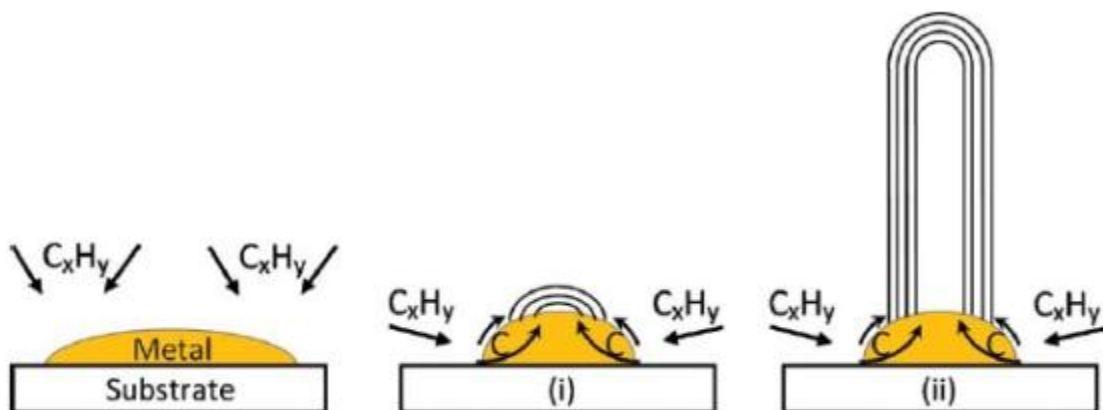


Figure 2.12 Base growth model (Kumar, M. and Ando. A, 2010)

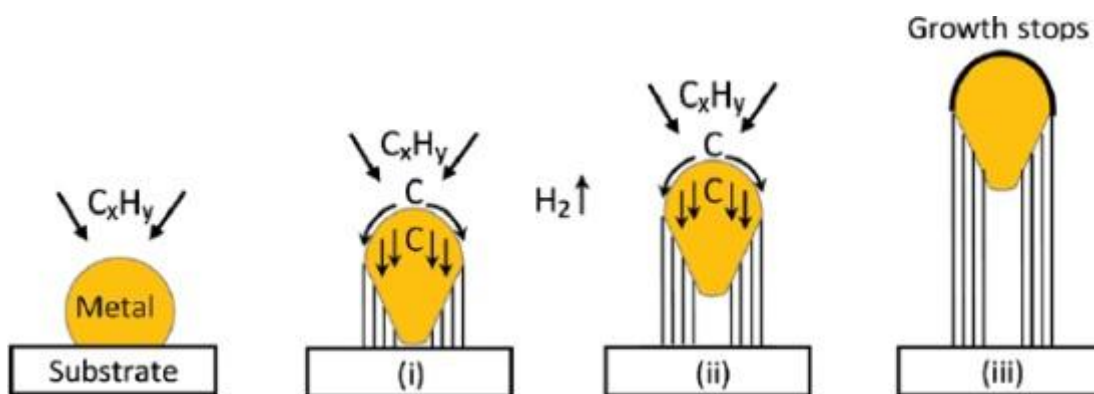


Figure 2.13 Schematic view of widely accepted growth mechanism; tip-growth model (Kumar, M. and Ando. A, 2010)

The second involves solution-based methods where a solid solution of two metal oxides is formed on substitution of different metal ions. For example, a solid solution of Fe_2O_3 (Ferrous Oxide) and Al_2O_3 are employed to form $\text{Al}_{2-2x}\text{Fe}_{2x}\text{O}$ complex solid solution. Both are homogeneously inter-dispersed. Solid solutions of this type may be prepared in various ways for example, co-participation of mixed oxides. Homogeneous dispersions of catalytic oxide can produce very small catalytic metal oxides at high temperatures. 18% CH_4 in H_2 decompose between 850-1050 °C. Nanotubes obtained are typically gathered into small diameter bundles less than 15 nm with lengths of 100 μm . The CNTs types are predominantly SWNTs and DWNTs with diameter ranging between 1-3 nm. The defining issue is the ability to remove the catalyst and obtain pure CNTs.

When oxides such as Al_2O_3 or SiO_2 are used removal requires the usage of aggressive chemical treatments. Hot KOH (Potassium Hydroxide) or NaOH (Sodium Hydroxide) are used for Al_2O_3 and HF (HydroFuran) is used to remove SiO_2 . These solutions have no effect on other impurities such as other forms of carbon. Treatments such as oxidation in air, HNO_3 (Nitric acid), KMNO_4 (Potassium Permanganate) and H_2O_2 (Hydrogen Peroxide) are required to remove carbon-containing impurities. However, the yield of CNTs attained is dependent on these oxidizing treatments.

MgCoO (Magnesium Cobalt Oxide) solid solution has been previously used to prepare SWNTs and DWNTs. These may be easily be separated from the support by washing in aqueous HCl (Hydrochloric acid) solution without damaging the CNTs formed (Flahaut, Peigney et al. 2000). In addition, there is a homogeneous CCVD process, which has also been used to synthesize SWNTs and MWNTs. This method employs a hydrocarbon gas with H_2/Ar mixture along with gaseous metal containing a precursor such as

ferrocene. The reactor contains two zones. The first zone is of a lower temperature and second zone is of a high temperature between 700-1200 °C. The metal precursor may be $\text{Fe}(\text{CO})_5$, ferrocene, nickelocene or cobaltocene (Awasthi, Kumar et al. 2011).

In the first zone the metal organic compound decompose to generate metal particles, possessing a size in the nanometre range. The particles act as a catalyst for the CNTs synthesis. Both SWNTs and MWNTs may be formulated by this method. Difficulties experienced are again in the formation of several types of materials, control of particle size and removal of impurities. Often metal particles are too large to form CNTs but can still decompose the carbon containing precursor and form layers of graphene on the surface. Process parameters that affect the quality of CNTs are similar to the heterogeneous process such as the nature and size of the catalyst particles, reactor temperature, flow rate, residence time and composition of incoming gases and state of hydrogen.

Notably the HiPCo (High Pressure Carbon Monoxide) process developed at Rice University has been used to produce high quality SWNTs. This process implements CO and $\text{Fe}(\text{CO})_5$ (Iron Pentacarbonyl) in order to produce SWNTs relatively free of impurities. Hydrocarbon gases are required; however no alignment of CNTs can be recovered by dissolving the template (Bronikowski, Willis et al. 2001).

2.5 Biomedical applications of CNTs

CNTs are novel carriers for small and large therapeutic molecules and may be functionalized using functional groups such as $-NH_3$, $-OH$, $-COH$ and $-PEG$ in order to manipulate their physical or biological properties. These may be added to various locations in the CNTs such as within (encapsulation), tips and sides depending on the intended application (Figure 2.14) (Bhirde, Patel et al. 2009). Furthermore, CNTs are able to act as carriers for therapeutic molecules, due to their large surface area and the manipulation of their surfaces and physical dimensions (Foldvari and Bagonluri 2008).

There is a huge and increasing interest among biomedical scientists in the exploration of all of the above-mentioned properties which CNTs possess for Nano-biotechnology applications (Bianco, Kostarelos et al. 2005). CNTs are deemed a suitable substrate for the growth of cells for tissue regeneration, as delivery systems for a variety of diagnostic or therapeutic agents or as vectors for gene transfection (Becker, Fagan et al. 2007). CNTs may be offered as a novel vector or transport system for various therapeutic agents to treat a variety of diseases.

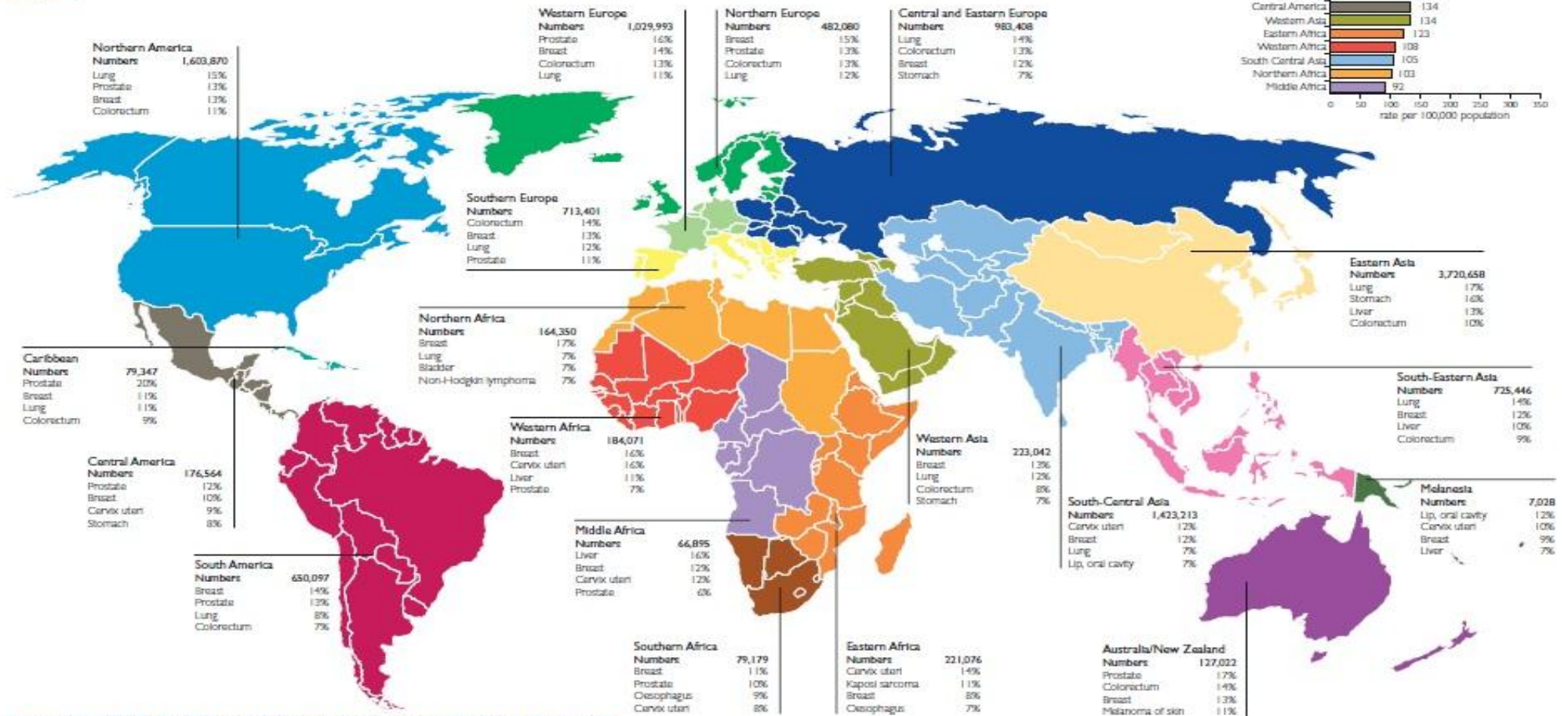
2.6 Cancer

Cancer is perhaps one of the most complex phenomena in biology and unfortunately each year more and more people are diagnosed with this often fatal disease. According to World Cancer Report 2008, there were 12.7 million new cases and an estimated 7.6 million deaths from the disease (**Error! Not a valid bookmark self-reference.**) (Boyle and Levin 2008).

Cancer can be broadly defined as a genetic disorder that is thought to be quite modern, although, the aphorisms of Hippocrates of Cos (born 460 BC) contains various references of malignant cancer, including “Every cancer not only corrupts the part it has seized but spreads further”. It is fundamentally a disease, whereby cell proliferation or apoptosis is disturbed (Figure 2.16). Typically, the human genome is very stable and many genetic alterations are required for cancer to occur. To elaborate, with the exception of reproductive cells, all cells divide by the process of mitosis which entails nuclear and cellular division. This process results in the production of two identical daughter cells. Any abnormality in one or both of the processes results in cell overgrowth which potentially may initiate cancer. Cell overgrowth can cause the formation of clusters remaining in a single mass in which the tumour is counted to be benign; this can more often not be completely cured. On the other hand a malignant tumour has the ability to invade the surrounding tissues; the end result may be secondary tumours or metastases. A cancerous tumour commonly originates from a single mutated abnormal cell (Alberts 1994).

Cancer Incidence Worldwide

Breakdown of the estimated 12.7 million new cases, World-age standardised incidence rates and the most commonly diagnosed cancers by the different regions of the world, 2008.



Source: GLOBOCAN 2008, v. 1.2, Cancer Incidence and Mortality Worldwide, IARC, 2010 (<http://globocan.iarc.fr>)
Map updated February 2011

<http://info.cancerresearchuk.org/cancerstats/>

© Cancer Research UK
Reproduced with permission of the Institute of Cancer Research (ICR) and the Wellcome Trust

Figure 2.15 World cancer incidence in 2008 (adapted from (Boyle and Levin 2008))

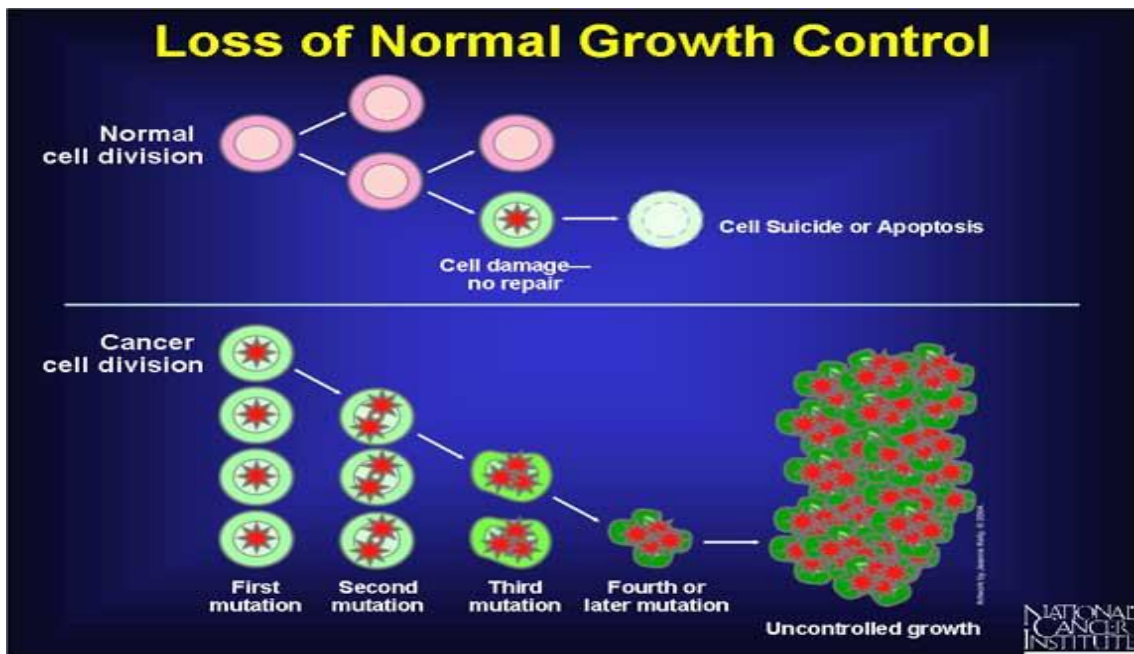


Figure 2.16 Typical growth of normal cells and cancerous growth in uncontrolled manner adapted from (National Cancer Institute, NCI Website: (<http://cancer.gov/cancertopics/understandingcancer>))

Cancer cells have specific characteristic that are distinct from normal cells. A study by Hanahan and Weinberg established a model that is proposed as the “Hallmarks of Cancer”, after a decade of research they have broadened the scope of the concept, for a better understanding of cancer cells (Hanahan and Weinberg 2000). These six biological capabilities are acquired during tumour development to allow continuous and independent cell proliferation. These aforementioned hallmarks include;

- Resisting apoptosis
- Self-sufficient on growth factor
- They can resist inhibitory signals from tumour suppressor genes
- Stimulation of angiogenesis
- Potential for limitless replication
- Tissue invasion and metastasis

The permutation of these characteristic make cancer a highly complex disease in terms of therapeutics. Apoptosis resistance is a crucial attribute of cancer cells along with

limitless replication, where they retain telomerase which sustains the telomere length of the chromosomes accomplishing a virtually immortal cell. A way in which cancer may metastasize is via the stimulation of angiogenesis this plays an important role in rapid growth, since the new cells are in deprivation of nutrients and oxygen, at the same time they are able to override anti-growth signals (Hanahan and Weinberg 2011).

Causes of cancer are dependent on internal and/or external factors. Internal factors may be attributed to genetic disorders, such as hormonal changes or immune system abnormalities. The environmental influences vary from; alcohol consumption, smoking tobacco to excessive sunlight exposure. Additional external factors may also include exposure to certain drugs, radiation and bacteria. Specific environmental factors may be linked to specific type of cancers; a key example would be the exposure of Benzidine resulting in a strong association with bladder cancer (You, Chen et al. 1990). Moreover, the smoking tobacco may cause various types of cancer such as; lung, bladder, lip, mouth and stomach cancer (Gandini, Botteri et al. 2008). In contrast, only one environmental factor is established for brain tumours, this is ionization radiation (Fisher, Schwartzbaum et al. 2007).

Over 90% of Central Nervous System (CNS) tumours are initiated in the brain (Boyle and Levin 2008) and are classified as primary brain tumours. This may occur on brain cells, the membranes around the brain (meninges), nerves or glands. There are approximately 100 types of brain tumour. The most aggressive type is Glioma (Louis, Ohgaki et al. 2007). In the UK Brain tumours are listed as one of the most 20 common cancers, as it can be observed in Figure 2.17.

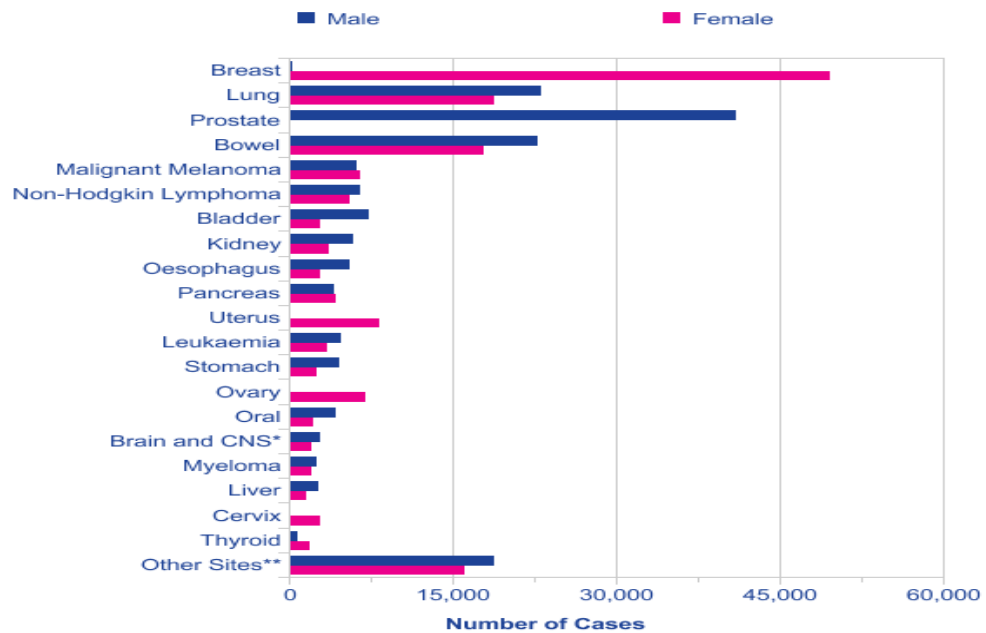


Figure 2.17 Twenty Most Commonly Diagnosed Cancers, adapted from Cancer Research UK statistics (2010)

The tumour is named according to the type of cells and the area of the brain from which the abnormality stems. The most common brain tumour begins in glial cells and is referred to as Glioma. It is known for being an extremely aggressive tumour as described further on.

According to the World health organisation (WHO) brain tumours can be classified and graded based upon their appearance under a microscope.

- **WHO grade I** – Benign tissue which resembles normal brain cells, growth rates are often slow, removable and curable with surgery.
- **WHO grade II** – Tissue is malignant and tends to spread, and looking less like normal cells. It often turns into high grade brain tumours with a poor prognosis.

- **WHO grade III** – In this grade the malignant tissue is anaplastic. (are actively growing)
- **WHO grade IV** – This grade of tumours has poor prognoses and progress rapidly. This is the most aggressive malignant tumour.

The possibility for low grade tumours to recur or to progress into higher grades (III and IV) is very common. However, the change is more common in adults than in children. The initial two types mentioned grow slower and can sometime be cured with treatment. The most common types of brain tumours are listed in table 2.2.

Table 2.2 Most common types of brain tumours

Glioma	Skull based tumours	Other types
<ul style="list-style-type: none"> • Anaplastic Astrocytoma (grade III glioma) • Astrocytoma (grade II glioma) • Brainstem Glioma • Ependymoma • Gangliogliomas • Ganglioneuromas • Glioblastoma (Grade IV glioma) • Glioma • Juvenile Pilocytic Astrocytoma (JPA) • Low-grade Astrocytoma (LGA) • Medulloblastomas • Mixed Gliomas • Oligodendroglioma • Optic Nerve Gliomas • Pilocytic Astrocytoma (grade I glioma) • Primitive Neuroectodermal (PNET) 	<ul style="list-style-type: none"> • Acoustic Neuroma • (vestibular schwannoma) • Acromegaly • Adenoma • Chondrosarcomas • Chordomas • Craniopharyngiomas • Epidermoid Tumours • Glomus Jugulare Tumours • Infratentorial Meningiomas • Meningiomas • Pituitary Adenomas • Pituitary Tumour • Rathke's Cleft Cyst • Vestibular Schwannoma 	<ul style="list-style-type: none"> • Choroid Plexus Papillomas • CNS lymphoma • Colloid Cyst • Cystic Tumours • Dermoid Tumour • Germinoma • Lymphoma • Nasal Carcinomas • Naso-pharyngeal tumors • Pineal Tumours • Pineoblastoma • Pineocytoma • Supratentorial Meningiomas • Vascular Tumors

2.6.1 Glioma

The most common type of primary brain tumour is Glioma and accounts for more than 50% of cancer types and more than 90% of all primary malignant CNS tumours. They originate in the brain or the spine, as they arise from the glial cells (Figure 2.18). These protect and support the nerve cells (Kaye and Laws 2001). Gliomas exist in IV grades and nomenclature is based on the cells from which they grow including; hence gliomas that originate from astrocytes, ependymal and oligodendrocytes are referred to as astrocytoma, ependymoma and oligodendrocytoma, respectively. Some Gliomas contain more than one cell type and thus have the characteristics of both tumours, therefore treatment is harder to obtain and full recovery is significantly reduced. The grading is confirmed by performing a pathological evaluation of the tumour. However, Gliomas are also classified according their histological cell features.

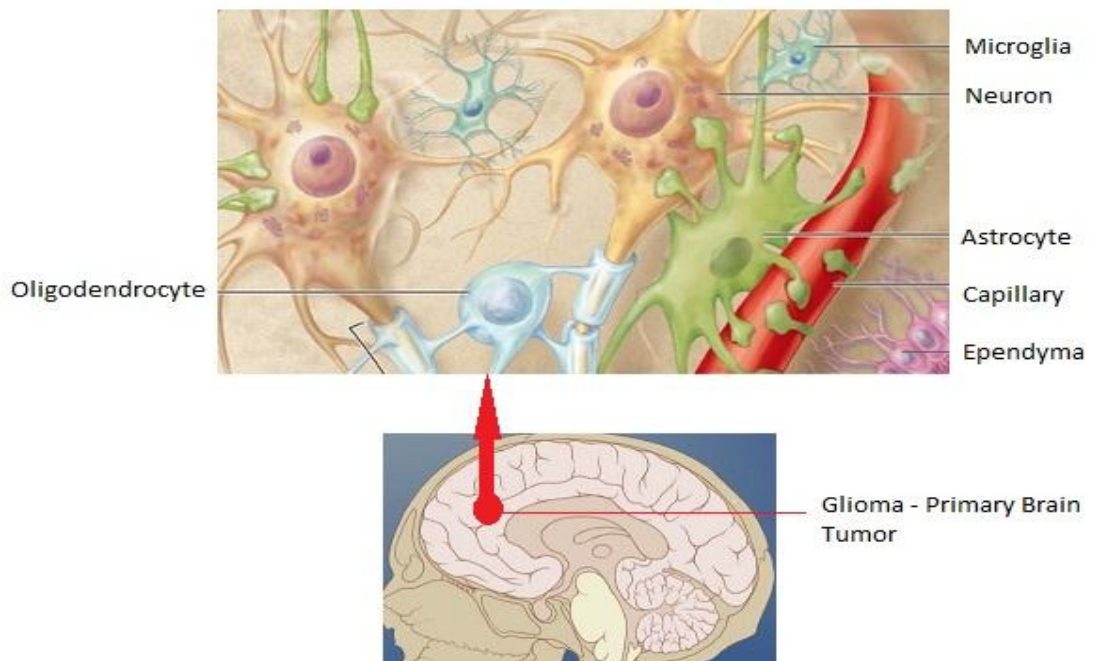


Figure 2.18 Microglia cells showing the Glioma in the brain

Low grade (I and II) Gliomas are not anaplastic, meaning they remain in the cell structure and are less aggressive, although they grow, the growth factor is much less in comparison to the high grade (III and IV) whereby the growth is rapid and are anaplastic and thus the patients have poor prognosis.

Histological nomenclatures of Gliomas:

- **Astrocytoma** can be located anywhere in the brain and vary from grade I to IV. These neoplasms arise from astrocytes, the star-shaped brain cells, their characteristics vary from slow growth, invasion of surrounding tissue any cyst formation (Walker and Kaye 2001; Ohgaki and Kleihues 2005)
- **Ependyomomas** are also glial tumour cells that usually occur in the lining of the ventricles (the brain passageways). Occasionally, this type of tumour does metastasise to the spinal cord but rarely originates from the cord itself. These neoplasms comprise approximately 5% of all CNS tumours and 15% of all spinal cord tumours. (Gilbert, Ruda et al. 2010; Nagasawa, Smith et al. 2011)
- **Oligodendroglioma** is a tumour that is derived from the oligodendrocytes cells and was firstly recognized by Robertson in the 1900 as part of a neuroglial that was found mainly in the white matter of the CNS (Earnest, Kernohan et al. 1950). Oligodendroglioma are classified into two forms: the well-differentiated oligodendroglioma and anaplastic oligodendroglioma. Additionally, oligodendrogliomas may occasionally contain clear evidence of neoplastic astrocytes and are considered as “mixed gliomas,” or most commonly as oligoastrocytomas. (Kleihues and Sobin 2000)

2.7 Cancer treatments

Innumerate therapies have been uncovered since the 18th century and already have been utilized for cancer treatment either solely or in combination with radiotherapy, chemotherapy, and/or surgery. Recently, however, a wide range of nanotechnology therapies have been shown to be effective in treatment of various cancers *in vitro* and *in vivo* (Misra, Acharya et al. 2010). This work focuses on chemotherapy and targeted delivery to cancerous regions specifically for primary central nervous system tumours. Brain tumours are considered to be the most difficult of cancers to treat, primarily due to the presence of the BBB and glioblastoma is the highest dedifferentiated form of astrocytic brain tumours, and it is refractory to chemotherapy in most cases.

2.7.1 Radiation therapy

Radiation therapy is used in conjunction to surgery and chemotherapy. The treatment consists of high energy beams that are produced by the accelerator to exterminate the cancer cells. However, the energy beams produced may kill surrounding healthy tissues, after extensive research in past decades doctors have determined the optimum doses for specific types of cancer that maximize effectiveness and minimize any harm to healthy tissues making radiotherapy a highly effective treatment. Various types of radiations exists, the most common type is however the external beam radiation therapy, whereby the high-energy beam is directed at the tumour (Hattangadi, Chen et al. 2010).

2.7.2 Surgery

Nowadays, surgery is used within the context of multidisciplinary management of cancer, where it plays a role as one of the components of modern cancer management. Surgery can be used for multiple motives such as; cancer screening and prevention, surgery of cancer staging and surgery for cancer treatment. The choice for surgical intervention can be dependent on the nature and stage of the cancer type (Boyle and Levin 2008).

2.7.3 Chemotherapy

The mechanism of action in chemotherapy is based on the prevention of the rapid growth of mitosis or destroying the malignant cells, although their mechanism of action may vary with different drugs and concentrations levels. However, the major drawback of these drugs is that they damage and/or kill the healthy cells during the treatment (Karnofsky 1968). Several antineoplastic drugs are potentially available and that has been used to treat all cancer types (Table 2.3), among all only a number of them are more effective for treatment of brain tumour (Bredel 2001).

Table 2.3 Anticancer drugs that have been used in the past decades

Chloroethylnitrosoureas (CENUs)	Antimetabolites	Protein kinase C (PKC) inhibitors
Carmustine (BNCU)	Methotrexate (MTX)	Tamoxifen
Lomustine (CCNU)	Edatrexate	Bryostatin
Nimustine (ACNU)	5-Fluorouracil (5-FU)	7-Hydroxystaurosporine (UCN-01)
Semustine (MeCCNU)	Cytosine arabinoside (Ara-C)	<i>Miscellaneous Agents:</i>
PCNU	6-Tioguanine (6-TG)	
HeCNU	5-Fluorocytosine (5-FC)	
NB-Fotemustine	Bromodeoxyuridine (BrdU)	
<i>Vinca alkaloids:</i>	Iododeoxyuridine (IUDR)	
Vincristine (VCR)	Methylprednisolone (MPred)	
Vinblastine (VBL)	<i>Alkylating agents:</i>	
<i>Epipodophyllotoxins:</i>	Temozolomide	
Etoposide (VP-16)	Procarbazine (PCB)	
Teniposide (VM-26)	Dacarbazine (DTIC)	
<i>Platinum compounds:</i>	Thiotepa	Lovastatin
Cisplatin (CDDP)	Chlorambucil	Methylglyoxal bisquanylhydrazide
Carboplatin	Busulfan	Benznidazole
<i>Phosphamides:</i>	Melphalan	Didemnin B
Cyclophosphamide (CPA)	Hydroxyurea (HU)	Acivicin
Ifosfamide	Gemcitabine	Boswellic acids
Mafosfamide	Spirohydantoin mustard (SHM)	Thalidomide
<i>Taxanes:</i>	<i>Antibiotics:</i>	Eflornithine
Paclitaxel	Doxorubicin	Piroxantrone
Docetaxel	Idarubicin	<i>Hexitol derivatives:</i>
	Epirubicin	
	Actinomycin D	
	Bleomycin (Bleo)	
	Aziridinybenzoquinon (AZQ)	Dibromodulcitol (DBD)
		Dianhydrogalactitol (DAG)

Drugs in bold are most commonly used for glioma. Temozolomide appears to be the current leading drug for high-grade gliomas. The efficacy of these anticancer drugs was determined to be only 20-25% in case of glioblastoma multiforme. Several factors apply for the poor prognosis, especially in the treatment of brain tumours. It originates at least in part from impermeability of the chemotherapeutic agents to BBB, inadequate drug exposure time, inadequate intracellular drug concentrations, and a number of other intracellular conditions (Bredel 2001). Paclitaxel is one of the chemotherapeutic agents that has been suggested as a therapeutic agent in treatment for Gliomas either alone or in combination with other approaches.

Paclitaxel is a natural product extracted from *Taxus yunnanensis* and a microtubule inhibitor causing mitotic arrest; however it has poor solubility and therefore has restricted effectiveness in treatment. Various strategies have been proposed to find alternative to PTX to be non-toxic and still have high drug loading capacity. PEG has been used into the excipient to increase solubility, control drug release profile and increase blood circulation. However, PTX has been used widely as a hydrophobic drug to evaluate for sequestration in nanoparticles (Bredel 2001). Generally, PTX is a white to off-white crystalline powder and is highly lipophilic. Various forms of Paclitaxel are shown in Figure 2.19.

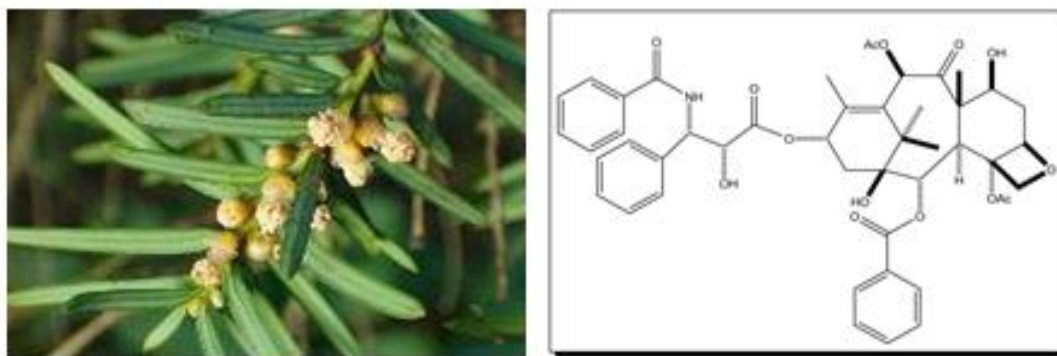


Figure 2.19 Various forms of PTX from natural and synthetic sources.

Paclitaxel treated cells have defects in mitotic spindle assembly, chromosome segregation, and cell division. It stabilizes the microtubule polymer and protects it from disassembly; its mechanism of action is shown in Figure 2.20.

Since it is known that GBM cells are sensitive to Paclitaxel *in vitro*, (Glantz, Choy et al. 1995) an enhanced delivery of Paclitaxel to the tumour cells in the CNS would be expected, to substantially help the chemotherapeutic prospect (Zhao, Liang et al. 2010).

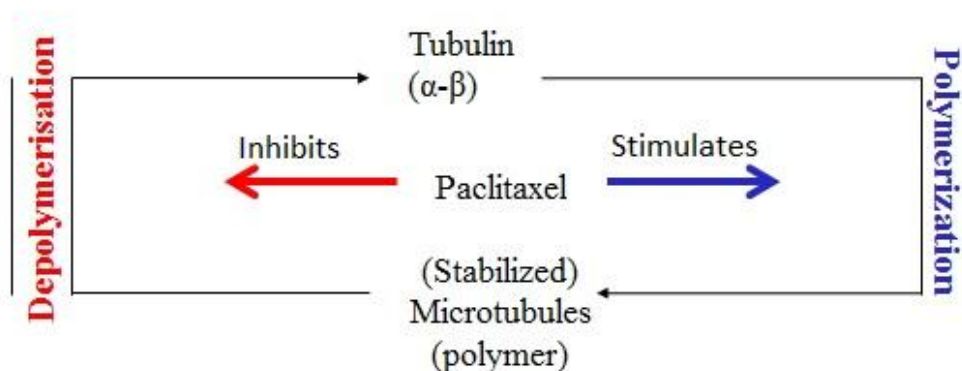


Figure 2.20 Paclitaxel mechanism of action

2.7.4 CNTs as carriers for cancer treatment

Advanced nanotechnology has been widely utilized in the treatment of cancer (Portney and Ozkan 2006; Nagahara, Ferrari et al. 2009; Zhao, Liang et al. 2010). Due to their unique physiochemical properties, CNTs have been exploited as multipurpose innovative carriers for cancer therapy (Lacerda, Bianco et al. 2006; Xu, Meng et al. 2010). The advantages of the utilization of CNTs in cancer therapy, specifically for brain tumours, is to improve the inadequate drug delivery, due to their properties that CNTs possess is to cross the BBB (Foldvari and Bagonluri 2008). Moreover, due to their distinct outer surface, wide range functional groups can be added to the tips and walls of CNTs making them amenable for functionalization with drug molecules (Chen, Chen et al. 2008; Chen and Schluesener 2010). A number of surfactants have been used to disperse and functionalize CNTs with PTX (Liu, Chen et al. 2008). The major advantage of non-covalent functionalization is that the electronic structure of the CNT's is preserved and the physical properties remain intact. CNT's have been used for cancer applications such lung, breast and brain tumours (Chen and Schluesener 2010).

Previous research has shown that, CNTs are retained in the lymph nodes for a longer period when compared to spherical nanocarriers such as liposomes and can treat lymph node cancers (Reddy, Rehor et al. 2006). Magnetic nanoparticles may be entrapped into the MWNTs complex using anticancer drug Cisplatin. These nanoparticles are then utilised to move the nanotubes using a magnetic field to the lymph nodes in mice injected subcutaneously and released over several days to inhibit breast and lung cancer (Misra, Acharya et al. 2010).

In another study, anticancer effects have been demonstrated to be dependent on the method used to entrap the drug in the CNTs, which highlighted the possible effects of preparation conditions on the therapeutic activity of therapeutic molecules associated with CNTs (Hampel, Kunze et al. 2008).

As can be seen in Figure 2.21 the structure morphology of CNTs may have various effects on cellular level whereby, the short CNTs can be engulfed and cleared out of the system through phagocytosis and long structures can have the adverse effect, of being toxic (Kostarelos 2008).

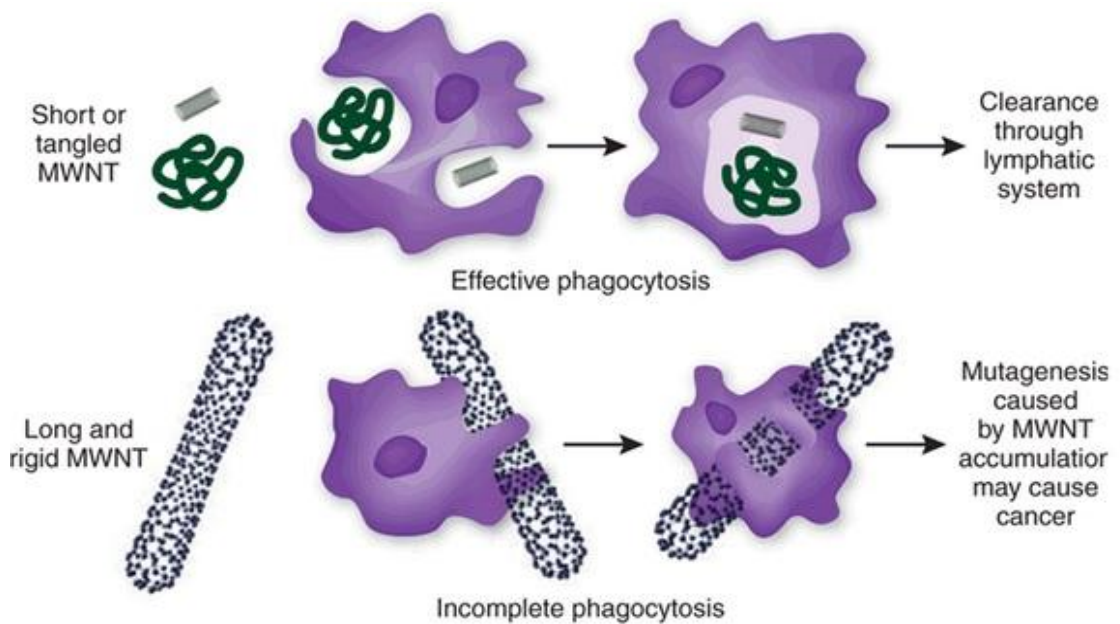


Figure 2.21 Phagocytosis process of long and short CNTs. Adapted from (Kostarelos 2008)

PEGylated nanotubes can prolong circulation and greatly enhance cellular uptake of the drug by the cancer cells (Liu, Chen et al. 2008). Anticancer activity was demonstrated by loading paclitaxel onto PEGylated SWNTs or MWNTs utilising HeLa cells and MCF-7 cancer cell lines (Lay, Liu et al. 2011). Using confocal microscopy hepatoma cell lines treated with PEGylated MWNTs accumulate in multidrug resistant cells with the same efficiency as in non-resistant cells (Cheng, Meziani et al. 2011). Liu et al interestingly reported that PEGylation of SWNTs prolongs blood circulation time of the associated anticancer molecule causing accumulation of the nanotubes in the dermal tissues of mice (Liu, Tao et al. 2011). Another remaining issue is that CNTs are cleared out of the body through the faeces (Liu, Cai et al. 2007).

2.8 Toxicity of CNTs

Whilst, CNTs have enormous potential in drug delivery, there are still concerns surrounding their toxicity, due to their small size and extremely high aspect ratio, they may still be a health hazard to living cells and the environment (Maurer-Jones, Bantz et al. 2009; Firme and Bandaru 2010). Generally, CNTs have been considered as being toxic due of their size although, the data are still fragmentary and subject to criticism.

Dumortier and co-workers prepared two types of functionalized CNTs, following the 1,3-dipolar cycloaddition reaction and the oxidation/amidation treatment, respectively and reported adverse effects that functionalized CNTs may have on cells of the immune system (Dumortier, Lacotte et al. 2006). Using *in vitro* studies, the uptake of functionalized CNTs were reported by B and T lymphocytes rapidly as well as macrophages without affecting the cell viability. Highly water soluble modified CNTs did not affect the functional activity of the immunoregulatory cells (Dumortier, Lacotte et al. 2006). Cui et al, examined the influence of single-walled CNTs (SWNTs) on human HEK293 kidney cells with the aim to explore SWNT biocompatibility (Cui, Tian et al. 2005) and found that SWNTs can inhibit cell proliferation and decrease the cell's ability to adhere in a dose and time-dependent manner. SWNT-treated HEK293 cells revealed acute and active responses to these nanotubes, such as the secretion of proteins, the aggregation of cells attached by SWNTs and the formation of subcellular nodular structures. Using cell cycle analysis they showed that 25 $\mu\text{g ml}^{-1}$ SWNTs could arrest cell division at stage G and induce apoptosis.

The potential pulmonary toxicity of SWNTs in revealed chronic inhalation and/or exposure to SWNTs could be a serious occupational health hazard (Lam, James et al.

2004). Histopathological studies on lungs treated for periods of 7 and 90 days after a single intratracheal instillation of SWNTs dispersion, showed that nanotubes induced epithelial granulomas and interstitial inflammation at day 7, which persist and developed to peribronchial inflammation and necrosis around day 90. Pharyngeal aspiration of SWNTs elicited unusual pulmonary effects in C57BL/6 mice, which resulted in acute inflammation accompanied with signs of the early onset of progressive fibrosis and granulomas (Shvedova, Kisin et al. 2005).

2.9 Conclusions

This chapter highlighted several of advances that have been made in the utilization of CNTs, their properties and applications in cancer therapy. However, there are still tremendous opportunities and significant challenges to be unravelled. The challenges integrating CNTs with biomolecules are still being addressed.

The small size and electronic properties of CNTs allow technologies to be developed that were otherwise not possible. Various of researchers have demonstrated that CNTs have the ability to enter cell membranes and were found to be non-toxic as these particles clear out from the body through faeces in the past years. The needle-like shape of the CNTs enables them to perforate cellular membranes and transport therapeutic molecules to the cellular components. This process is thought to take place via endocytosis. CNTs have exclusive properties that make them highly relevant in the medical field such as their ability to absorb pathogenic microorganisms and conduct heat. Furthermore, the results of the aforementioned studies are often inconclusive or contradictory. The data that has been presented in this review indicates that unrefined CNT possess some degree of toxicity mainly due to the transition metal catalysts presence. Exposures to pristine CNTs have been shown to elicit minimal cytotoxicity at higher concentrations (both *in vivo* and *in vitro*), whilst functionalized CNTs which enhance drug delivery without toxic effects.

Hence, CNTs have been introduced to drug delivery research for a limited number of years and therefore extensive investigation and maximization is expected in the forthcoming years to explore their potential. Furthermore, no pre-clinical therapeutic effectiveness data is available yet for any specific disease with CNTs conjugated drug complexes. Radically different delivery system specifications are necessary for successful intercellular delivery and guaranteed biological activity of CNTs.

CHAPTER 3

MATERIALS, METHODS &

TECHNIQUES

*“Curiosity is one of the permanent and certain characteristics of a
vigorous mind.”*

(Samuel Johnson, 1709-1784)

CHAPTER 3

3.1 Materials and methods

This chapter describes the materials and methods that have been used in this study. Initially, the purchased SWNTs and MWNTs were characterized using a range of techniques to demonstrate their size, morphology and structure. The materials were then functionalized to improve their solubility in aqueous solvents and increase their biocompatibility. Paclitaxel, a widely used anti-cancer drug, was attached to the functionalized CNTs. Glioma cell lines were employed for *in vitro* studies and subsequently, the CNTs complexes were investigated for cytotoxicity studies using MTT assay.

3.2 Materials

Materials that have been used for this study are described in the following chapter.

3.2.1 Carbon Nanotubes

SWNTs and MWNTs with purity of more than 98% were purchased from Chengdu Ltd with SWNT diameter in the range of 1-5 nm and lengths between 100-500 nm. Purchased MWNTs exhibited outer diameters in the range of 10-20 nm and were 500-1000 nm long. SWNTs and MWNTs were both produced by chemical vapour deposition (CVD).

3.2.2 Surfactant and Paclitaxel

Pluronic 127 (PF127), polyethylene glycol 400 (PEG400) and Paclitaxel (Taxol®) were purchased from Sigma Aldrich, UK and were prepared according to the material solubility. Paclitaxel was stored at -20 °C as received. The Paclitaxel stock solution was stored between 2-8 °C as it is not stable in aqueous solution and samples were discarded after 1 day.

3.2.3 Cell and MTT assay

SVGp12 normal astrocytes cells and U87-MG Grade IV glioblastoma cells were purchased from European Collection of Cell cultures (ECACC). The MTT assay kit suitable for *in vitro* cytotoxicity was purchased from Sigma, Aldrich, UK as well.

3.3 Characterization

Characterization has been carried out for all utilized materials in this study, including SWNTs, MWNTs and *f*-CNTs. SEM and TEM were used to study the size and morphology. Raman spectroscopy was implemented to determine various characteristics of the CNTs. Zetasizer implemented to determine the zeta potential. TEM allowed the observation of the internal structure of samples, visualise the structure, demonstrate the number of walls and diameter size of the nanotubes.

3.3.1 Scanning Electron Microscopy

SEM is utilized to determine the morphology of fine structures of materials and nanoparticles, including CNTs (Figure 3.1). Samples were obtained with Field Emission High Resolution Scanning Electron Microscopy, Hitachi S-4100 and Hitachi, SU 70. The resolution of secondary electron image of the microscope was 1.0 nm (at an accelerating voltage of 15 kV) or 2.5 nm at accelerating voltage of 1 kV. Accelerating voltage varied from 0.5 to 30 kV for low magnification from 25 to 19 000 times, and higher magnifications from 100 to 800 000 times in the high-resolution mode. The cold field emission Schottky Emitter gun was used as a source of electrons.

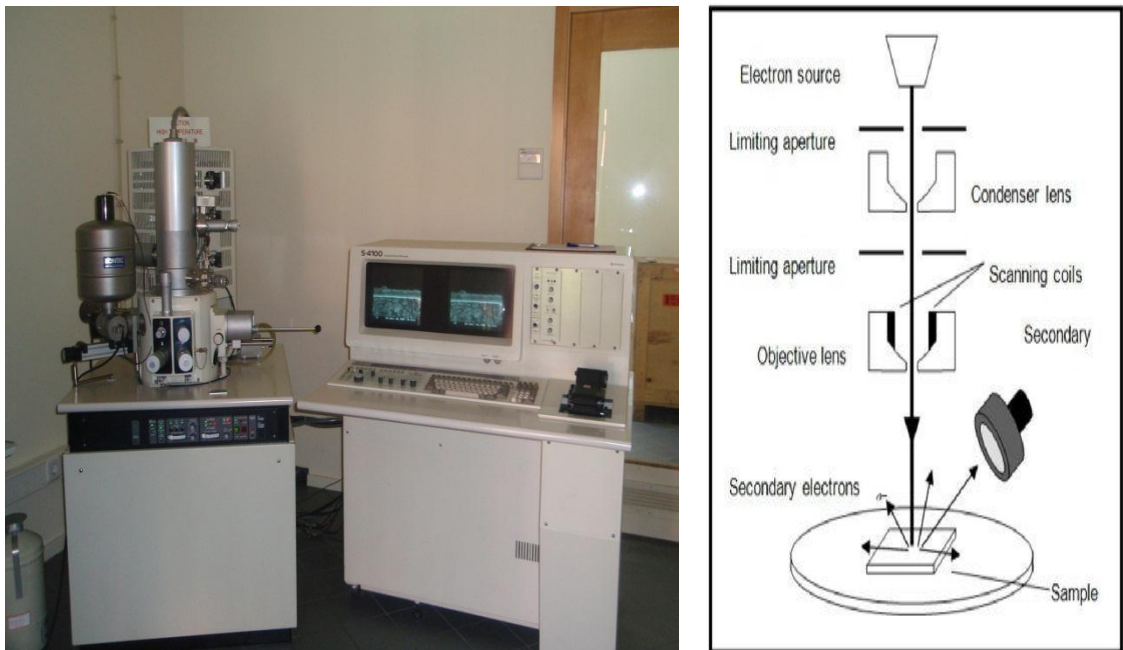


Figure 3.1 Picture and schematic view of Scanning Electronic Microscopy

3.3.2 Transmission Electronic Microscopy

TEM forms major analysis method in a range of scientific fields (Jinschek and Helveg 2012). In TEM, an electron beam from the electron gun passes through the electromagnetic condenser lens through the sample to an objective lens and then down to the phosphor screen or charge-coupled device (CCD) camera (Figure 3.2)

In transmission electron microscope a beam of electrons is transmitted through an ultra-thin sample. The condenser lens controls the size and intensity of the beam hitting the sample and the objective lens controls the magnification. TEM shows internal structures of specimen with magnification up to one million times revealing the structures in atomic resolution. Morphological and size examinations of freshly prepared blank, CNTs were done using negative staining solution. A droplet of the spontaneously formed CNTs samples, were placed onto a carbon-coated copper grid (400 mesh) for about 3 minutes in order to reach absorption equilibrium. The droplet was then wicked to dryness using pieces of filter paper before leaving the grid for another 1 minute.

Next, a droplet of the negative stain solution (2% Uranyl Acetate) was added to the surface of the grid. After 1 minute, the copper mesh grid was dried using pieces of filter paper and kept in a filter paper lined petri dish. The size, morphology and lamellarity of carbon nanotube samples were then viewed on Philips CM12 transmission electron microscope and photographed at an accelerating voltage of 8 kV.

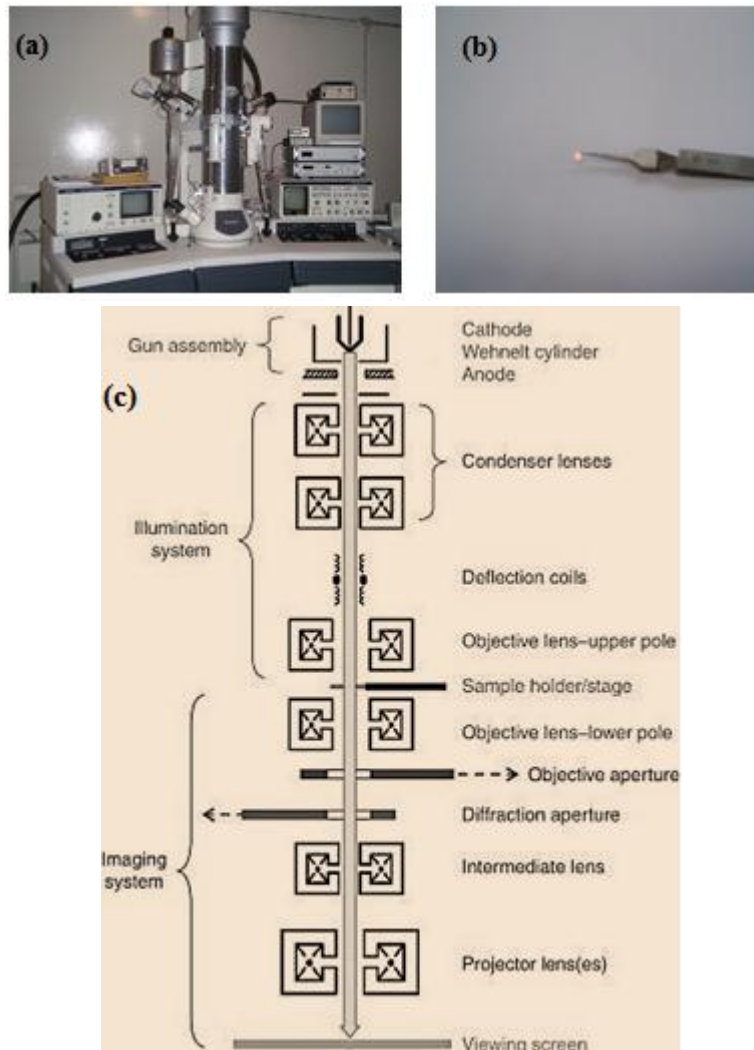


Figure 3.2 (a) Transmission Electronic Microscopy (b) TEM grid where the sample is to be viewed on (c) Schematic view of TEM adapted from (Marassi and Nobili 2009)

3.3.3 Raman Spectroscopy

Raman spectroscopy principle is based on inelastic light scattering (Figure 3.3) complemented by the shift in photon frequency due to excitation or deactivation of molecular vibrations in which either the photon loses a proportion of energy or gains energy. The G-Line is a feature of the graphite layer which corresponds to the tangential vibration of the carbon atoms and second-order related harmonic G'-band. The D-band sets the sign of the typical defects on the graphite structures. Comparison of the two peak intensities gives a measure of the quality of the CNTs. The third feature of Raman spectroscopy is the Radial Breathing Mode (RBM) which is sensitive to the diameter of SWNT (Figure 3.4).

Raman spectra gives qualitative and quantitative information including; diameter, electronic structure (semi-conducting, metallic), purity, crystallinity and allows for the distinction between metallic and semiconducting components.

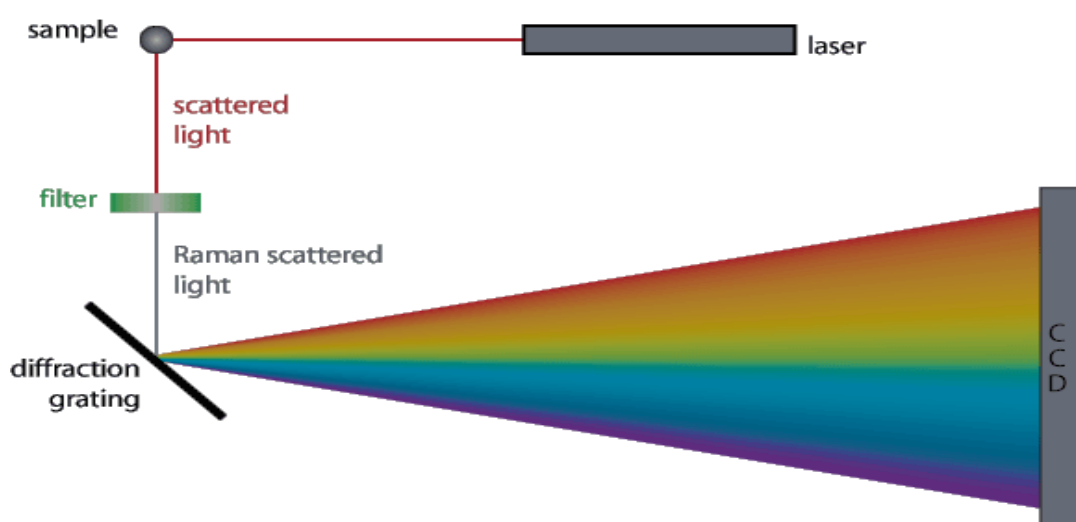


Figure 3.3 Schematic overview of Raman scattering

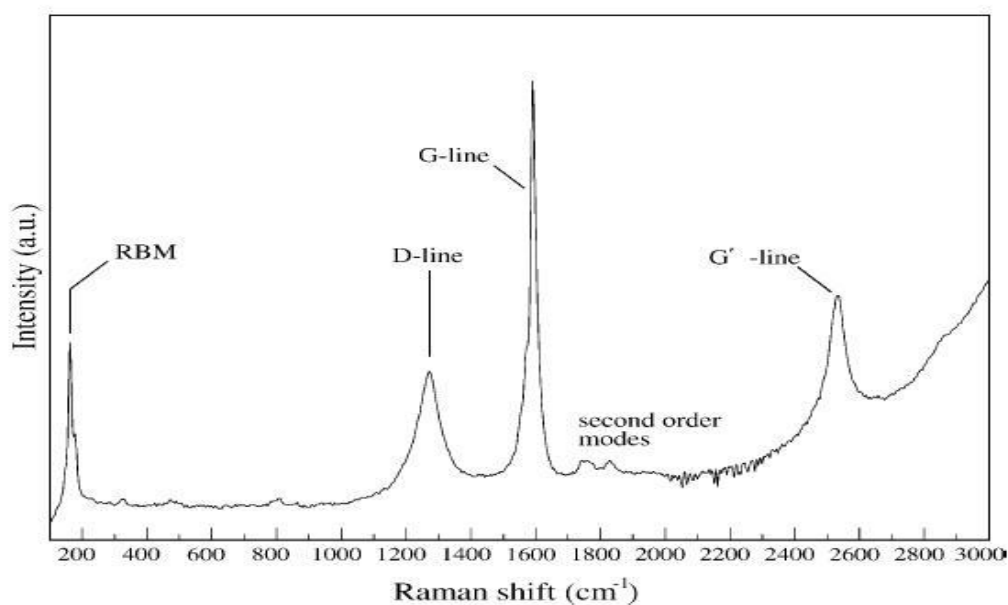


Figure 3.4 Raman Spectra showing the characteristic features of CNTs (Belin and Epron 2005)

Two different wavelength laser excitations were used to characterize the materials and are mentioned in the forthcoming paragraph;

UV set up; Raman spectra were obtained at room temperature in back scattering configuration with a Jobin-Yvon LabRam HR equipped with a Multichannel air cooled (-70 °C) CCD detector. An objective of x40 magnification was used to focus the surface of sample pellet excited with the 325 nm HeCd laser line.

Visible set up; Spectra were recorded on a triple subtractive Jobin Yvon T64000 Raman spectrometer equipped with a liquid-nitrogen-cooled charge-coupled device (CCD) detector. The emission line at 488 nm from the Ar + ion laser was focused on the sample under the microscope. The time of acquisition was adjusted according to the intensity of the Raman scattering. The wavenumber values reported from the spectra are accurate to within 1 cm⁻¹.

3.3.4 ζ -potential measurements

Zeta potential (i.e, surface charge) of CNTs were analysed by injecting the sample into the plugs and voltage was applied through two gold plated electrodes (

Figure 3.5). The particle movement under the influence of an applied field was exploited to determine the zeta potential or effective charge of the particle on the basis of their electrophoretic mobility. This shows the amount of light scattered for the various contributions from the different charge. This process was established through the Zetasizer (Zetasizer nano zs, Malvern) that is equipped with the Zeta potential option.

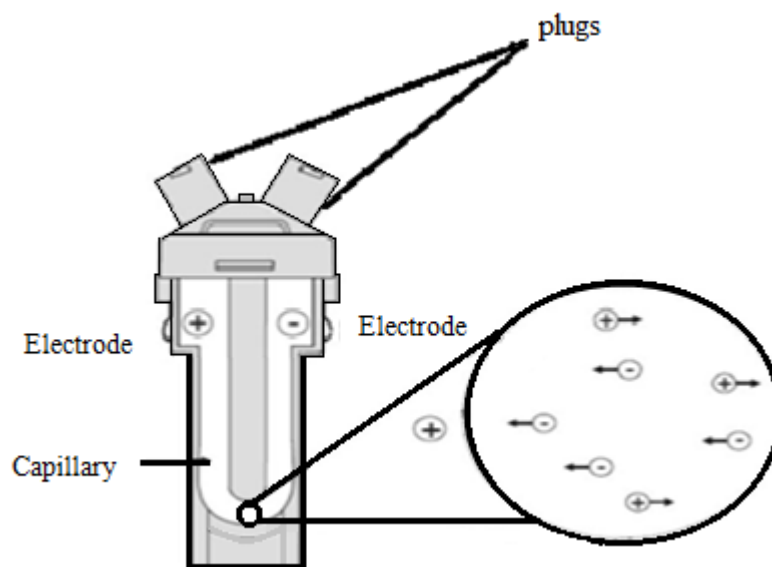


Figure 3.5 Schematic overview of zeta potential cuvette that has been used for measurements

3.4 Non-covalent functionalization

Functionalization is a process where modification and coating of materials and functional groups can be added onto the CNTs surface. This process increases their solubility, dispersion in aqueous solutions and biocompatibility for biomedical applications. A vast range of functional groups may be added to the tips and walls of CNTs (Klumpp, Kostarelos et al. 2006).

Two methods are commonly implemented to functionalize CNTs; these are covalent (Tagmatarchis and Prato 2004) and non-covalent bonding routes (Lay, Liu et al. 2011). Non-covalent functionalization holds the advantage that the structure of the CNTs is preserved with their physical properties remaining intact. Covalent functionalization also improves the solubility, however it has the disadvantage of altering the physical properties of CNTs. Hence non-covalent procedures were preferred for this study. There are a number of advantages and disadvantages to functionalization, these include the following:

- The solubility in aqueous solvents is increased
- The stability of the CNTs is improved considerably
- Small drug molecules can be attached via chemical bonding onto the walls, the tips or they can be encapsulated
- The cell toxicity is reduced significantly

Two surfactants including PEG400 and PF127 were chosen for this study and are described in the following sections.

3.4.1 Functionalization of CNTs with Pluronic

PF127 has been employed to functionalize the CNTs and are commonly used in biomedical applications due to their low toxicity and non-irritating behaviour. A multitude of methods have been employed to achieve these objectives (discussed in the previous chapters). For non-ionic polymers the dispersion is achieved due to hydrophilic counterparts.

PF127 is a non-ionic triblock copolymer (Figure 3.6) with an additional property in aqueous solution: at or above room temperature, a solution of PF127 will convert from its liquid state to a non- fluid hydrogel. PF127 has already demonstrated significant ability to preserve polypeptide bioactivity *in vitro* and *in vivo*. It is also deemed one of the most efficient and non-destructive surfactant amongst various compounds and highly biocompatible when used in low concentrations. With non-ionic surfactant CNT suspensions solubility appears to be due the size of the hydrophilic group. Higher molecular weights suspend a greater amount of nanotube due to the enhanced steric stabilization with longer chain polymeric groups being present (Klumpp, Kostarelos et al. 2006).

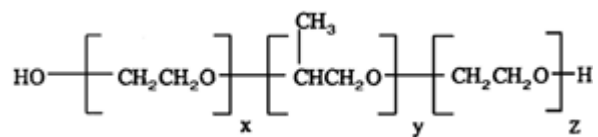


Figure 3.6 Chemical formula of Pluronic F127 with hydrophilic chains of polyoxyethylene, hydrophobic chain of polyoxypropylene and Hydrophilic chains of polyoxyethylene

I. PF127- suspension

PF127 was dissolved in a weight ratio of 1% wt in deionised water (DI) at room temperature.

II. PF127 – CNT

The appropriate amounts of 1:5 and 1:1 of SWNTs and MWNTs were added to the PF127 suspension whilst on bath sonication and left for 1 hour at high power. The suspension was then centrifuged to separate the *f*-CNT from the unreacted PF127-CNT at 122,000 g for 1 hour. The supernatant was used for characterization and sediment was re-suspend for Paclitaxel drug loading.

Table 3.1 Concentrations of CNTs in PF127

Functionalization of SWNT and MWNT-Concentration 1:1 with PF127	
SWNT 10 mg (SWNT-PF127)	9 ml
MWNT 10 mg (MWNT-PF127)	9 ml
Functionalization of SWNT and MWNT-Concentration 1:5 with PF127	
SWNT 1 mg (SWNT-PF127)	4 ml
MWNT 1 mg (MWNT-PF127)	4 ml

3.4.2 Functionalization of CNTs with PEG400

The process where CNTs are non-covalently functionalized with PEG is called PEGylation. This involves the use of PEG functional groups onto the CNTs to alter solubility (Figure 3.7). Polyethylene glycols are addition polymers of ethylene oxide and water, identified by a number which approximates their corresponding molecular weight. In order to prolong the circulation and minimize the opsonisation of CNTs, this is necessary for successful drug targeting. This can be achieved by coating of the CNTs with hydrophilic polymers/surfactants. Using a branched PEG for functionalization of CNTs enables more functional amine groups to be attached at the PEG terminal for more efficient drug conjugation.

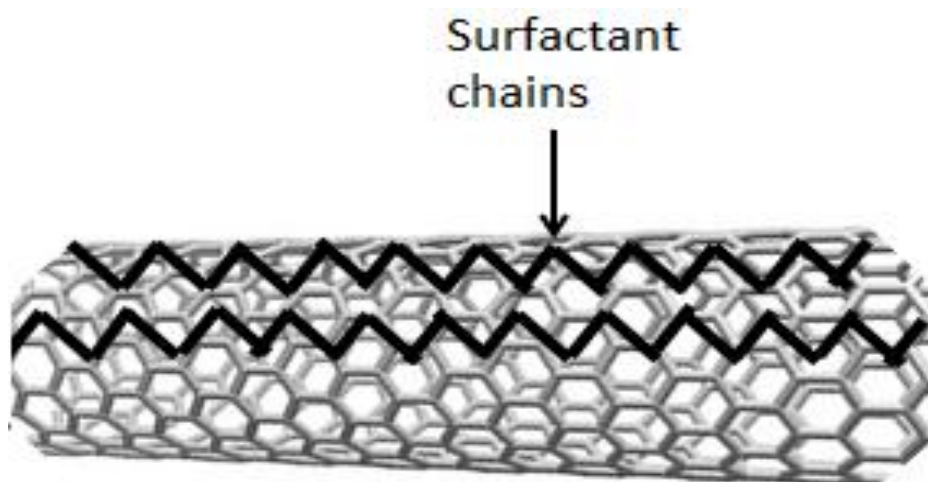


Figure 3.7 Non-covalent functionalization; surfactant chains onto the CNT

I. Polyethylene glycol solution

PEG400 was mixed with 1% w/w DI through gentle shaking.

II. PEGylation

Ratios were weighed and then transferred into 20 ml vial containing PEG400-DI. SWNTs and MWNTs were added to the solution and then ultrasonicated for approximately four hours until clear black suspension was obtained. For the *f*-CNT separation, the suspension obtained was centrifuged at 150 000 g for 1 hour and the supernatant was filtered with a molecular weight cut-off of 100 kDa (Millipore). This was followed by adding the suspension and then washed with DI six times to completely remove the unreacted PEG.

Table 3.2 Concentrations of CNTs in PEG400

Functionalization of SWNT and MWNT- Concentration 1:1 with PEG400	
SWNT 10 mg (SWNT-PEG)	9 ml
MWNT 10 mg (MWNT-PEG)	9 ml
Functionalization of SWNT and MWNT- Concentration 1:5 with PEG400	
SWNT 1 mg (SWNT-PEG)	4 ml
MWNT 1 mg (MWNT-PEG)	4 ml

3.4.3 Paclitaxel

Paclitaxel (PTX) stock solution was prepared, followed by mixing the appropriate concentration with the CNTs formulation (Table 3.3).

I. Stock solution

25 mg of Paclitaxel was weighed in a 100 ml volumetric flask which was then filled with absolute ethanol to make up the volume to 100 ml. The resultant solution was stirred until the paclitaxel was completely dissolved in the ethanol. A calibration curve of Paclitaxel was produced by making a serial dilution of 50-250 $\mu\text{g/ml}$ using the equation: $V_1 C_1 = V_2 C_2$ from the stock solution and additional ethanol that was required.

II. PTX-*f*-CNT method

Each functionalized and pristine (p) (SWNT – MWNT) sample reacted with the required concentration of the modified PTX. PTX was weighted and modified according to concentration in glass vials and appropriate amounts of 10 ml for *f*-CNTs and 10mg of p-SWNT and p-MWNT were slowly added to each vial. After six hour reaction of ultrasonication, the resulting surfactant-CNT-PTX was purified to remove unconjugated PTX by filtration through 5 kDa MWCO filters and extensive washing.

Table 3.3 Dilutions of stock solution for calibration curve

Concentration $\mu\text{g/ml}$	Stock amount	Dilution with ethanol
50	20 μl	80 μl
75	30 μl	70 μl
100	40 μl	60 μl
125	50 μl	50 μl
150	60 μl	40 μl
175	70 μl	30 μl
200	80 μl	20 μl
225	90 μl	10 μl
250	1 ml	0 μl

3.5 Techniques

The following techniques have been implemented for the purposes of functionalization, characterization and entrapment efficiency of PTX into CNT formulations.

3.5.1 Probe-and Ultrasonication

Sonication is one of the most commonly used methods, where a transducer is used to irradiate a liquid with a high pressure sound field with the resultant growth of cavities which implode violently with a localised release of energy. In a bath-type sonicator the sound field is almost uniform, with homogenous treatment of the suspension. Sonication has been used to disperse CNTs to in the aqueous solvents to improve efficiency and yield.

3.5.2 Centrifugation technique

Centrifuge technique is based upon the principle that particles of different density respond differently to gravity. With respect to this work low speed centrifugation has been used to separate amorphous carbon leaving behind the CNTs. CNTs sediment to the bottom of the centrifuge tube, whilst single nanotubes remain in the upper part. Sonication in aqueous solutions of surfactant followed by ultra-centrifuging is used to separate the individual CNTs.

3.5.3 High performance liquid chromatography – loading efficacy of PTX

Prior to the injection of the drug solution, the column was equilibrated for a minimum of 30 minutes with the mobile phase flowing through the system. High performance liquid chromatography (HPLC) is a chromatographic separation technique. In this study, the separation was achieved by HC-C18 column (250 × 4.6 mm, 4 μm, C18,

Agilent Technologies) at 35 °C. The CNT-PTX was dissolved in methanol, HPLC grade and sonicated for 10 minutes, thereafter centrifuged at 1000 g for 5 minutes. Once centrifuged, the supernatant was used for HPLC analysis (HPLC1200 instrument, Agilent, UK).

Mobile phase: A = Water, B = acetonitrile; Injection volume: 5 µL; Temp: 25 °C; Flow rate: 1.0 ml/minutes; Gradient: at 0 minutes 50% B, at 10 minutes 90% B, Column wash: at 12 minutes 50% B; Stop time: 12 minutes; Post time: 5 minutes (Table 3.4).

Table 3.4 HPLC gradient phase used for Paclitaxel

Time in minutes	A% (HPLC water)	B% (Acetonitrile)
0	50	50
10	10	90
10.01	50	50
17	50	50

3.6 Cell culture: Materials and Methods

Cell culture procedures were conducted under aseptic conditions. Also all materials were sterilised via autoclaving prior to use. Step and procedures were carried out under a laminar flow hood.

3.6.1 Glioma cell lines tissue culture to study glioma growth

The growth of tissue or a cell on a surface e.g. glass or plastic, separated from the organism or *in vitro* growth in nutrient medium is commonly refers to the culture of animal cells and tissues. This is ordinarily facilitated via use of growth media or semisolid growth media such as broth or agar. Typically, there are two types of cell culture which employ similar practical sterile techniques (Mather and Roberts 1998).

- a. Primary cell culture** - Culture consists of mixed population of cell types and the growth derived from the living organisms. Commonly, some of the cells may survive without proliferation and will therefore be lost in the increasing population of those which are able to multiply in *in vitro*.
- b. Established cell line** - These cells are derived from a primary culture which can be sub-cultured in the medium indefinitely.

3.6.2 Media importance in tissue culture

Medium is essential to support the growth of the cells in tissue culture. A sample of tissue is either spread onto or added to a culture biological medium (e.g. blood serum) of either synthetic or mixed origin, having the appropriate nutrients, temperature and pH for the cells incubation. The media used for Glioma cell culture is Dulbecco's Modified Eagle Medium (DMEM) and Eagle's Minimal Essential Medium (EMEM). Cultured

materials must be incubated as close to the normal tissue environment. Sterile conditions are a requirement to maintain and to prevent contamination.

3.6.3 Eagle's Minimal Essential Medium and Dulbecco's Modified Eagle Medium used for the proliferation of cells

Development of Eagle's Minimum Essential Medium (EMEM), by Harry Eagle is one of the most widely used of all synthetic cell culture media for the cultivation of mammalian cells (Eagle 1955). EMEM has been broadly used for growing a wide variety of cells in mono-layers. It has to be stored at 15-30 °C. EMEM formulation may contain Earle's salts and a group of amino acids that are generally referred to as essential amino acids and non-essential amino acid (Table 3.5). There are twelve amino acids that are essential and can be used for the development of medium. The non-essential amino acids are optional and can be added to supplement the growth of cells.

In their absence, irregularity in cell growth due to malnourishment of cells would cause an incorrect growth.

Table 3.5 List of essential and non-essential amino acids in EMEM.

Essential Amino acids	Non- Essential amino acids
L-arginine	Alanine
L-cystine	Aspartic Acid
L-glutamine	Asparagine
L-histidine	Cysteine
,L-isoleucine	Cystine
L-leucine	Glutamine
L-methionine	Glutathione
L-phenylalanine	Glycine
L-threonine	Proline
L-tryptophan	Serine
L-tyrosine	Threonine
L-valine	Taurine

EMEM contains higher concentrations of amino acids so the medium is more similar to the protein composition of mammalian cells. EMEM also requires FBS supplementation for providing growth promoting factor. Moreover, EMEM requires Sodium Pyruvate as a supplement for the growth of cells as Pyruvate is an intermediary organic acid metabolite in glycolysis and the first of the Embden Myerhoff pathway that can pass readily into or out of the cell. Thus, its addition to tissue culture medium provides both an energy source and a carbon skeleton for anabolic processes. Its addition may also help in maintaining certain specialized cells in cloning and may be necessary when the serum concentration is reduced in the medium (Culture of Animal Cells).

A variation of this EMEM is called Dulbecco's Modified Eagle Medium (DMEM) (Dulbecco and Freeman 1959), this contains up to four times more vitamins, glucose and amino acids which are present in the original formula but it does not contain any proteins or growth promoting agents. Therefore, it requires supplementation to be a complete medium. Fetal bovine serum (FBS) is the most widely used growth supplement for cell culture media due of its high content of embryonic growth promoting factors and is usually supplemented to the media in concentration ranging from 5-10%. DMEM requires artificial levels of CO₂ to maintain the required pH and therefore carbon dioxide (CO₂) levels around 5-10% may be optimal for cell culture. Additionally, it contains iron and phenol red. DMEM is suitable for most types of cells, including human, monkey, hamster, rat, mouse, fish and chicken cell lines (Ham and McKeehan 1979).

3.7 Equipment and materials used for cell culture

The materials and equipment that has been used for cell culture are shown in Table 3.6.

Table 3.6 Materials and equipment used for cell culture

Materials
Cryovials, “Mr. Frosty” freezing container and liquid nitrogen
DMSO (Sigma Aldrich, UK)
Glioma cell lines (U87-MG, SVGp12) (ECACC, UK)
Equipment
New Brunswick Scientific (CO ₂ 81R)- water jacketed CO ₂ incubator,
Water bath
Laminar flow hood
Inverted phase contrast microscopes
Weighing balance
Tecan plate reader (Manufacturer: Tecan Austria GmbH, 2004 model)
Refrigerator, freezer (- 20 °C) and deep freezer (-80 °C)
Centrifuge machine
Electrical aspirator

Equipment (continued from previous page)
Vortex mixture
2, 20, 200 and 1000 μ l pipettes and pipette tips and motorized pipette controller
75 cm ² /25 cm ² culture flasks and 5 ml volumetric flask
Sterile forceps
5 and 10 ml disposable plastic pipettes and 15 ml and 50 ml centrifuge tubes
0.22 μ m and 0.44 μ m sterile filters (Fisher Scientific, UK)
Syringes (Fisher Scientific, UK)
Universal bottles, glass funnel and sterile spatula
Clear bottom white 96 well plates (Grenier, UK).

3.7.1 Chemicals and Reagents in cell culture

Chemicals and reagents used for cell culture are described in this section.

- Ethanol and Methanol (Fisher Scientific, UK)
- Phosphate Buffered Saline-2 tablets was dissolved in 400 ml of water and stored the solution at 4 °C (Sigma, Aldrich, UK)
- MTT assay kit (Sigma Aldrich, UK)

3.7.2 Composition of medium and supplements required for cell culture

The essential medium and supplement was DMEM and MEM (Minimal Essential Medium), Fetal bovine serum (FBS), trypsin, L-Glutamine, non-Essential Amino Acid (NEAA) and sodium pyruvate (All from Lonza, UK).

The composition requirement for U87-MG was Minimal Essential Medium (MEM-500 ml), 10% Fetal bovine serum (FBS-50 ml), 2 mM L-glutamine (5 ml), 1% Non-Essential Amino Acids (NEAA- 5 ml), 1 mM sodium Pyruvate (5 ml) and for SVGP12 was Eagle's Minimal Essential Medium (EMEM-500 ml) and 10% Foetal bovine serum (FBS-50 ml).

3.8 Cell culture passaging

Prior to experimentation, air removal was carried out for 10 minutes in a laminar flow hood inside the cabinet. Medium, trypsin (sterile) and PBS were removed from the fridge freezer 4 °C and then placed in a water bath at 37 °C for 30 minutes to allow equilibration.

3.8.1 Cell culture and passaging of the Primary Glial Cells (U87-MG and SVGP12)

Cells were encouraged to grow until they were 70-80% confluent, medium was then removed from the cultured flask and was washed with Phosphate Buffer Solution (PBS) (5 ml for 75 cm² flask and 2 ml for 25 cm² flask) to remove the serum from the cells, to prevent inactivation of Trypsin serum. Trypsin solution (2 ml for 75 cm² flask and 1 ml for 25 cm² flask) was pipetted in the flask and incubated at 37 °C in an atmosphere of 5% CO₂ in air for 4-5 minutes until the cells started to detach, this was observed at intervals under an inverted microscope. The cells were left in trypsin for an appropriate length of time to avoid damage. Complete growth medium (2 ml) was then added to the flask to inactivate the trypsin and the cells were pipetted up and down to break down any large cell aggregates. The cell suspension was removed from the flask into a 15 ml centrifuge tube and centrifuged at 1000 r.p.m for 5 minutes. After centrifugation, the supernatant was removed and the cells were pelleted at the bottom of the centrifuge tube. Density dependent cell pellet, a volume of 1 ml to 2 ml of fresh medium was added and properly suspended in the centrifuge tube. Subsequently, the cells were incubated at 37 °C in an atmosphere of 5% CO₂ in air. Thereafter, the cells were examined under an inverted contrast microscope to note their general health and confluences.

3.8.2 Haemocytometer and cell quantification

A volume of 20 μl of cell suspension and 80 μl of trypan blue were pipetted into a micro centrifuge tube and mixed. The cover slip was placed over the chambers of the haemocytometer as shown in Figure 3.8.

A volume of 20 μl of cell suspension was pipetted against each side of the cover slip to facilitate the spreading of the suspension into each chamber. The haemocytometer was placed onto the stage of an inverted phase contrast microscope and focused on the centre 25 squares of one chamber. The number of cells in these squares were then counted. These above steps were repeated for the other chambers.

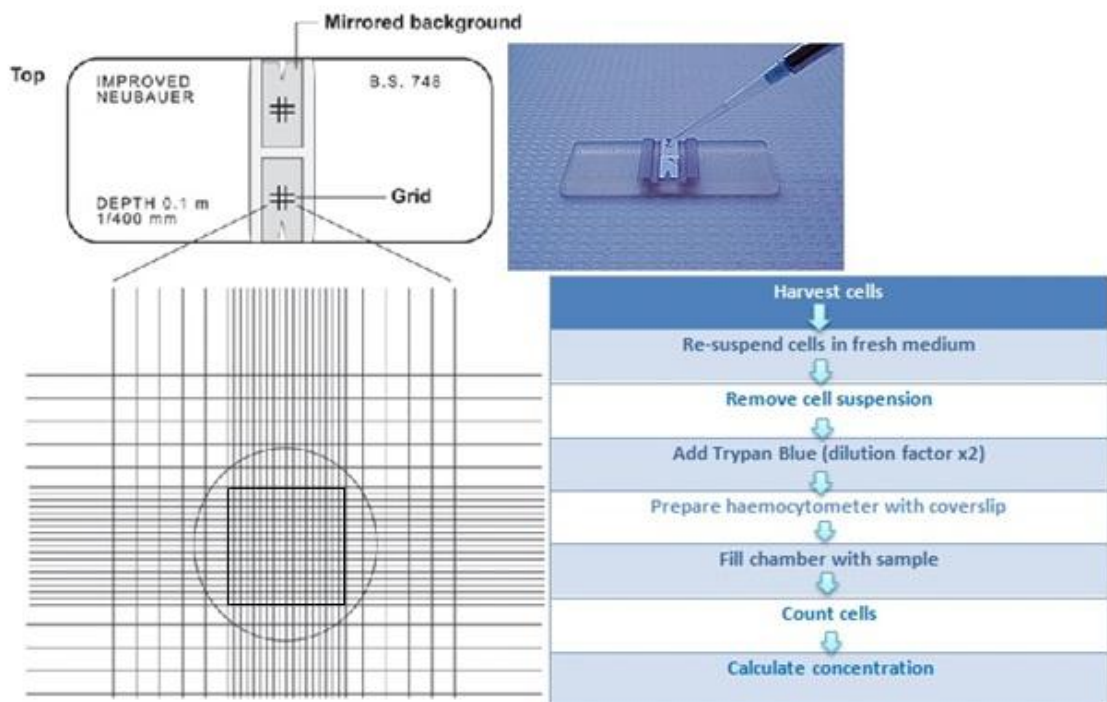


Figure 3.8 Neubauer Haemocytometer: each large square gives an area of 1 mm² (1 mm x 1 mm) with a depth of 0.1 mm

The average number of cells in the centre grid (1 mm²) of each chamber was calculated. This number was multiplied by 10⁵ to obtain the number of cells per 1 ml of suspension. The total number of cells was calculated by multiplying the number of cells per 1 ml by the total volume of the cell suspension. Cell numbers were calculated according to equation in 3.1.

$$\frac{\text{Total number of cells in 9squares}}{\text{Total number of squares counted}} \times \text{Dilutions} \times (1 \times 10^5) = \text{Cell number/ml}$$

Equation 3.1 Cell number equation to calculate cells/ml

3.8.3 Cryopreservation of cells

Cryopreservation is where a cell suspension is obtained during passaging and cells are allowed to be stored for longer periods in liquid Nitrogen. In this process the cells were supplemented with a cryoprotactant which prevents the cells from rupture due to formation of ice crystals are slowly frozen down in culture medium. The most important principle involves freezing the cells between a range of 1-3 °C and then defrosting quickly in a 37 °C water bath. Dimethyl sulphoxide (DMSO) is one of the most commonly used cryoprotectant. The frozen cell suspension contained of 10% DMSO, yield approximately more than 1 million cells. The frozen vial container was in a bath of Isopropanol named “Mr. Frosty”, which mediated a 1 °C/minute cooling of the cryovials in a – 80 °C freezer prior to storage at a temperature below -135 °C in either vapour or liquid phase nitrogen.

3.8.4 Growth curve

Demonstration of a standard growth curve for Glioma cell was established when the master flask was passaged and cell count was noted. Approximately, 0.23×10^6 (day-0) cells were taken and were seeded in five sub flasks. The sub flasks were incubated at 37 °C in 5% of CO₂ incubator. Each sub flask was passaged on regular basis from day-1 until day-6 and the cell count was noted down.

3.9 Plating of cell lines

Cell suspensions of U87-MG, and SVGp12 were acquired during passaging and were diluted in 1:10 ratio of cell suspension media. The amount of fresh medium and cell suspension were calculated based on cell counts. The dilutions were made till 200 µl suspensions consisted of 5000 cells. 200 µl of suspension was added into each well on 96 well plates. Thereafter, the plates were incubated at 37 °C for 24 hours in 5% CO₂ incubator. The media in the plates were removed on sterile tissue paper. To each well 100 µl of sample and 100 µl of media was added. PTX and/or CNTs solutions were added to the wells and incubated in 5% CO₂ incubator at 37 °C for another 24 hours and 48 hours. The suspension from the plates was again removed and all the plates were washed with 1 x PBS (7.4 pH). Plates were treated according to Figure 3.9 and the sample description is given in section 3.9.1.

To each well of the 96 well plates, a volume of 100 µl of sample and 100 µl of media was added, subsequently the plates were incubated at 37 °C for 24 and 48 hours in 5% CO₂ incubator. The suspension from the plates was again removed after 24 and 48 hours and all the plates were washed with 1 x PBS (7.4 pH) where MTT assay was ready to be performed.

3.9.1 Plating of cells with PTX-f -CNTs

Appropriate amounts of PTX was added to the S1 to S8, the suspensions were sonicated for 6 hours and centrifuged for 5 minutes at 1000 rpm. The samples were washed with PBS 7.4 pH and were put in the shaker for 6 hours. Then an amount of 100 µl of sample and 100 µl of media was added, subsequently the plates were incubated at 37 °C for 24

and 48 hours in 5% CO₂ incubator. After 24 and 48 hours the plates were removed for the incubator and suspension was aspirated from the plates and washed with 1x PBS.

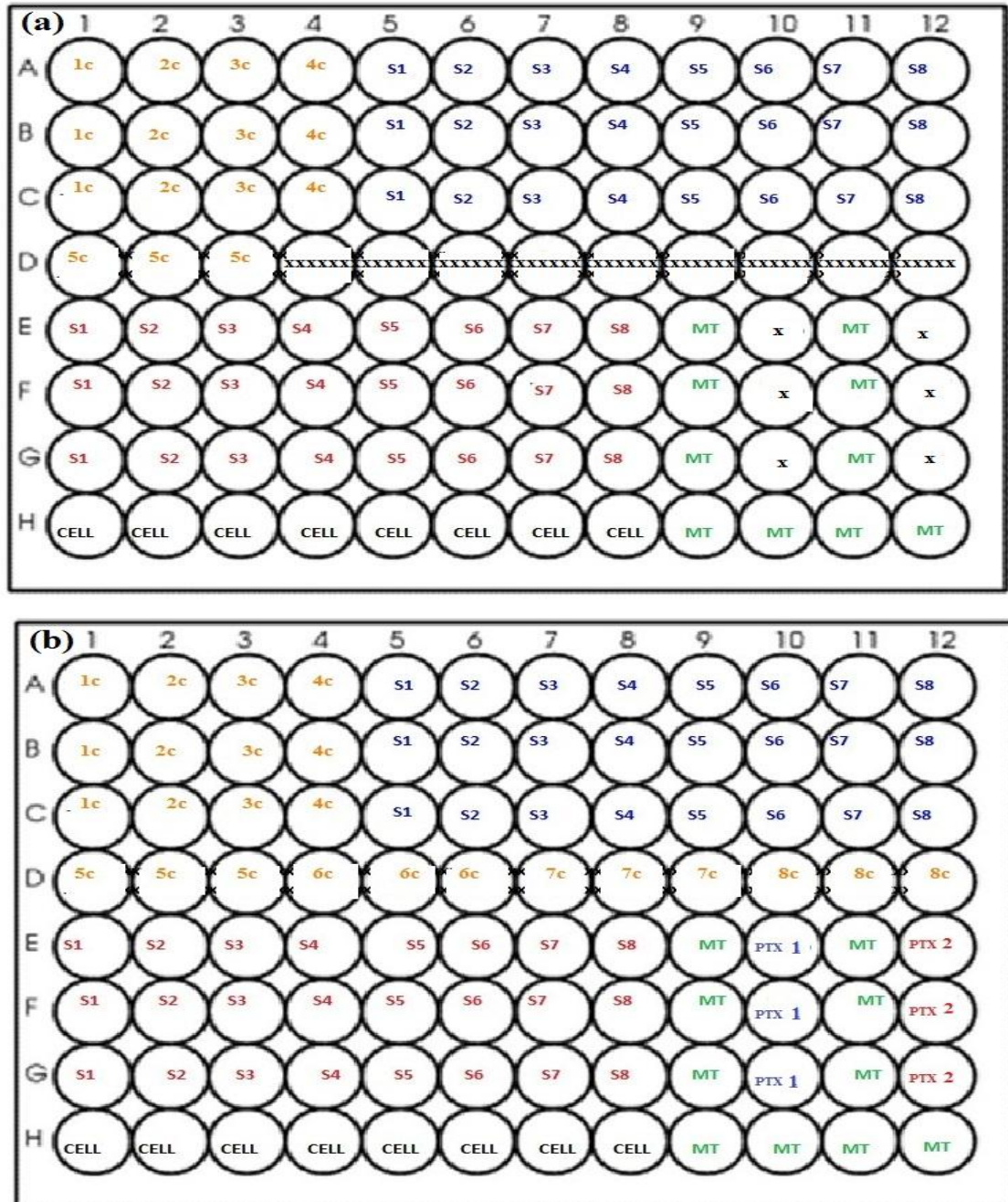


Figure 3.9 Schematic view of a 96 well plate with recorded samples (a) without PTX and (b) with PTX, where; C is CONTROL, S is SAMPLE, MT is no cells and CELL is untreated seeded cells

Table 3.7 Samples and controls description used for plating of SVGp12 and U87-MG on the 96 well plates with PTX

Control labels	Samples
1c	SWNT
2c	MWNT
3c	PEG 400
4c	PF127 1%
5c	SWNT-PTX 100
6c	SWNT-PTX 150
7c	SWNT-PTX 200
8c	SWNT-PTX 250
9c	PTX-100
10c	PTX-200
11c	MWNT-PTX 100
12c	MWNT-PTX 150
13c	MWNT -PTX 200
14c	MWNT-PTX 250
15c	PTX-150
16c	PTX-250

The capacity of each well is 200 μ l for each set of experiment; four 96 well plates were prepared for PTX of each concentration of 100-250 μ g/ml. The total quantity is shown in Table 3.8.

Table 3.8 Control labels have been described for each sample with and without PTX

Samples (with and without PTX) 1= 1:5 2= 1:1	Quantity needed for cell culture per 96 well plate (0.200 μl)
S1 = SWNT- PEG 1	2.4 ml
S2 = SWNT-PEG 2	2.4 ml
S3 = MWMT-PEG 1	2.4 ml
S4 = MWNT-PEG 2	2.4 ml
S5 = SWNT-PF127 1	2.4 ml
S6 = SWNT-PF127 2	2.4 ml
S7 = MWNT -PF127 1	2.4 ml
S8 = MWNT -PF127 2	2.4 ml

Plates were prepared, seeded and cytotoxicity was measured according to the following plate structures:

PLATE I

1. SGVp12 at 10^5 cells/well → Plates were seeded as per lay out → subsequent incubation for 24 hours
2. Controls were added and drugs at appropriate concentrations in medium
3. Cells were incubated for 24 hours as per standard tissue culture
4. Media were removed and cells were subsequently washed with PBS
5. 180 µl of media was added and MTT assay was performed by the addition of 20 µl and left for 2 hours
6. The assayed media was discarded and MTT was added in each well to dissolve the crystals of dye
7. Plates were read at 492 nm wavelength

PLATE II

1. SGVp12 at 10^5 cells/well → Plates were seeded as per lay out → subsequent incubation for 24 hours
2. Controls were added and drugs at appropriate concentrations in medium
3. Cells were incubated for 48 hours as per standard tissue culture
4. Media were removed and cells were subsequently washed with PBS
5. MTT assay was performed by the addition of 20 µl and left for 2 hours
6. The assayed media was discarded and 200 µl of acidified Isopropanol (0.33% v/v HCl in Isopropanol) was added in each well to dissolve the crystals of dye
7. Plates were read at 492 nm wavelength

PLATE III

1. U87-MG at 10^5 cells/well → Plates were seeded as per lay out → subsequent incubation for 24 hours
2. Controls were added and drugs at appropriate concentrations in medium.
3. Cells were incubated for 24 hours as per standard tissue culture
4. Media were removed and cells were subsequently washed with PBS
5. MTT assay was performed by the addition of 20 μ l and left for 2 hours
6. The assayed media was discarded and 200 μ l of acidified Isopropanol (0.33% v/v HCl in Isopropanol) was added in each well to dissolve the crystals of dye
7. Plates were read at 492 nm wavelength

PLATE IV

1. U87-MG at 10^5 cells/well → Plates were seeded as per lay out → subsequent incubation for 24 hours
2. Add Controls and drugs at appropriate concentrations in medium
3. Controls were added and drugs at appropriate concentrations in medium.
4. Cells were incubated for 48 hours as per standard tissue culture
5. Media were removed and cells were subsequently washed with PBS
6. MTT assay was performed by the addition of 20 μ l and left for 2 hours
7. The assayed media was discarded and 200 μ l of acidified Isopropanol (0.33% v/v HCl in Isopropanol) was added in each well to dissolve the crystals of dye
8. Plates were read at 492 nm wavelength

3.10 MTT assay

MTT assay is the most popular colorimetric assay in which the compound 3-(4,5-dimethylthiazol-2-yl)-2,5-diphenyl-2H-tetrazolium bromide is converted by mitochondrial enzymes to a coloured insoluble formazan product, which is solubilised in alcohol or detergent followed by absorption measurement. The amount of colour produced is proportional to the number of live cells. This assay has been used by many investigators as a reliable method of chemosensitivity testing in malignant Gliomas (Ferrari, *et al.*, 1990).

Values obtained were expressed as a percentage of control cells to which no formulation were added, and comparison was made between *f*-CNTs-PTX complexes and Control (C) samples. Based on the results of the test, the IC₅₀ doses (the concentrations which kill 50% of cells) were calculated.

3.10.1 MTT assay protocol

1. Media was removed and cells were washed with PBS
2. PBS was filtered and sterilised to prepare MTT solid and 3 ml of filter PBS
3. 90 µl of filtered medium was added to 10 µl of MTT which was made up to 3 ml of medium and added to each well (96 well plate would require 9 ml of media and 1 ml of diluted MTT)
4. Samples were incubated for 2 hours at 37 °C
5. The dish was foiled wrapped as a result of MTTs sensitivity to light
6. Medium was not discarded from the wells. A 100 µl of the clear solubilisation reagent in the kit was added

7. The plates were agitated at 240 rpm for 10 minutes to enhance dissolution and measure absorbance at 590 nm

3.11 Statistical analysis

The results were expressed as the mean \pm Standard Deviation (SD) from three independent experiments and were analysed using the software SPSS 14.0 and Graphpad Prism 6.0 to calculate the significance between groups. A difference was considered to be significant if the *P*-value was less than 0.05.

CHAPTER 4
CHARACTERIZATION of PRISTINE
& FUNCTIONALIZED CNTs
(RESULTS AND DISCUSSION)

*“The aim of argument, or of discussion, should not be victory, but
progress”*

(Joseph Joubert)

4.1 Characterization and functionalization

A wide range of techniques have been used to characterize the morphology and structures of the materials utilized in this research. Two different types of CNTs with various characteristics have been studied, including SWNTs and MWNTs. These have been characterized for structure and impurities. MWNTs and SWNTs were also functionalized in order to improve their solubility in aqueous solvents using two polymeric systems polyethylene glycol (PEG) and Pluronic 127®. The samples were homogenised and sonicated. The results presented are Pristine (p-CNT) before and after sonication and after filtration.

The first section covers Raman spectroscopy which provides qualitative data in relation to the impurities and structure of CNTs. Thereafter TEM micrographs are shown for the samples, followed by SEM, XRD and zeta potential.

4.2 Raman Spectroscopy visible 488 nm - Ultra violet 325 nm

Raman has different characteristic features for analysing CNTs samples. The G-band is a feature of the graphite layer which corresponds to the tangential vibration of the carbon atoms and second-order related harmonic G'-band. The D-band sets the sign of the typical 'defects' on the graphite structures. Comparison of the two peak intensities gives a measure of the quality of the CNTs. The third feature of Raman spectroscopy is the Radial Breathing Mode (RBM) which is sensitive to the diameter of SWNT.

The RBM is directly dependent on the CNT diameters through the relation shown in Equation 4. 1:

$$\omega_{\text{RBM}} = A/d_t + B$$

Equation 4. 1 Equation for the diameter calculation of SWNTs

Where d_t is the CNT diameter, A and B parameters can be determined experimentally (Jorio, Pimenta et al. 2003). For this Raman study A is 234 cm⁻¹ and B is 10 cm⁻¹ this is an estimate to the correction of the breathing mode restoration due to tube-tube interaction within the bundles (Milnera, Kurti et al. 2000).

4.2.1 Raman spectra SWNT

The Raman spectrum of SWNT has been illustrated in Figure 4.1. The D-band is visible in between 1200-1500 cm^{-1} and confirms the scattering from a defect that breaks the basic symmetry in the graphite sheet (Figure 4.1(b)). A Shift of 1574 cm^{-1} is typical for G-band of SWNTs (Dresselhaus, Dresselhaus et al. 2005). Also the Radial Breathing Mode (RBM) peak is prominent and appears to be in the range of 200 cm^{-1} and 400 cm^{-1} . This suggests that the sample that has been investigated can be confirmed to be SWNTs and tube diameter can be determined.

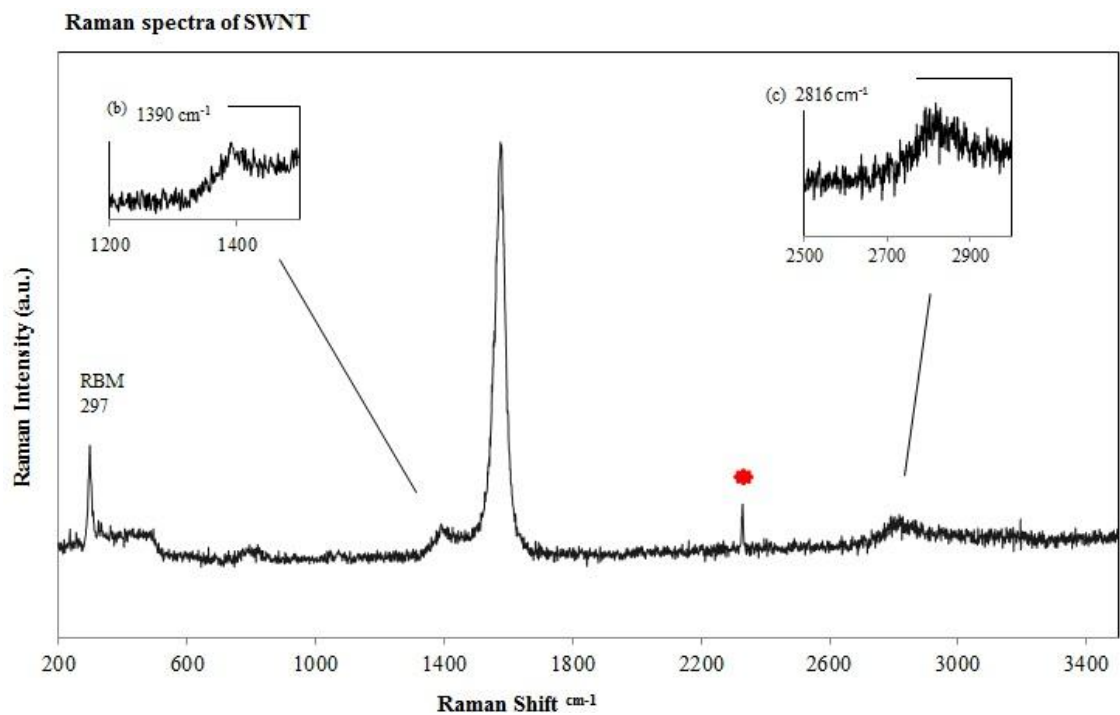


Figure 4.1 (a) Raman Spectra of SWNT with Ar + laser (488 nm) the peak marked with * is Hg calibration peak (b) expanded spectra of D-band (c) Expanded spectra of second order G'-band.

Figure 4.1 (c) is the second order G'-band and is identified as a higher order peak of the D-band featured at 1390 cm⁻¹ (Figure 4.1(b)) (Dresselhaus, Dresselhaus et al. 2005).

In Figure 4.2 the low frequency of 200-400 cm⁻¹ region spectra has been shown and frequencies of 236, 255, 297, 324, 332 and 359 have been observed, whereby the tube diameter was calculated.

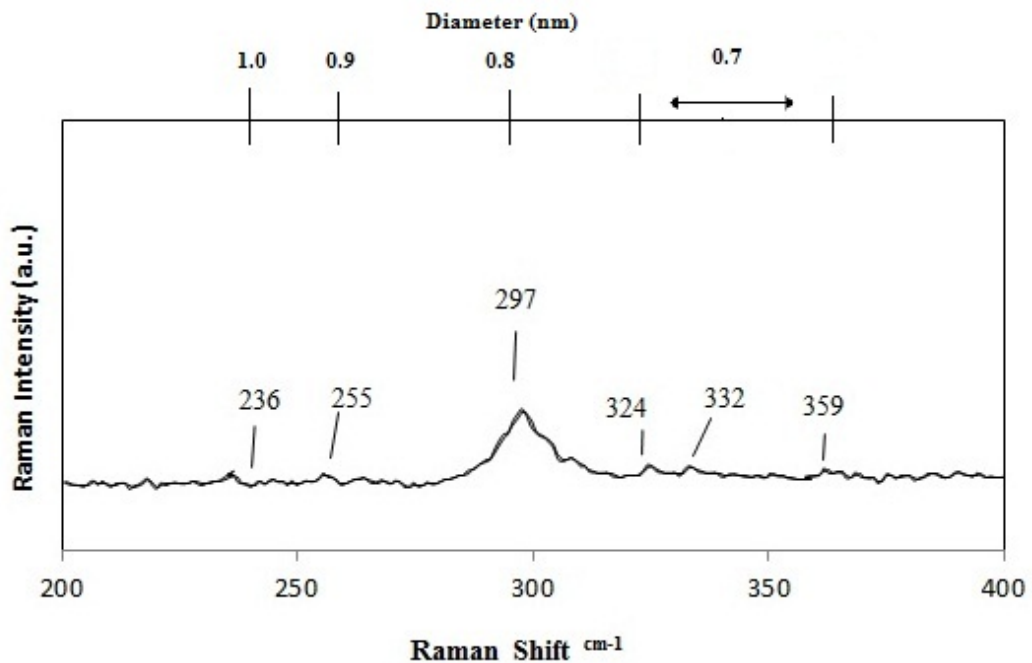


Figure 4.2 Room temperature Raman spectrum of SWNT on the expanded scale show the details of RBM and tube diameter (nm)

The tube diameter is calculated and is presented in Table 4.1 and the diameter of the SWNT have been plotted against the RBM frequency showing a linear relationship i.e. the higher the RBM frequency the lower the tube diameter as seen in Figure 4.3.

Table 4.1 Tube diameters calculated from radial breathing mode (RBM) frequencies using the relation $\omega_{\text{RBM}} = 234/d_t - 10$

	ω_{RBM} (cm-1)	d_t (~ nm)
Excitation 488 cm-1	236	1.03
	255	0.95
	297	0.81
	324	0.74
	332	0.72
	359	0.67
Average		0.80

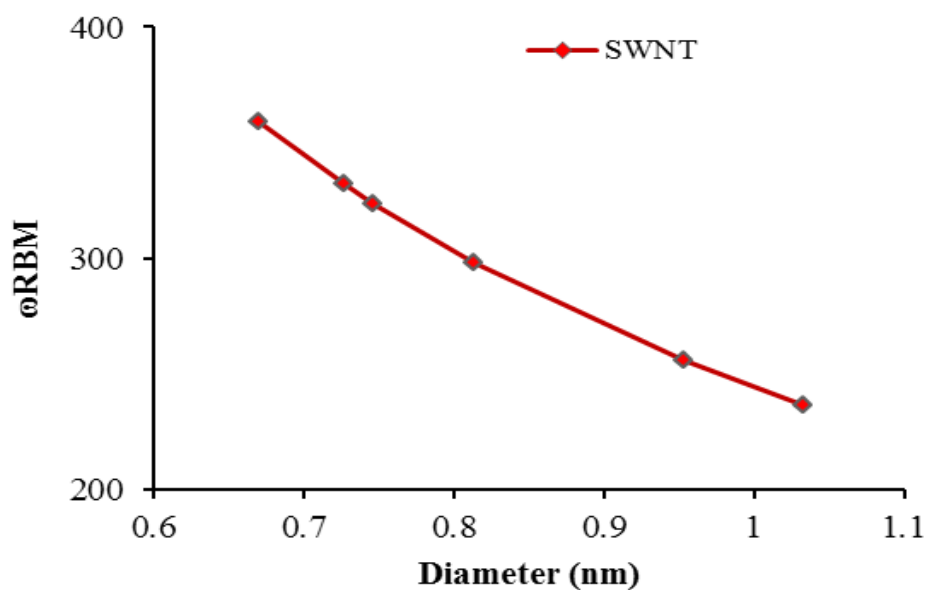


Figure 4.3 RBM frequencies vs tube diameter (nm)

It is also evident that RBM frequency is diameter dependent. It can be seen that SWNTs has diameters ranging from ~ 0.67-1.03 nm providing an average diameter of 0.8 nm.

This is in agreement with the TEM micrographs (Figure 4.4) shown in which SWNTs are obvious and an estimate of the tube diameter can be concluded from the scale to confirm the data observed from Raman Spectra. The length of the SWNTs can be confirmed from in which it is to be in the range of 50 ± 250 nm (Figure 4.5). However, when morphology of the CNTs where characterized with SEM (Figure 4.6) merely a rough estimate of length could be observed.

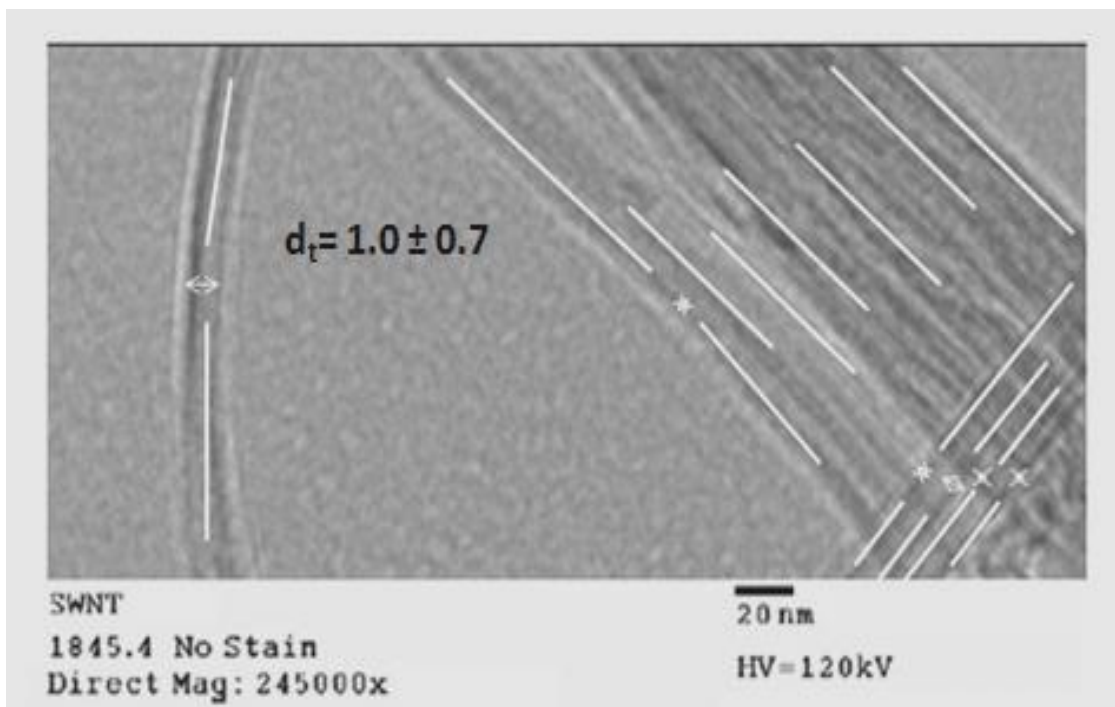


Figure 4.4 TEM micrograph of SWNT at x 245000 magnification



Figure 4.5 TEM micrographs of SWNT x 65000 magnification

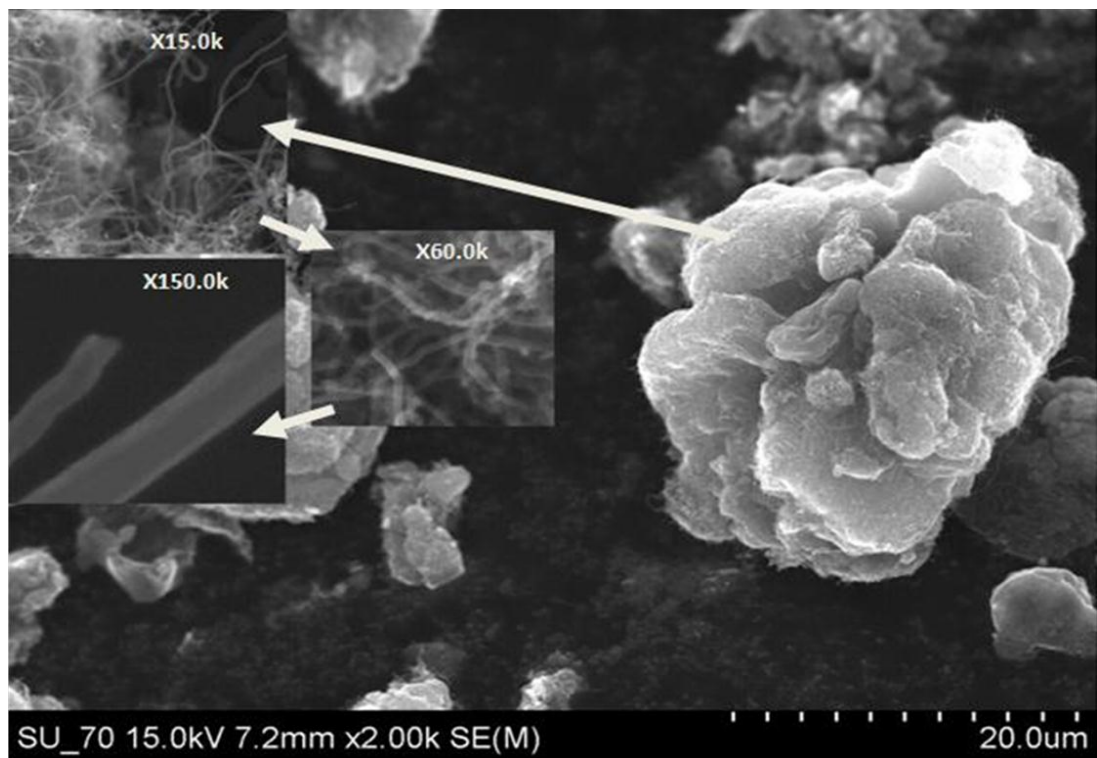


Figure 4.6 SEM micrographs at various magnifications

4.2.2 Raman Spectra of MWNT

Since the geometry, number of walls and tube diameter of MWNTS varies from SWNTs; Raman spectra of MWNTs are expected to slightly differ. A typical G-band shift of 1578 cm^{-1} (Figure 4.7) is expected for MWNTs that are synthesized with CVD (Lee, Kim et al. 1999).

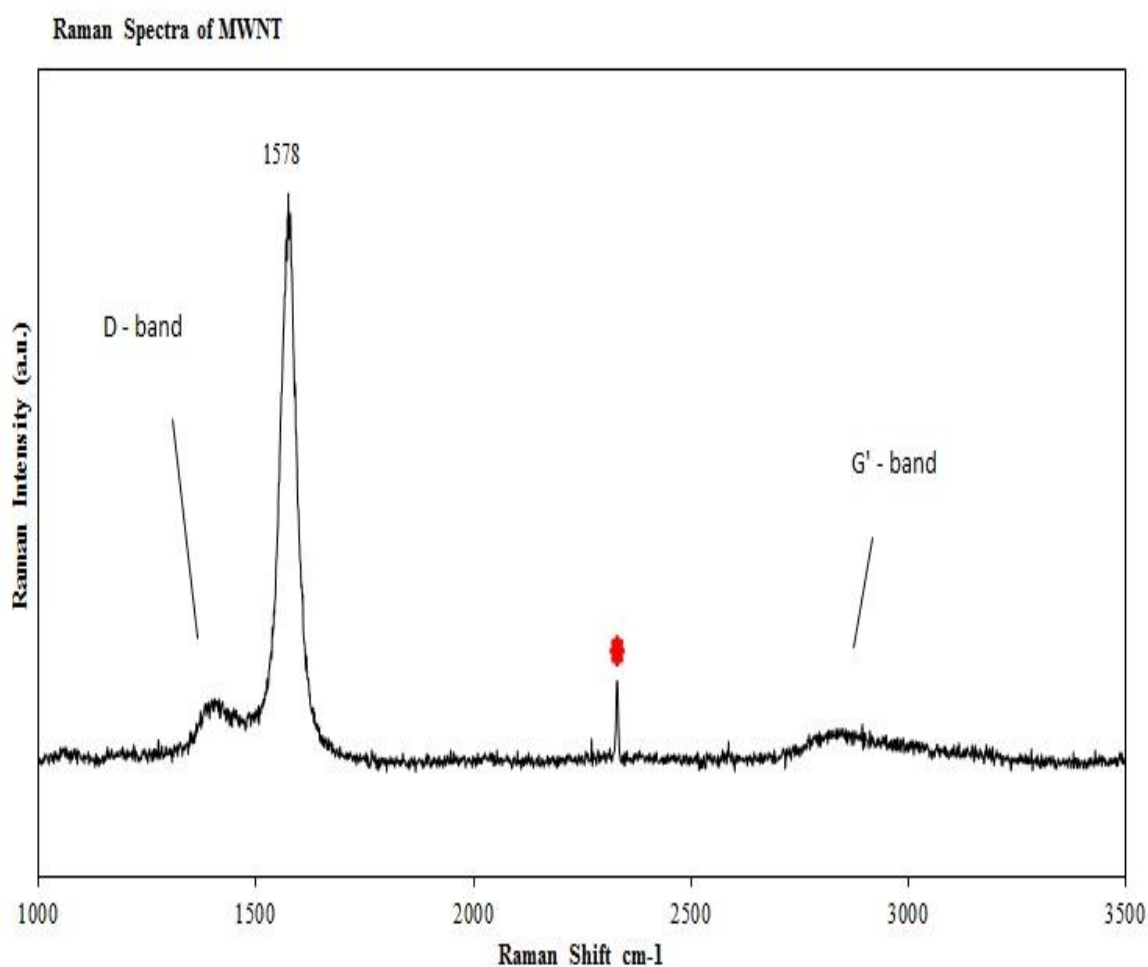


Figure 4.7 Raman Spectra of MWNT with 488 nm, the peak marked with * is Hg calibration peak

No RBM Peak was determined for MWNT in the 200-400 cm^{-1} range, as this was expected and confirmed. This also can be a confirmation that the MWNT samples do

not contain any SWNT. Due to the large diameter of MWNTs, the signal of RBM is too weak to be observed.

The D-band at 1385 cm⁻¹ (Figure 4.7) is mainly derived from the disordered carbon and defects of MWNTs, a feature common to *sp*² hybridized disordered carbon materials (Arbizzani, Righi et al. 2011) that have been utilized through laser excitation of 352 nm. Furthermore, the sample has a typical G-band of 1578 cm⁻¹, second order G'-band is in the range of 2700-2800 cm⁻¹ that is established for MWNT. For MWNTs length determination TEM micrographs have been utilised. Sample contained various tube lengths ranging from 50-1000 nm with an average of 580 nm (Figure 4.8). With higher magnifications (Figure 4.9) the nature of MWNT becomes clearer. The inner and outer diameters was determined and found to range from ± 10-20 nm Inner diameter (I.D) and ± 30-40 nm Outer diameter (O.D). CNTs were arranged in a concentric arrangement and in one MWNT 8 walls can be counted showing 4 concentric CNTs of increasing diameter. Nevertheless, it is of great difficult to identify their precise structure through SEM (Figure 4.10).

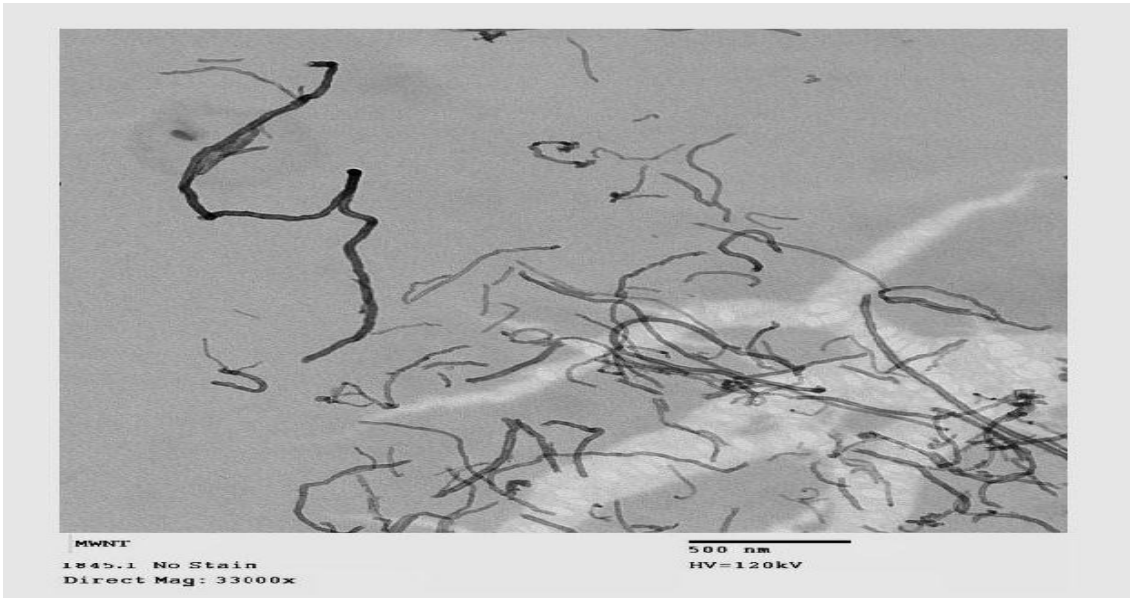


Figure 4.8 TEM micrograph of MWNT x33000 magnification

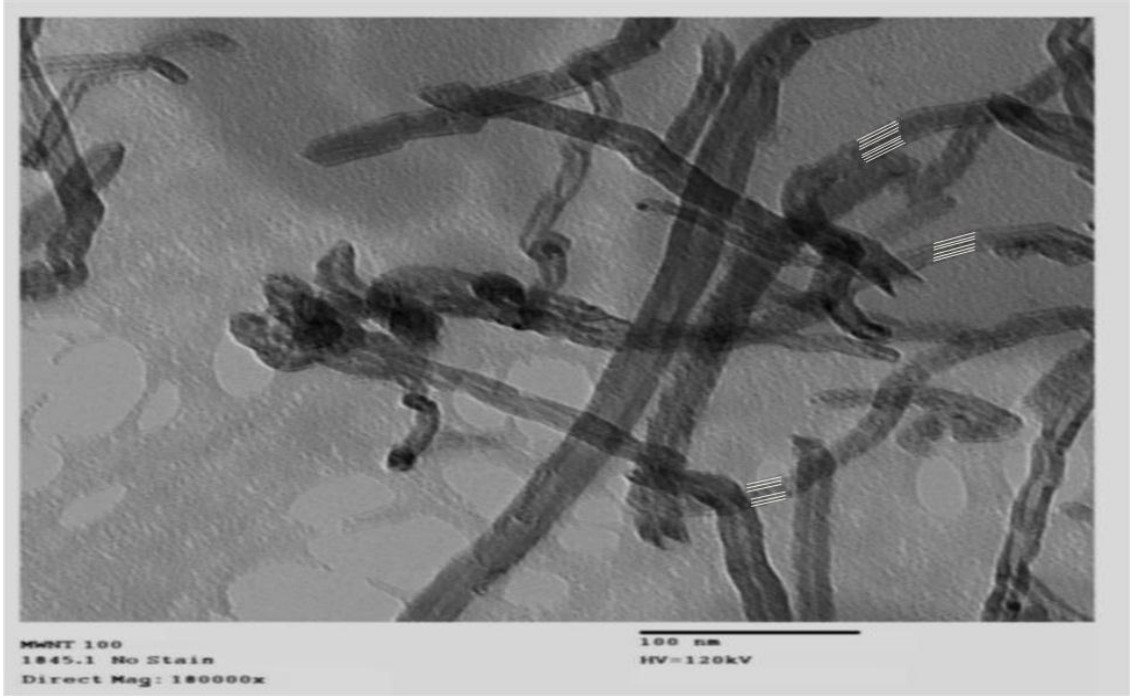


Figure 4.9 TEM micrograph of MWNT at x180 000 magnification

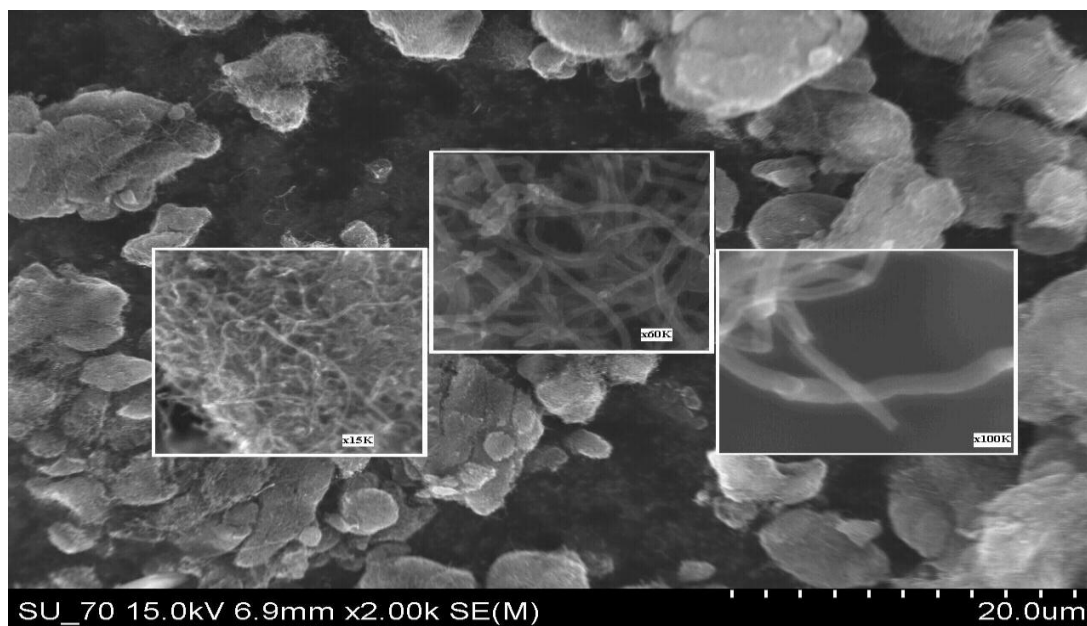


Figure 4.10 SEM micrograph of MWNTs with various magnifications

4.2.3 Raman comparison of SWNT and MWNT

As stated earlier, CNTs are made up of graphene rolled up into a tubular geometry. MWNTs contain a number of sheets rolled in a concentric manner with a range of diameters in the nanometre range. MWNTs elicited a wider range of outer diameters. Therefore the Raman spectra for MWNTs are not as distinct compared to that of SWNTs. For example, RBM signal (Figure 4.11) is normally too weak to be observed as it gives an average diameter which broadens the signal (Costa, Borowiak-Palen et al. 2008).

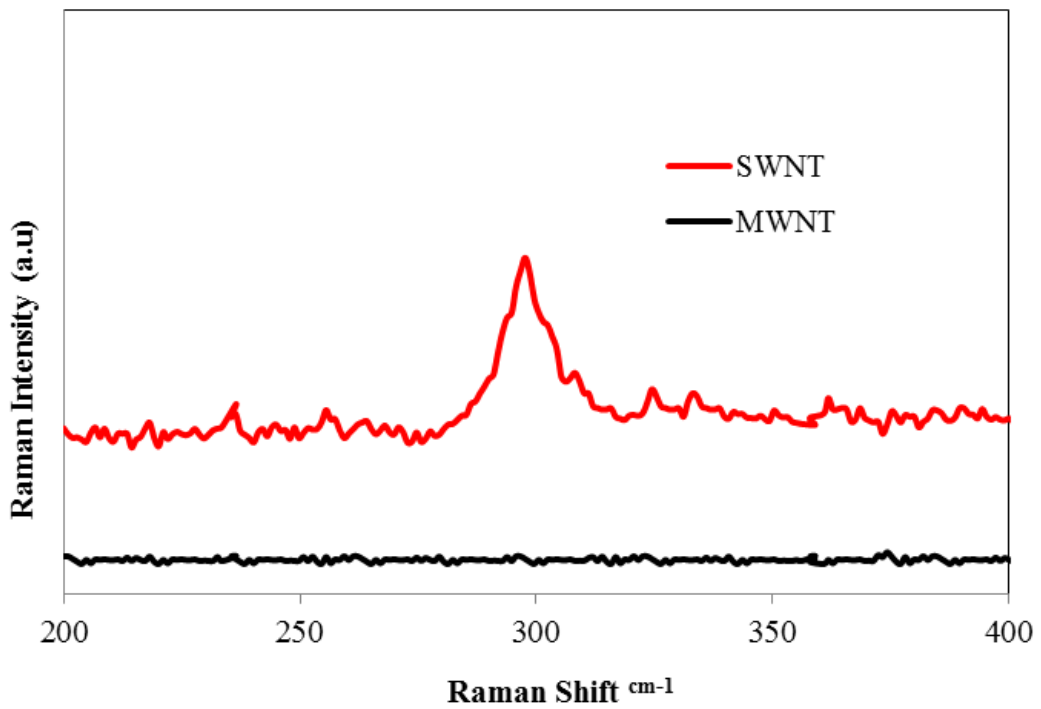


Figure 4.11 Raman Spectra of MWNT and SWNT with 325 nm

It is clear that the G-band for MWNT is small in intensity comparing to SWNT, this can be related to the diameter distribution within the individual MWNTs. An alternative explanation is the variation between the tubes. The D- and G-bands confirm investigation of the ‘defects’ on CNTs. When these two bands present similar intensity, this indicates a high quantity of ‘defects’. On examination it was seen that MWNTs had similar intensities, meaning high quantity of structural defects due to its multilayer of graphite sheets.

4.2.4 Raman spectra of pristine and *f*-CNTs

Raman spectra of dispersed SWNTs showed a significant G-band peak shift confirming the presence of the surfactants that were utilised to functionalize the CNTs (Figure 4.12). The D- and G-bands shifts confirmed investigation of the ‘defects’ on CNTs.

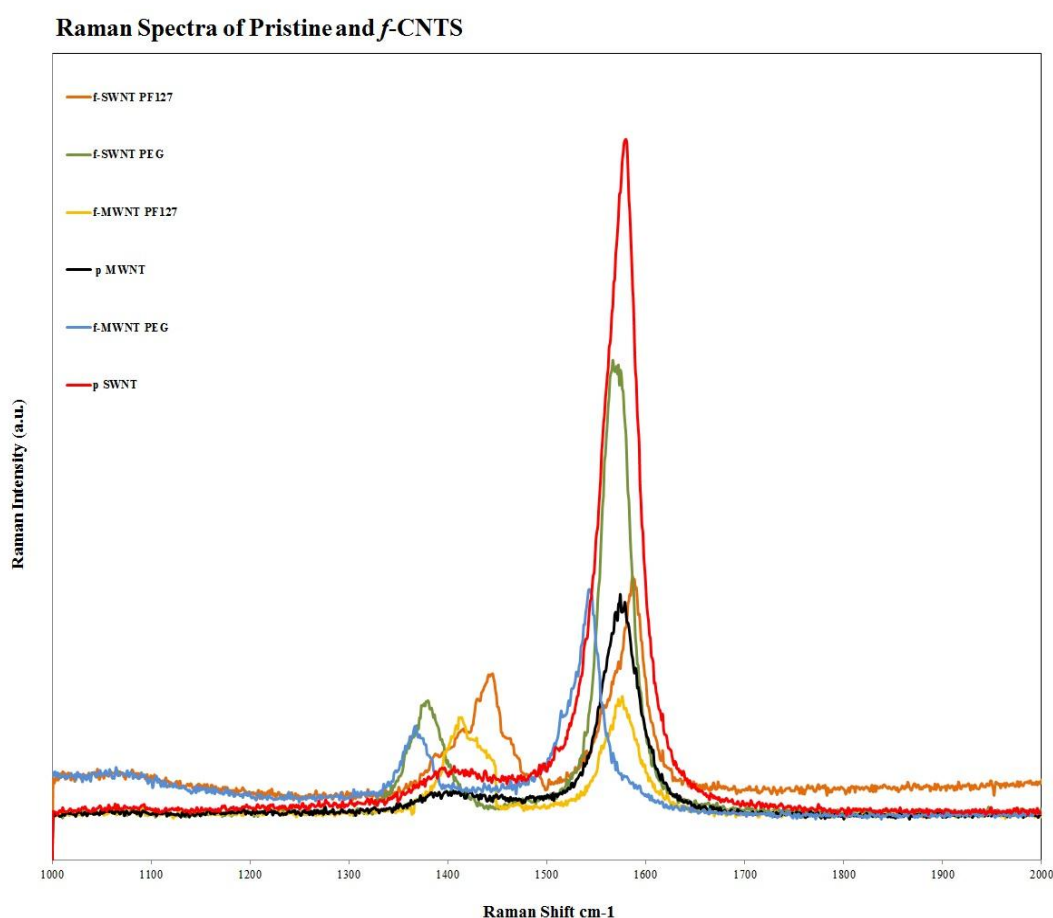


Figure 4.12 Raman Spectra of functionalized CNTs

Similar intensity presented by these two bands indicated a high quantity of ‘defects’. Evidently MWNTs had similar intensities suggesting high quantity of structural defects due to the multilayer of graphite sheets, there was significant change in the D-bands for both SWNTs and MWNTs that were functionalized with the two polymeric systems.

The decrease of the Raman intensity of G-band and increase of D-band observed for the functionalized CNTs could be attributed to a change in the electronic properties and/or an alteration of the vibrational modes of the tubes (Figure 4.12).

4.3 X-ray diffraction for sample purity

X-ray diffraction (XRD) is a non-destructive method for characterising CNTs. The technique gives information about interlayer spacing, structure and impurities. Arrangements of CNTs were random; however diameter and chirality could be determined. The XRD of CNTs is similar to graphite. A peak at (002) can be used to obtain the interlayer spacing a family of $(hk 0)$ peaks due to the honeycomb lattice of single graphene sheet. However, in this study XRD is not used to determine the micro structural details but to provide information about sample impurities (catalyst and functional group). Data comparison between MWNTs and literature has been illustrated in Figure 4.13.

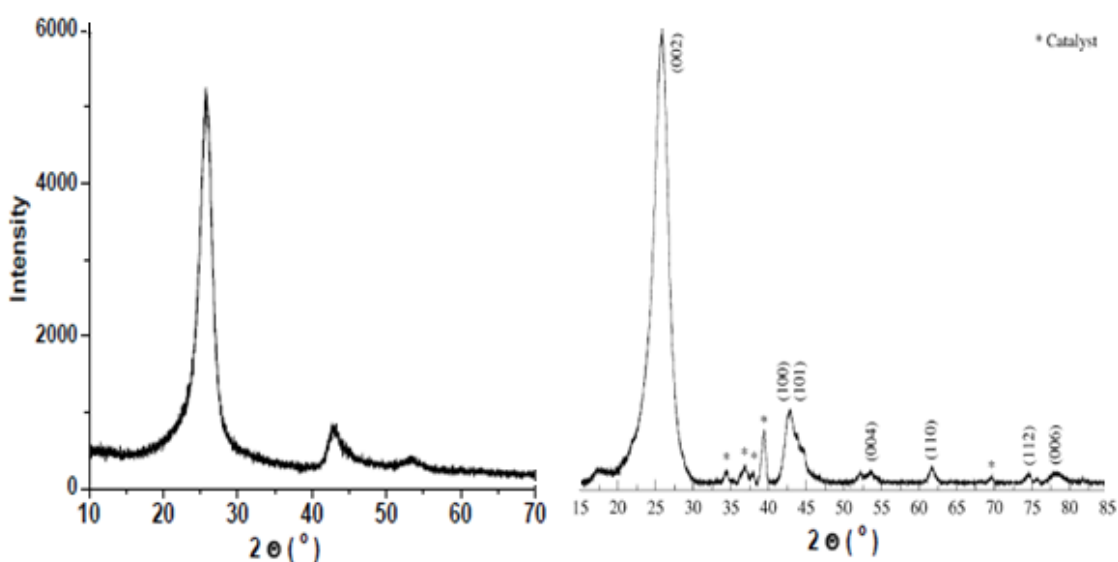


Figure 4.13 XRD spectra of MWNTs (left) from this study and (right) from (Belin and Epron 2005)

MWNTs in this study and those from literature were synthesised using chemical vapour deposition method, both samples showed a (002), (100) and (004) peaks, however in this study there was an absence of additional peaks. This suggests that the sample in this study is of high purity free from catalyst impurities. Similarly, a comparison of spectra has been shown for SWNTs in Figure 4.14 and they exhibit similar peaks and were also free from impurities. The graphite spectrum is also shown for comparison.

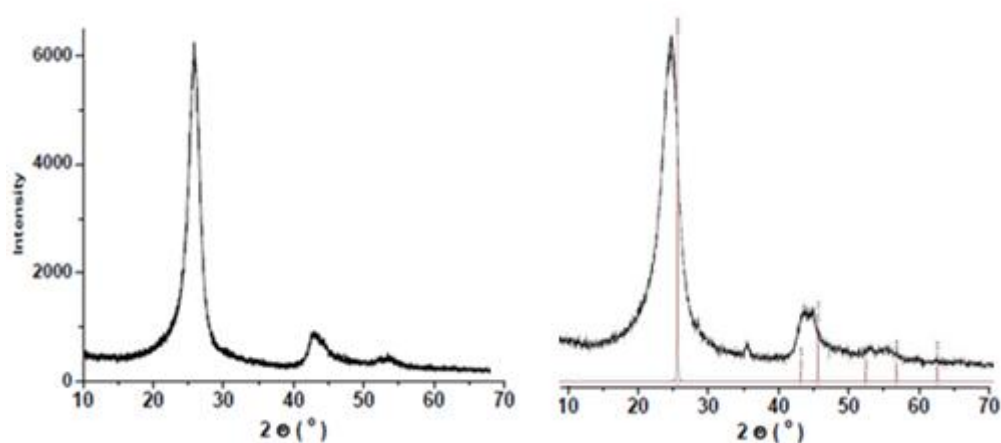


Figure 4.14 XRD spectrum of SWNTs (left) and Graphite (right) in red line

4.4 Functionalization and comparison of aqueous stability of CNTs with Polyethylene glycol 400 and Pluronic 127

Functionalization of CNTs has been established using PEG400 and PF127; and comparison has been conducted before and after sonication and homogenisation (Figure 4.15). TEM and SEM micrographs were taken to characterise the dispersion. Furthermore, ζ -potential was measured to note the aqueous dispersion stability. Additionally to confirm the presence of the *f*-CNTs, Raman spectra were recorded.

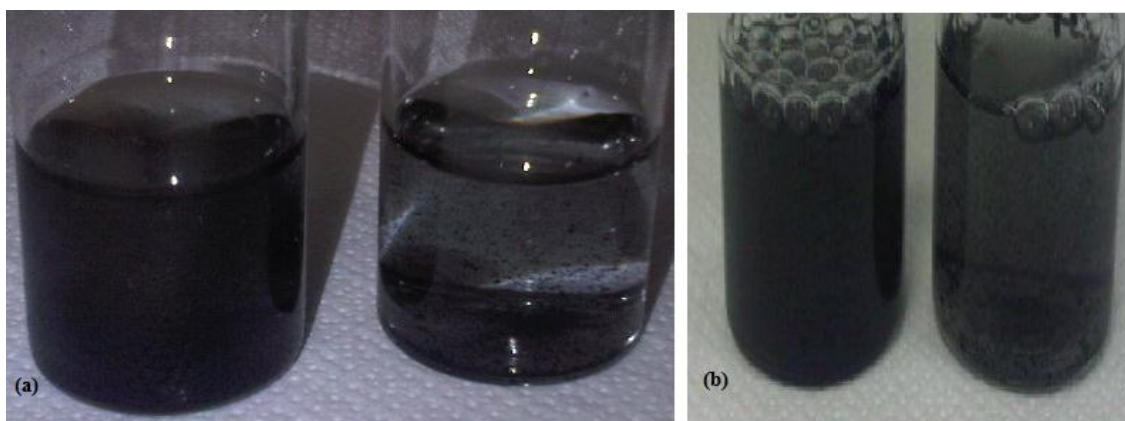


Figure 4.15 SWNT and MWNT in PEG400 and PF127 (a) SWNT (left) and MWNT (right) in PEG400, (b) dispersion of SWNT (left) and MWNT (right) in PF127 prior homogenising and sonication

Clearly SWNTs show a better dispersion in both polymeric systems prior to any mixing. Dispersion improvement was seen Figure 4.16 in after 10 minutes sonication, however the dispersion is unstable and particles were visible, it is not uniformly dispersed.

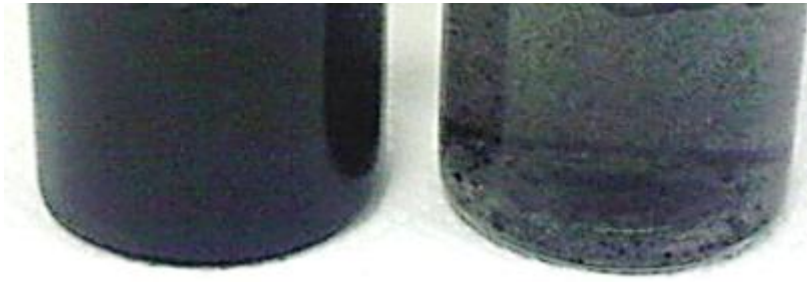


Figure 4.16 Shows the dispersions of SNWTs after 10 minutes ultrasonication

After the dispersion were sonicated for 1 hour and filtration was achieved, a significant difference was noted (Figure 4.17). Both SWNTs and MWNTs show a better dispersion in PEG400 in comparison to the dispersion in Figure 4.15.

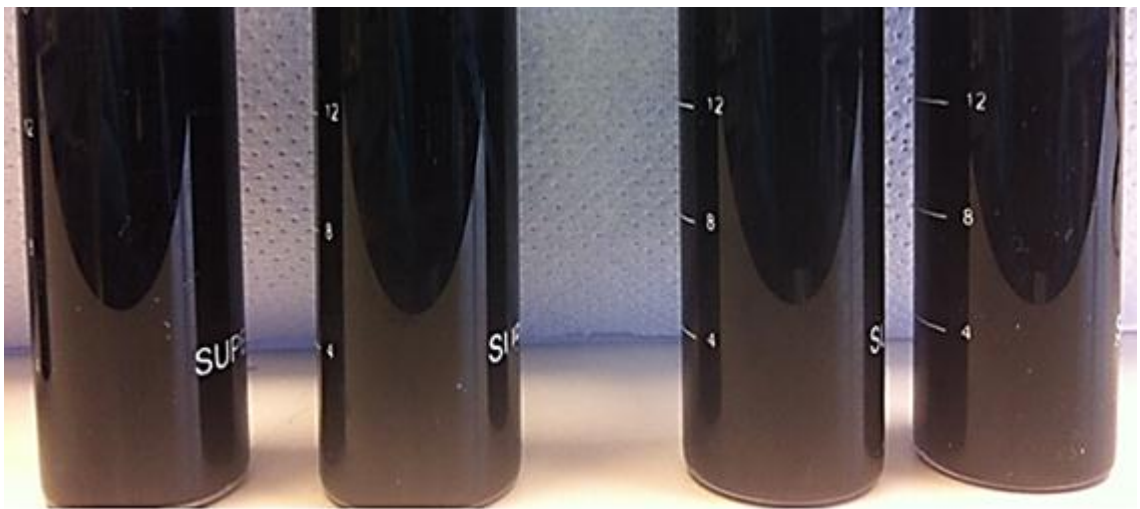


Figure 4.17 MWNT (left) and SWNT (right) in PEG

To confirm the uniformity of the dispersions of PEG400 with SWNTs and MWNTs, TEM micrographs were taken. As it can be seen in Figure 4.18, SWNTs in PEG400, show a clear uniform dispersion.

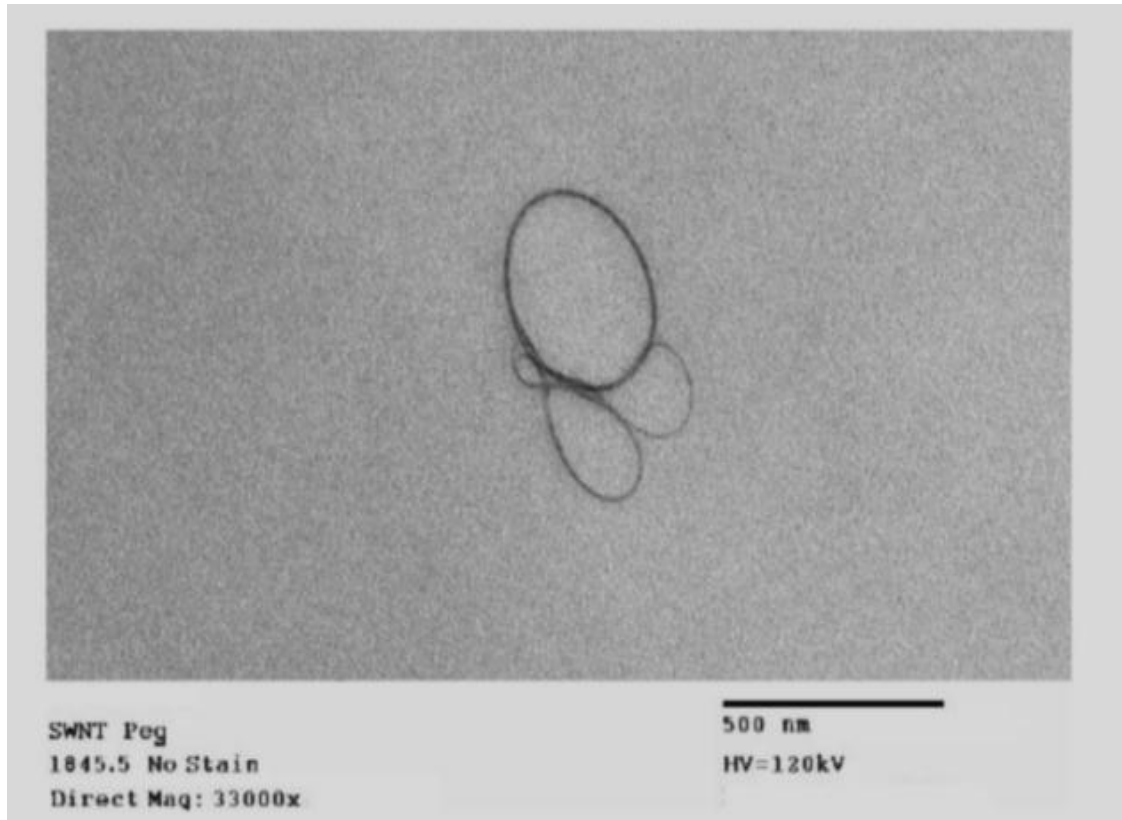


Figure 4.18 TEM Micrographs of *f*-SWNT in PEG400

From the Raman spectra in Figure 4.19 no significant G-band shift was observed. However, there is a significant decrease of D-band indicating the degree of disorder present in the nanotube. The new peak of D-band at 1375 cm^{-1} confirms modified SWNTs.

Different intensity of the G-band of *f*-MWNTs with PEG (Figure 4.20) was observed, as well as a shift difference of 35 cm^{-1} that changed from 1575 cm^{-1} to 1540 cm^{-1} during the functionalization process as an enhancement of defects was expected, which subsequently supports the attachment of molecules (Rajalakshmi, Ryu et al. 2005). Moreover, a significant higher intensity was observed in the D-band, which is due to its multilayer graphite sheet modification.

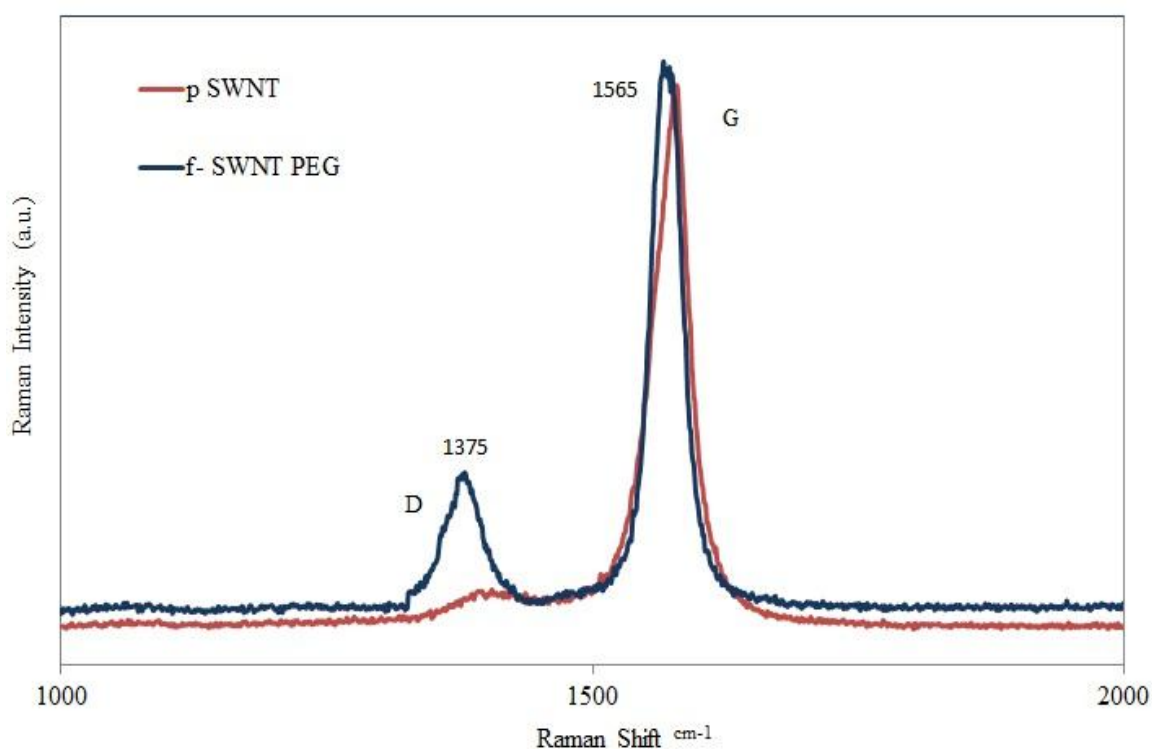


Figure 4.19 Raman spectra showing a shift and decrease in intensity of *f*-SWNT

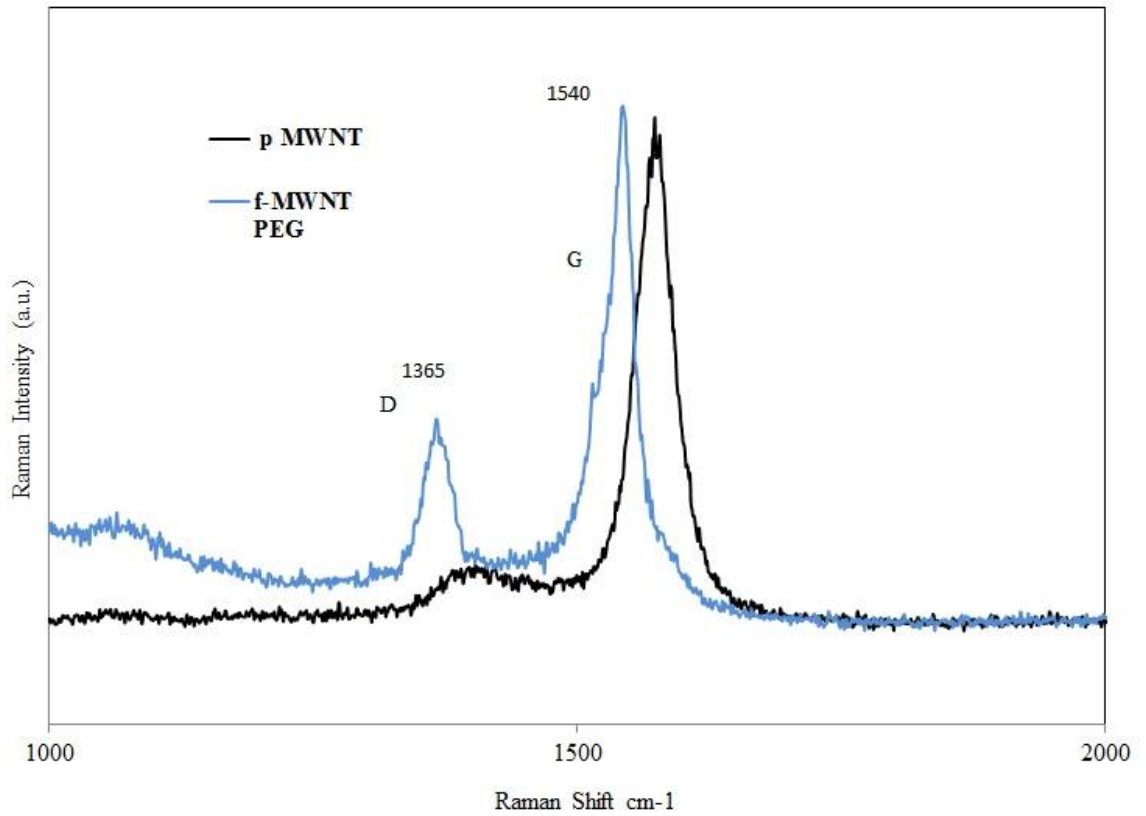


Figure 4.20 Raman spectra of *f*-MWNT in PEG

Nevertheless, not all CNTs concentrations achieved a uniform dispersion in PF127 as can be noticed in Figure 4.21.



Figure 4.21 MWNT (left) and SWNT (right) in PF127

Concentration of 1:5 MWNTs was shown to be the least dispersed. However, both 1:1 and 1:5 concentration of SWNTs in PF127 demonstrated a homogenised dispersion presented a number of different trends (Figure 4.22 and Figure 4.24).

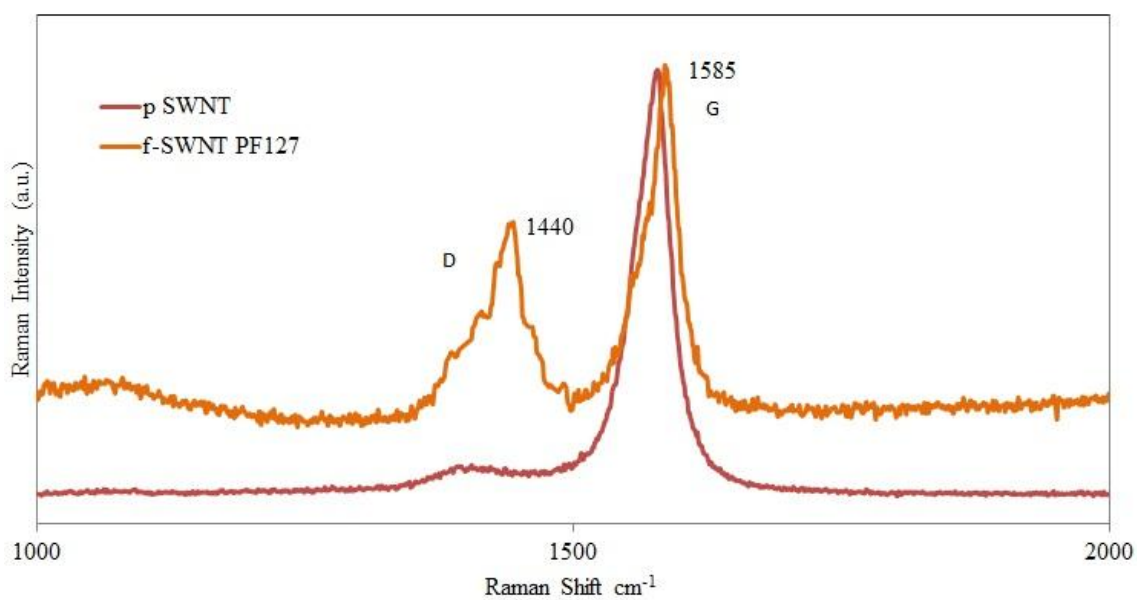


Figure 4.22 Raman spectra of p-SWNT and f-SWNT-PF127

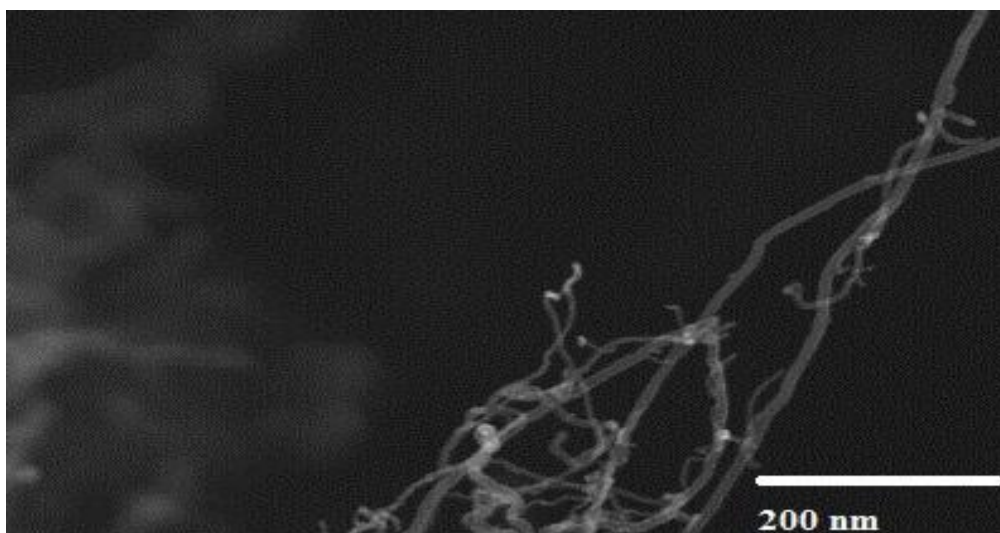


Figure 4.23 SEM micrograph of f-SWNT-PF127

From MWNT, merely 1:1 ratios to PF127 showed a better dispersion and this in agreement with the Raman spectra in Figure 4.24. For example the D-band peak for *f*-MWNT-PF127 1:1 ratio elicited substantially greater Raman intensity than its counterpart formulations; this may be explained by changes within the surface of the formulation specifically the CNT component.

Raman spectra of *f*-MWNT–PF127 were reordered and shifts were observed for both concentrations. However, a more prominent shift was seen with the 1:1 ratio, this may be due to the CNT surface and surfactant interaction.

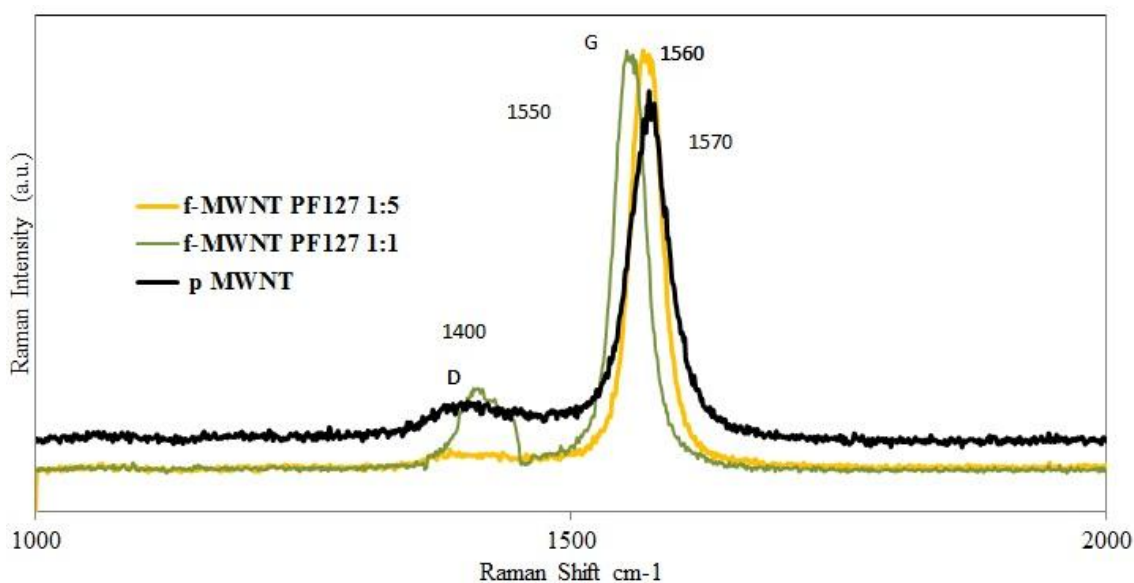


Figure 4.24 Raman spectra of p-MWNT and *f*-MWNT-PF127

4.5 ζ -potential

To evaluate the CNTs conjugates further with regards to their surface charges and functional groups, zeta potential analysis has been performed. The zeta potential of a system gives an indication of its stability. When particles in a solution have a large ζ -potential, whether positive or negative, they will repel each other and will not aggregate together. Low zeta potential infers low repulsive forces to push the particles apart and therefore they will tend to aggregate together. The zeta potential measurements are essential for CNTs in drug delivery to monitor their stability and to determine their behaviour. The ζ -potential records of pristine (p) and functionalized CNTs are presented in Table 4.2

Table 4.2 ζ -potential Mean \pm SD of Pristine and *f*-CNTs

Concentrations / MWNT/SWNT	ζ-potential Mean \pm SD	ζ-potential after <u>10days</u> Mean \pm SD
p- MWNT	-9.47 \pm 0.3	-9.57 \pm 0.3
MWNT-PEG 1:1	-20.00 \pm 0.2	-18.47 \pm 0.4
MWNT-PF127 1:1	-15.40 \pm 0.4	-15.61 \pm 0.7
MWNT-PEG 1:5	-22.23 \pm 0.5	-19.60 \pm 1.5
MWNT-PF127 1:5	-12.00 \pm 0.6	-8.67 \pm 0.8
p-SWNT	-7.81 \pm 0.25	-7.81 \pm 0.9
SWNT-PEG 1:1	-19.30 \pm 0.6	-19.3 \pm 0.6
SWNT-PF127 1:1	-13.10 \pm 0.4	-11.8 \pm 1.6
SWNT-PEG 1:5	-17.30 \pm 0.4	-15.3 \pm 0.8
SWNT-PF127 1:5	-15.30 \pm 0.3	-16.8 \pm 1.6

ζ -potential of p-CNT were presented to be -7.81 mV for p-SWNTs and -9.47 mV for p-MWNTs, with PEG400 -20.0 mV for SWNTs and -19.3 mV for MWNTs and with PF127 -13.10 mV for SWNTs and -15.4 mV (Figure 4.25).

Interestingly, no significant difference was observed in the two concentrations of p-SWNTs and p-MWNTs. However, there was significant difference between the p-CNTs and *f*-CNTs for both surfactants at any given ratio ($p < 0.05$).

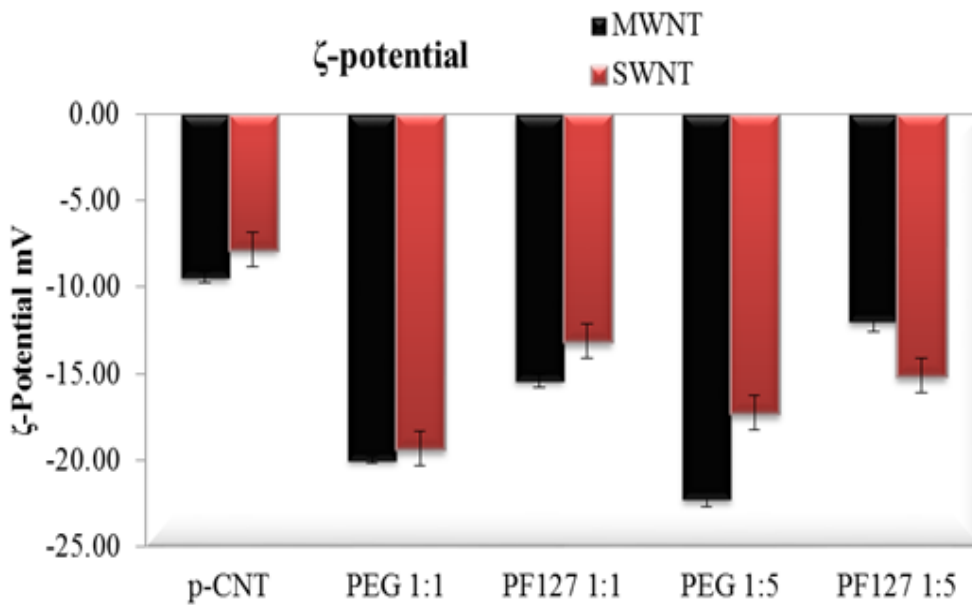


Figure 4.25 ζ -potential of pristine CNTs (p-CNT), CNT-PEG and CNT-PF127 were demonstrated. The error bars represent the standard deviation (SD) of three samples

On carrying out a multiple comparison test, a significant difference between SWNT-PEG 1:1 and MWNT PF127 1:1 ($p < 0.05$) was observed. In order to show a difference in ζ -potential for all formulations, samples were left to settle and measurements were repeated after 10 days.

As shown in Figure 4.26, no significant difference was observed for SWNTs freshly prepared and measurements after 10 day.

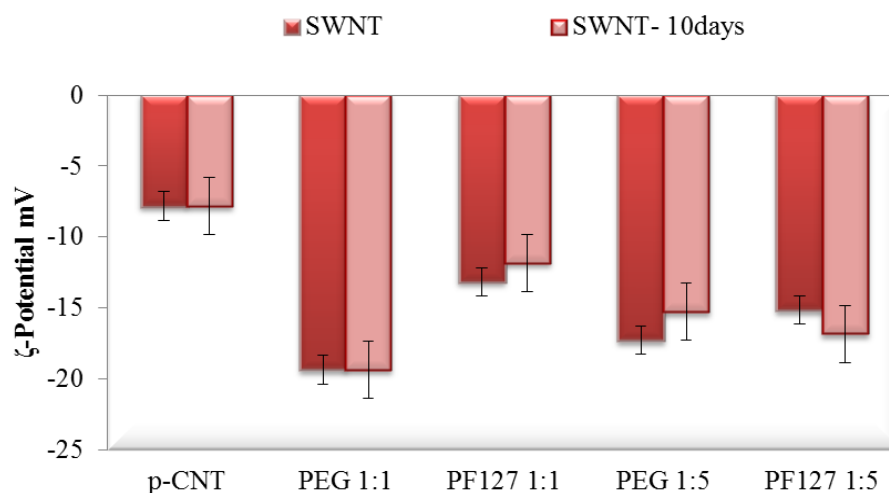


Figure 4.26 ζ -potential of SWNT in PEG and PF127 on preparation day and after 10 days. The error bars represent the standard deviation (SD) of three samples

The graph presented in Figure 4.27 shows the ζ - potential of freshly prepared and after 10 days samples of p-MWNTs and f-MWNTs. Measurements after 10 days showed no significant between p-MWNTs immediately and after 10 days. However, there is a significant difference between all the formulations when compared to one another ($p < 0.05$). Only PF127 ratios showed no significant difference when compared in ratios and with p-MWNTs.

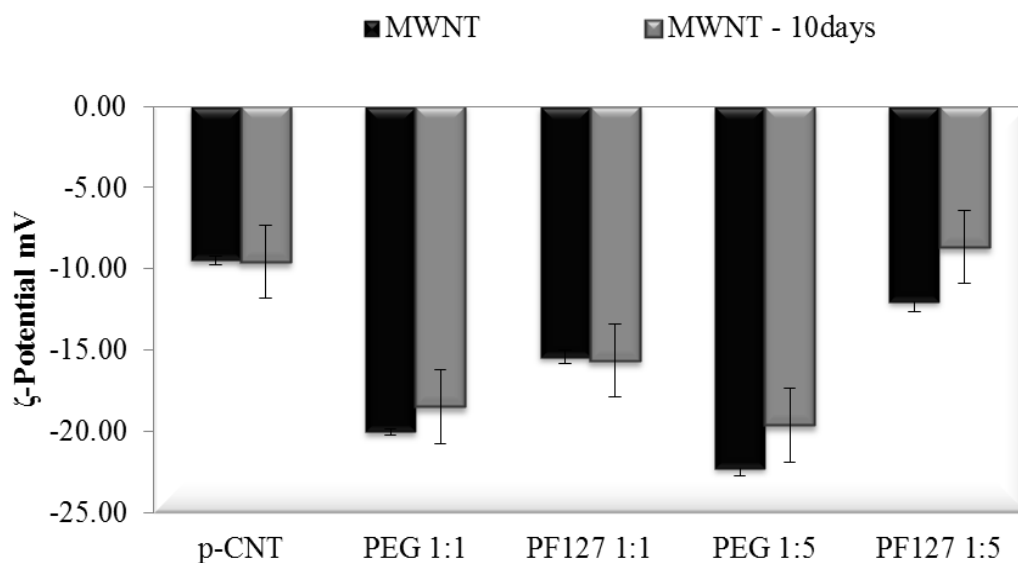


Figure 4.27 ζ -potential of MWNT in PEG400 and PF127 on the preparation day and 10 days after. The error bars represent the standard deviation (SD) of three samples

Moreover, a comparison of both SWNTs and MWNTs has been plotted in Figure 4.28, with both surfactants showing that MWNT-PF127 ratio 1:5 after 10 days has significantly lower ζ -potential than any presented formulation, at any ratio and time ($p < 0.05$). To elaborate more and to confirm that all samples were of acceptable quality, a phase plot was conducted and it showed to be satisfactory (Figure 4.29).

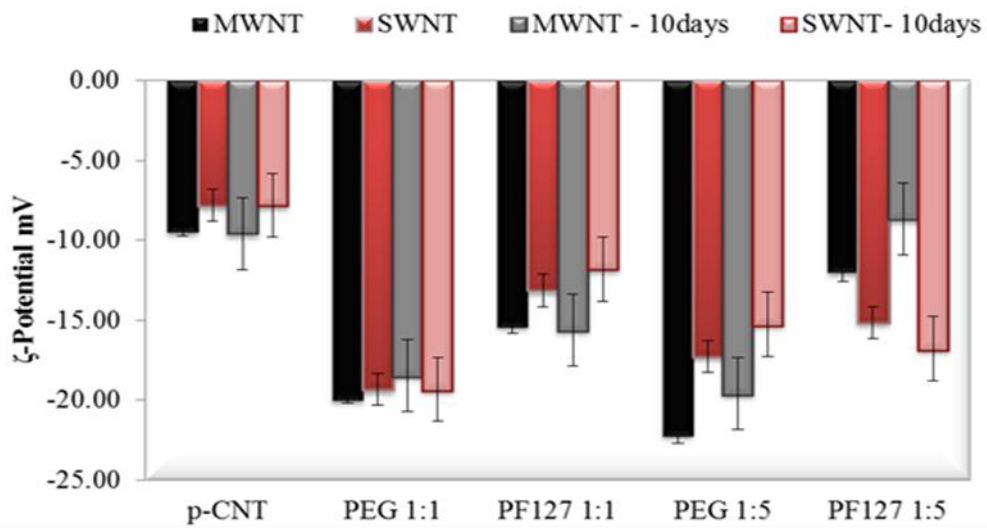


Figure 4.28 ζ -potential of SWNT and MWNT in PEG and PF127 1% on preparation day and 10 days after. The error bars represent the standard deviation (SD) of three samples

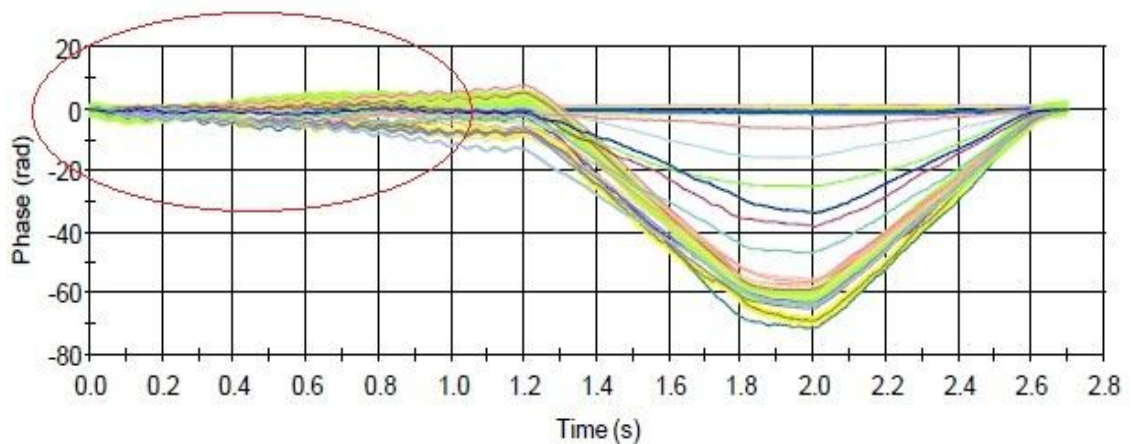


Figure 4.29 Phase plot that shows the quality of the samples used for ζ -potential measurement

In conclusion the characterization of the samples of both SWNT and MWNT in PEG has been shown to be significantly more dispersed and achieved a maximal decrease in Raman intensities as well as shifts in the G-bands; furthermore it also appears to be most stable as the ζ -potential shows a high charge ($p < 0.05$).

4.6 Paclitaxel *f*-CNTs

Determination of the Entrapment Efficiency (EE%) of PTX, was established through the conduction of a calibration curve that was measured from the stock solution. Thereafter, the formulations wer analysed with HPLC to define their entrapment efficiency using the respective linear regression equation.

4.6.1 Calibration Curve

Calibration curve of Paclitaxel concentration ranging from of 50-250 ug/ml was plotted using HPLC. The plot was used to obtain the equation R^2 for Paclitaxel; this is shown in Figure 4.30. Observably, a good linear relationship ($r = 0.9997$) was established. As the concentration increases there is a linear increase in absorbance. Using the respective linear regression equation $y = 655679x + 209811$, the entrapped Paclitaxel with CNTs can be found

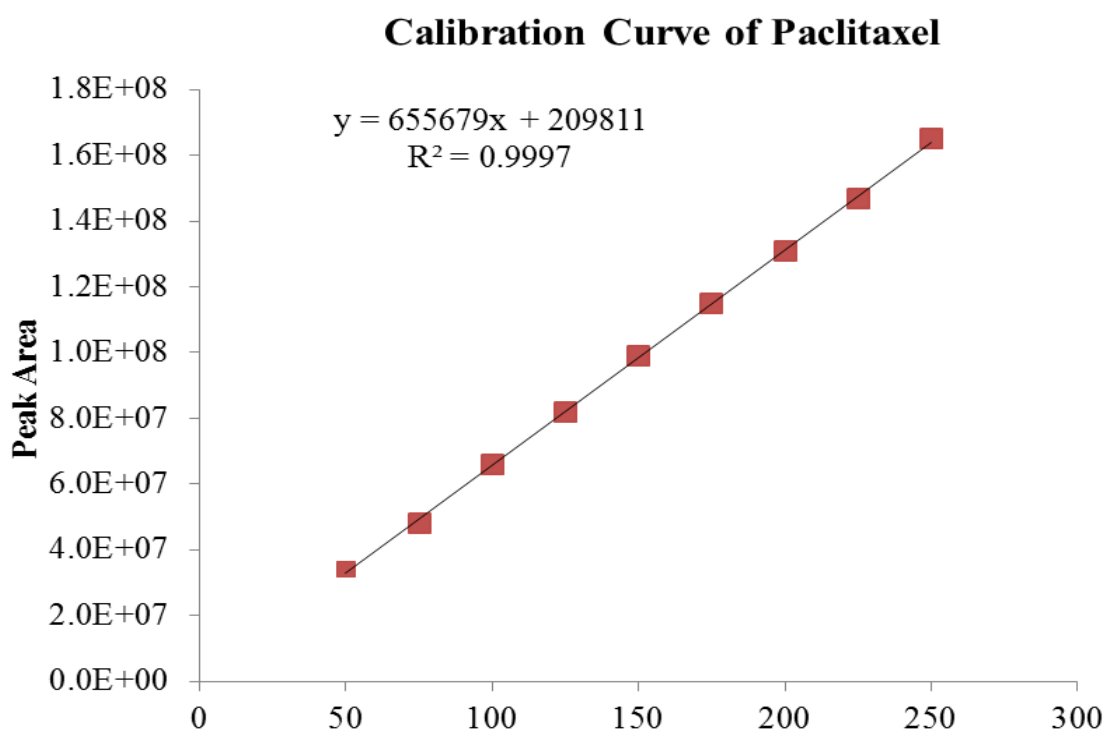


Figure 4.30 Paclitaxel calibration curve

4.6.2 Entrapment efficiency of *f*-CNTs

Loading efficiency of paclitaxel in the CNT- Surfactant was dependent on type of CNTs, surfactant and concentrations of drug. For this experiment a One-way ANOVA statistical test has been used where $p < 0.05$ is considered as significant. With the below equation the entrapment efficiency was calculated.

$$\%EE = \frac{\text{(Calculated drug content)}}{\text{(Theoretical drug content)}} \times 100$$

The entrapment efficiency of the formulations is demonstrated in Table 4.2 and it was found that PTX concentrations of 200 μg showed significantly ($p < 0.001$) higher percentage entrapment for *f*-CNTs in comparison to 100 μg , 150 μg and 250 μg concentrations. However, p-CNTs entrapment percentage showed to be concentration dependent, and had achieved maximum entrapment efficiency with PTX of 200 $\mu\text{g/ml}$.

Table 4.2 Entrapment efficiency of pristine (p) and functionalized (f) CNTs

<i>f</i> -CNTs	Entrapment efficiency in % \pm μ g/ml			
	PTX 100 μ g	PTX 150 μ g	PTX 200 μ g	PTX 250 μ g
p SWNT	7.45 \pm 7.4	13.35 \pm 20.0	25.11 \pm 50.2	32.92 \pm 82.3
SWNT PEG 1:1	12.15 \pm 12.1	27.07 \pm 40.6	71.33 \pm 142.7	39.38 \pm 98.5
SWNT PEG 1:5	12.45 \pm 12.5	29.65 \pm 44.5	87.56 \pm 175.1	41.94 \pm 104.8
SWNT PF127 1:1	15.27 \pm 15.3	31.16 \pm 45.7	86.23 \pm 172.5	52.30 \pm 130.8
SWNT PF127 1:5	15.23 \pm 15.2	32.03 \pm 48.1	87.24 \pm 174.5	49.92 \pm 124.8
p MWNT	14.02 \pm 14.0	32.19 \pm 48.3	46.29 \pm 92.6	57.54 \pm 143.9
MWNT PEG 1:1	12.27 \pm 12.3	27.11 \pm 40.7	72.74 \pm 145.5	40.13 \pm 100.3
MWNT PEG 1:5	12.99 \pm 13	11.58 \pm 17.4	17.55 \pm 35.1	41.91 \pm 104.8
MWNT PF127 1:1	14.68 \pm 14.7	31.09 \pm 46.6	85.94 \pm 171.9	50.47 \pm 126.2
MWNT PF127 1:5	15.18 \pm 15.2	31.44 \pm 47.2	86.42 \pm 172.8	50.65 \pm 126.6

The entrapment efficiency expressed as a percentage of the total concentration of PTX for p-MWNT and p-SWNT is shown in Figure 4.31.

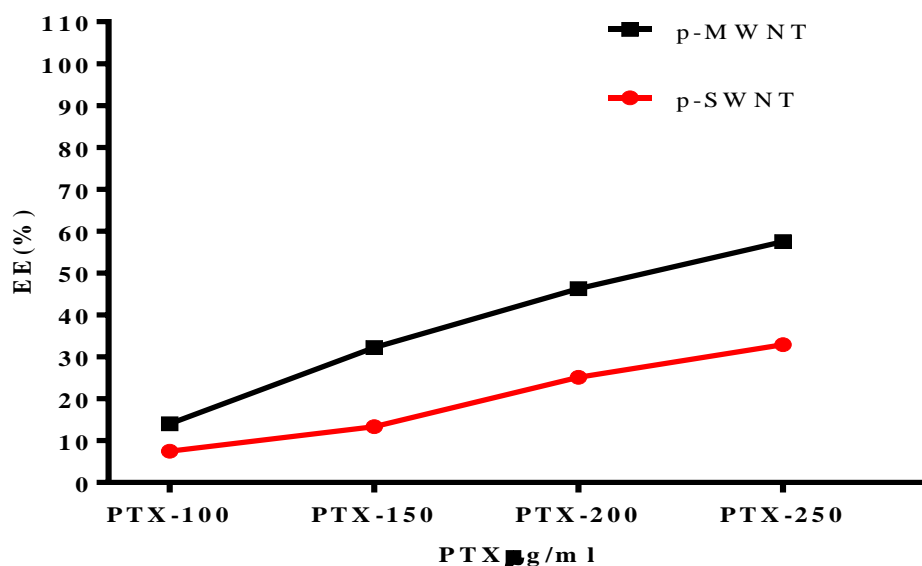


Figure 4.31 Entrapment efficiency of p-MWNT and p-SWNT

As the concentration of PTX is increasing from 100 µg/ml to 250 µg/ml the entrapment efficiency increases linearly in both cases for p-MWNTs and p-SWNTs. For p-SWNTs the entrapment efficiency increases by a factor of 5 from 7% to 33%, whereas for p-MWNTs the increase is less prominent by a factor of 4.1. However, the entrapment efficiency is considered very significant and is approximately double that of p-SWNTs ($p < 0.001$). The trend is as expected, and when MWNTs are used there is more space to entrapment for the drug onto the nanotubes. The PTX is attached to the outer surface of the CNTs. TEM micrographs shown the outer diameter (O.D.) of SWNT is in between 15-20 nm and the MWNT is between 30-40 nm. The diameter of MWNT is twice the size of SWNT. Hence, we can conclude that the entrapment efficiency of PTX increases

with the outer diameter of CNTs. However, further investigation would be required to verify this theory.

The entrapment efficiency of SWNTs (Figure 4.32) has been demonstrated and was observed that for SWNTs concentrations, highest entrapment efficiency were only achieved with 200 μ g/ml. The MWNTs formulations also show similar behaviour in Figure 4.33 .

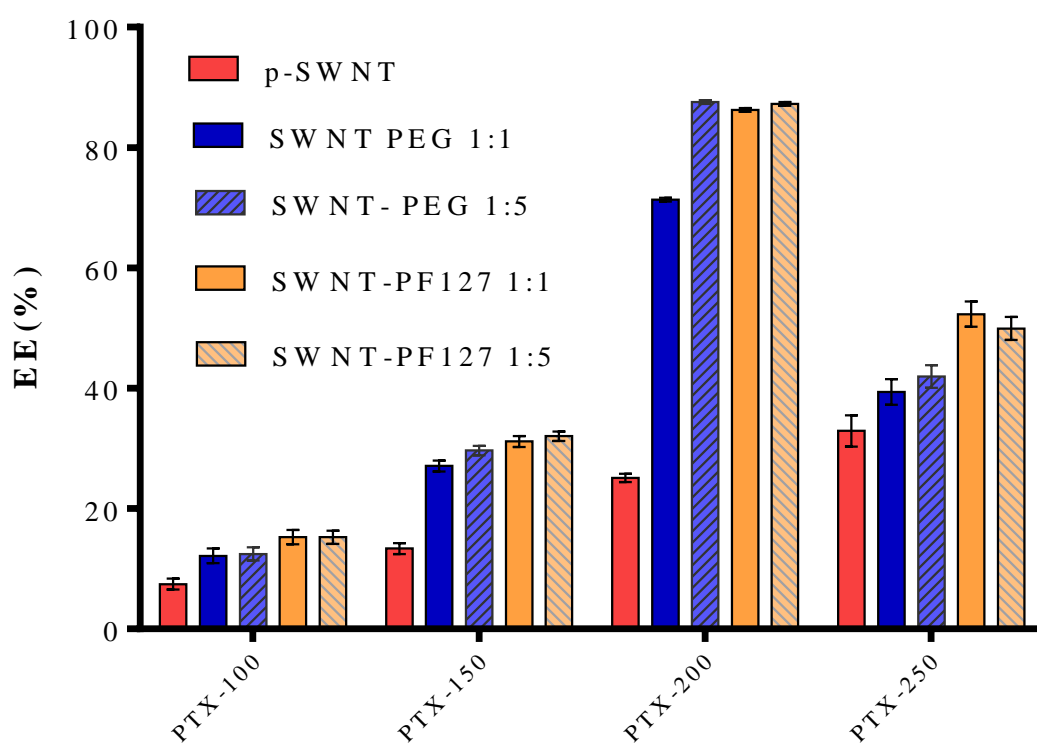


Figure 4.32 Entrapment efficiency of *f*-SWNT

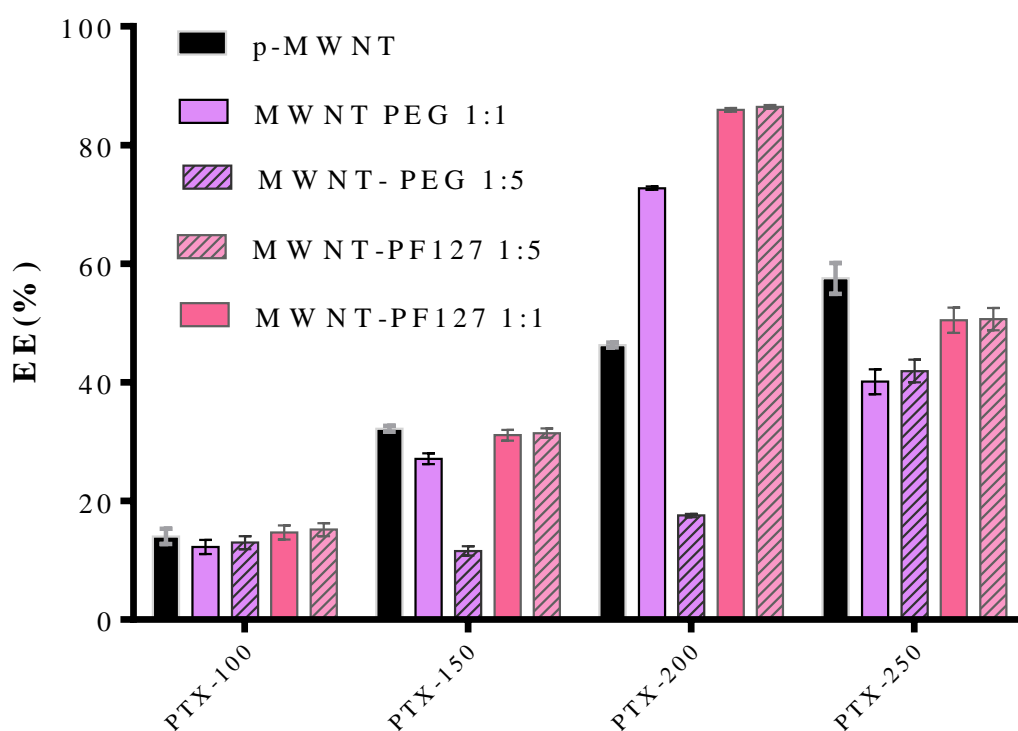


Figure 4.33 Entrapment efficiency of *f*-MWNT

The bar representing the formulation MWNT-PEG 1:5 has not been carried out in calculations as results were anomalous (Figure 4.34). For a significant difference between concentration 200 µg/ml Vs. formulations, the Bonferroni's multiple comparisons test has been carried out for all concentrations. Significantly higher entrapment efficiency was achieved with SWNT-PEG 1:5 and SWNT-PF127 ratios 1:5, respectively ($p < 0.05$).

To understand the correlation between the PTX concentrations and CNTs a graph has been plotted for all formulation (Figure 4.34).

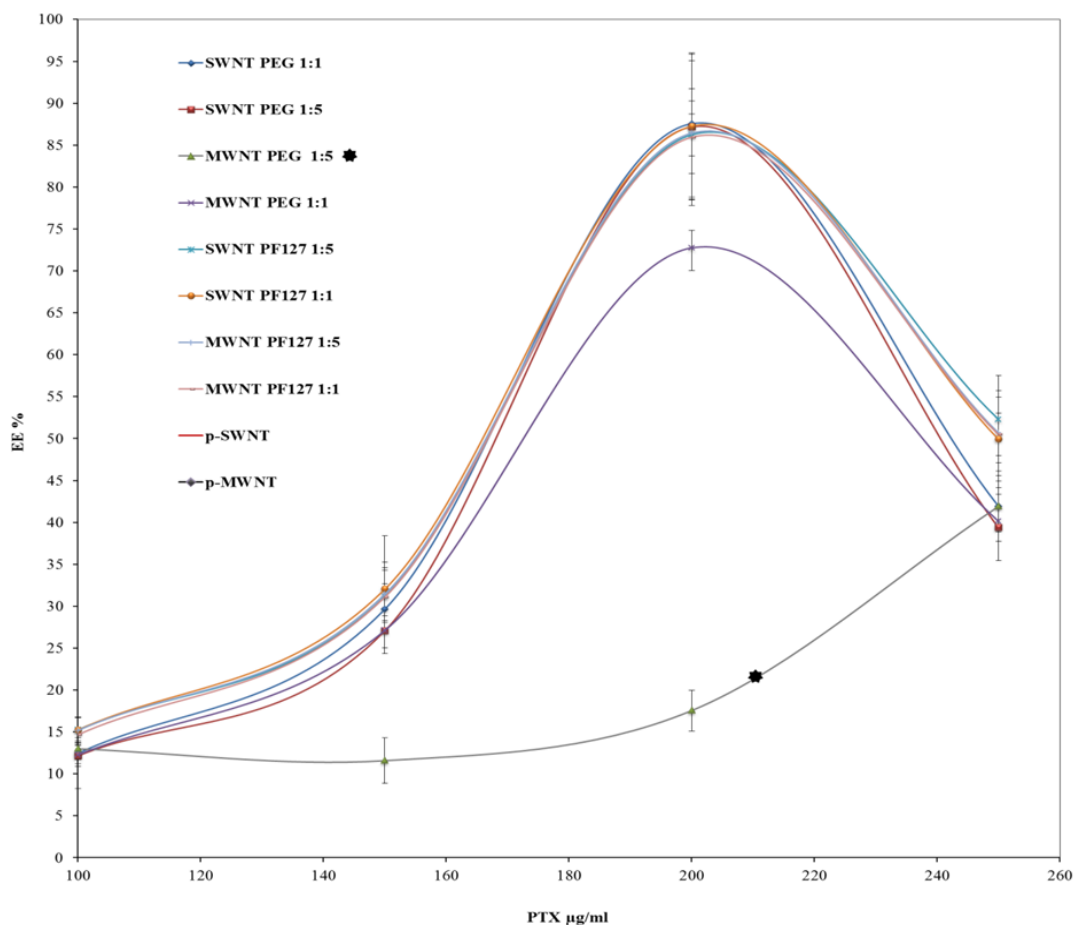


Figure 4.34 Paclitaxel *f*-CNTs and their entrapment efficiency

Entrapment efficiency has been plotted against PTX concentrations for all formulations investigated. The trends for all formulations were similar with the curves being bell shaped. Whilst the majority of formulations followed a set trend an anomaly was observed in the form of the curve generated by MWNT-PEG 1:5. The curve generated for this combination is significantly different from of other formulations. There are a number of different possible explanations for this. There is a very significant difference when all concentration compared to one another ($p < 0.001$). Also a significant difference was observed within the formulations ($p < 0.05$). In all CNTs formulations the entrapment efficiency has increased as the PTX concentration has increased achieving the maximum entrapment efficiency of 200 µg/ml. Thereafter, a negative trend was

observed for all formulations containing PTX. Peak entrapment efficiency of 200 $\mu\text{g/ml}$ PTX is shown in Figure 4.35.

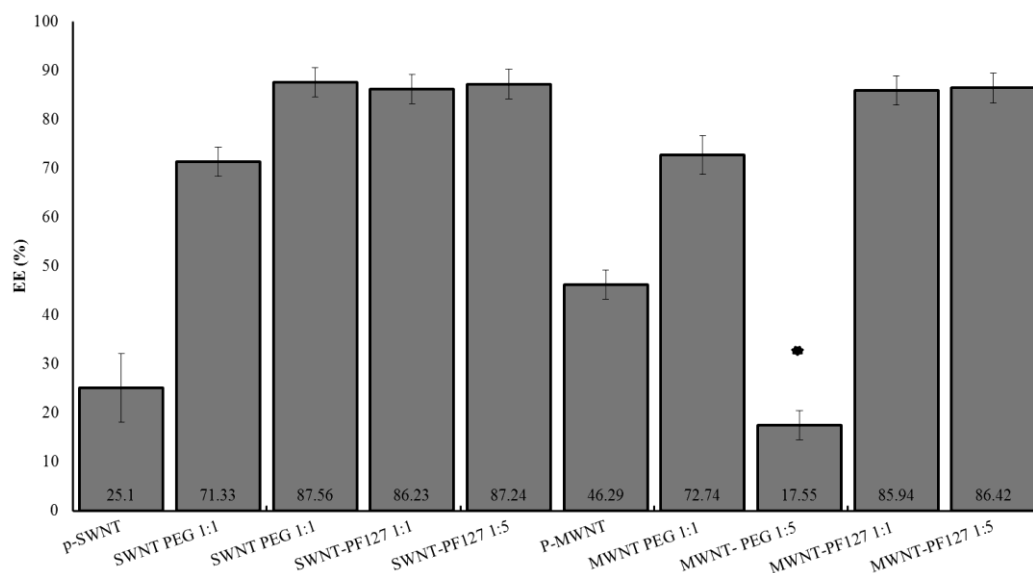


Figure 4.35 Entrapment efficiency achieved with all formulations at 200 $\mu\text{g/ml}$; the bar represent with * is anomalous and not calculated with other formulations

When SWNTs are compared, as expected the addition of both surfactants PEG and PF127 to the CNTs increases the entrapment efficiency. As the amount of PEG is increased the entrapment efficiency increases from 71.33% to 87.56%. The addition of PEG at a ratio of 1:1 increases the entrapment efficiency from 25% to 71%, representing a 3 fold increase. The results suggest a stoichiometric effect due to non-covalent bonding of the surfactant onto the walls of CNTs and only as for the PTX molecules in solution. However, further work is required to investigate and verify this hypothesis.

4.6.3 Saturation effect

From Figure 4.34, maximum entrapment efficiency was reached at 200 $\mu\text{g/ml}$, thereafter a decreasing trend was observed. As constructed in Figure 4.36 the concentration increases when surface side of the CNTs become occupied by surfactants or PTX and thus all the sides are saturated. Further increases of concentration results in collision behaviour to PTX in solution and the non-covalently attached PTX, the CNTs carry it to desorb.

This process of detachment of PTX from CNTs increases these results in decreasing of entrapment efficiency.

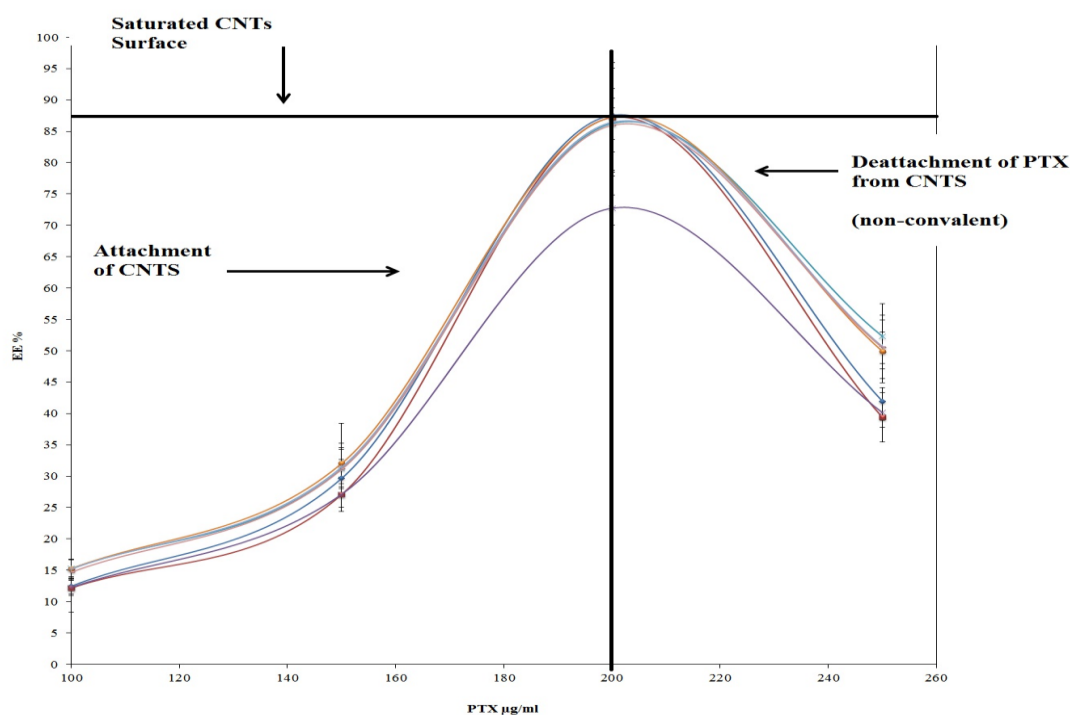


Figure 4.36 Correlation of SWNTs and MWNTs against PTX concentrations

4.7 Conclusions

The characterization and functionalization of both SWNTs and MWNTs using various techniques has been presented. Results confirmed and showed that samples were utilized in this study were SWNTs and MWNTs. It was concluded that SWNTs have diameters ranging from 0.67 ± 1.03 nm ($p < 0.05$) which is in agreement with small CNT diameter that are favourable for studies for biomedical applications (Yang, Thordarson et al. 2007).

Also an establishment was confirmed that CNTs were functionalized with two different biocompatible surfactants, including PEG400 and PF127 and their ζ -potential were measured for their stability. The decrease of the Raman intensity of G-band and increase of D-band were observed for the functionalized CNTs were due to a change in the electronic properties and/or an alteration of the vibrational modes of the tubes.

Loading efficiency of Paclitaxel onto CNT-Surfactants was dependent on the type of CNTs, surfactant and concentrations of drug. However, PTX entrapment percentage showed concentration dependency, and to have reached the maximum entrapment efficiency at 200 $\mu\text{g/ml}$.

CHAPTER 5

In Vitro Cytotoxicity of *f*-CNTs (RESULTS AND DISCUSSION)

“Science never solves a problem without creating ten more”

(George Bernard Shaw)

5.1 In Vitro Cytotoxicity

Various types of CNTs have been utilised for *in vitro* studies in cancer treatment. Its purpose was to achieve a greater decrease of cell viability in cancer cells in combination of drug CNTs formulations. Paclitaxel (PTX) is an anti-cancer drug that has been used for various types of cancer. The purpose of cytotoxicity test is to assess the effect of PTX, *f*-CNTs and PTX-*f*-CNTs and compare between the concentrations and types of CNTs.

In this chapter, cell culture studies are demonstrated and related results are presented. Two cell lines were investigated in order to analyse cytotoxicity; including SVGP12 (normal human brain cells known as astrocytes) and human glioblastoma-astrocytoma grade IV Glioma cells (U87-MG). Cell density selection was based on cell growth curves that was generated and curve line were established for both cell lines. Cell viability in percentage was analyzed with the following equation:

$$\text{Cell Viability (\%)} = \frac{\text{Absorbance of treated group}}{\text{Absorbance of control group}} \times 100$$

Data was analyzed and $p < 0.05$ was found for treated cells compared to untreated (controls), which was considered significant. Statistical analysis were performed using One-way ANOVA followed by Tukey's multiple comparison test (to compare all groups) or Two-way ANOVA followed by Bonferroni's multiple comparison test (Pristine and Functionalized CNTs and PTX various concentrations).

5.2 Growth curve of cell lines

For both cell lines, varied densities were assessed ranging from 10^3 - 10^5 cells/well. Cells were seeded and allowed to grow for seven days and their densities were of 10^3 , 10^4 and 10^5 cells/well. Each day their absorbance was measured. Measurements values in between 0.7-0.9 (pure media) were expected for appropriate seeding densities. This information was needed to perform the cytotoxicity assay and identify the effect.

5.2.1 Growth curve of SVGp12

The absorbance values for the growth curves of SVGp12 cell lines were significantly different for all three seeding densities measured each day ($p < 0.05$). Their seeding densities were plotted and it was observed in microscopic picture of cell density of 10^5 (Figure 5.1).

Density of 10^3 cells/well increased to nearly $198 \pm 6.56\%$ and the absorbance readings were in the range of 0.1-0.15 units at day 7. Whereas, density of 10^4 cells/well was increased to $251 \pm 7.5\%$, however the absorbance readings were in the range of 0.3-0.33 units. Subsequently, once 10^5 cells/well density reached $260 \pm 8.9\%$ and their absorbance values in the range of 0.78-0.81 units.

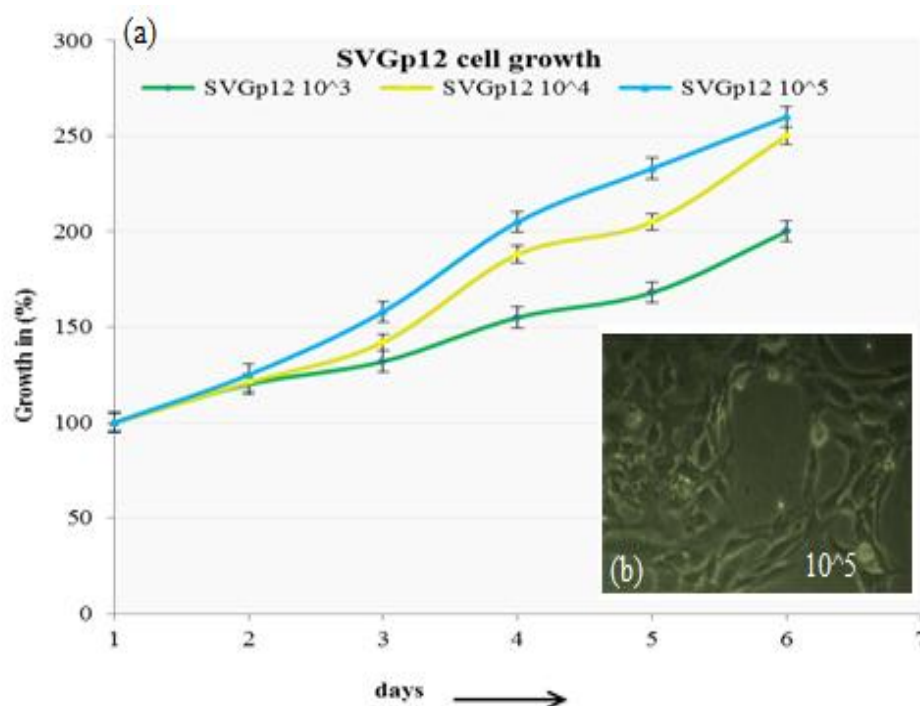


Figure 5.1 (a) Growth percentage of SVGp12 from three densities and (b) microscopic picture of 10^5 cell/well (x100)

5.2.2 U87-MG growth curve

Significant differences were observed for all three densities 10^3 , 10^4 and 10^5 ($p < 0.05$). According to Figure 5.2(a), highest cell absorbance in the range of 0.92-0.96 units and approximate cell growth of $301 \pm 6.6\%$ was achieved through 10^5 cells/well density at day 6. This also is in agreement with the microscopic picture shown in Figure 5.2(b). In contrast, the growth for 10^3 and 10^4 cells/well densities at day 6 demonstrated values in the range of 0.16-0.19, 0.31-0.35 units with cell growth of $240 \pm 5.6\%$ and $285 \pm 6.5\%$, respectively. The images were in accordance with growth curves obtained via the absorbance readings as the number of cells per well is directly proportional to the absorbance or cell viability.

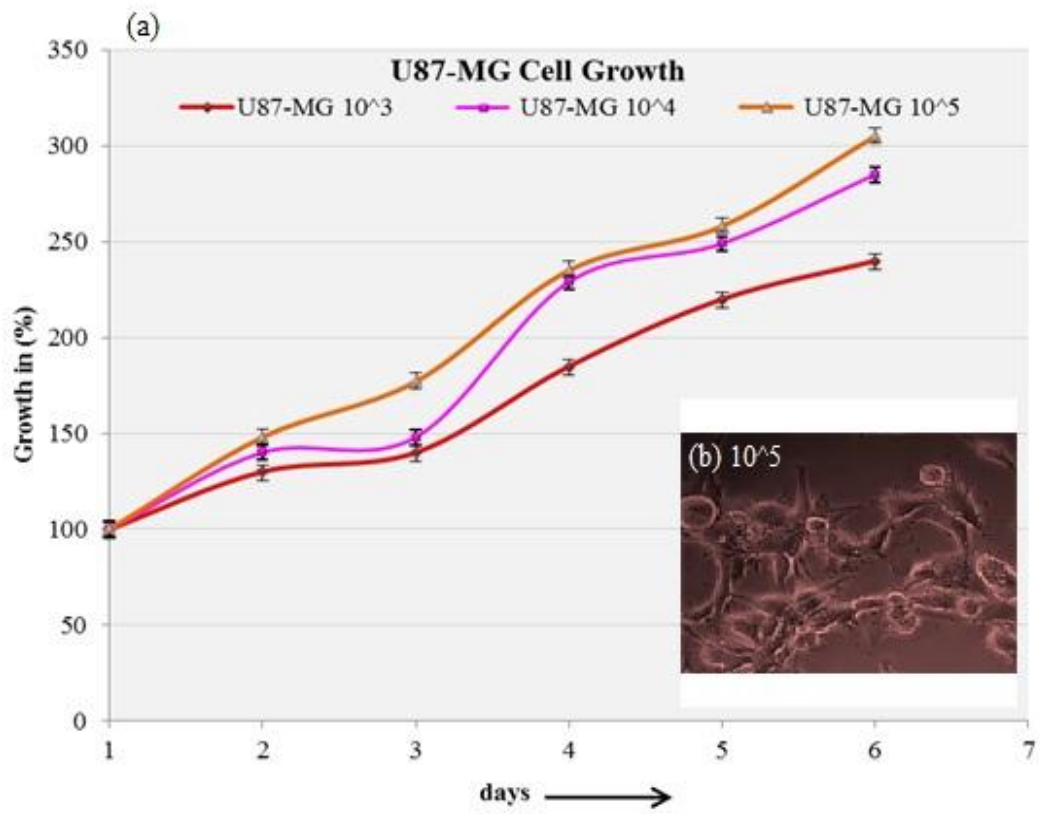


Figure 5.2 (a) Growth percentage of U87-MG from three densities and (b) microscopic picture of 10^5 cell/well density (x100)

5.3 Effects of PTX on SVGp12 and U87-MG

To measure the effect of PTX on SVGp12 and U87-MG grade IV glioblastoma, cells were treated for 24 and 48 hours, respectively. Data obtained are expressed as mean% \pm SD, n = 3 and p-value of <0.05 for untreated (control) compared to treated cells are demonstrated.

5.3.1 Effect of PTX concentrations of SVGp12

SVGp12 cell lines were treated for 24 and 48 hours with four different concentration ranging from 100-250 μ g/ml. Evidently, there was a decrease of cell viability and showed to be PTX concentration dependent (Figure 5.3).

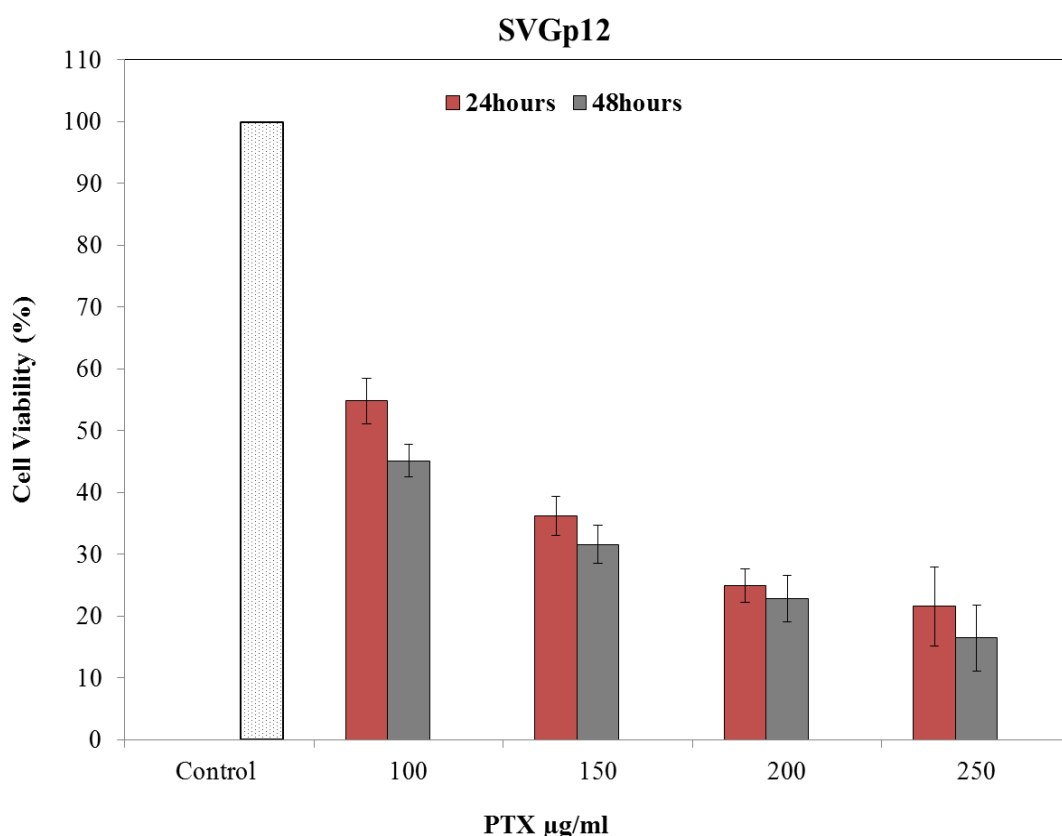
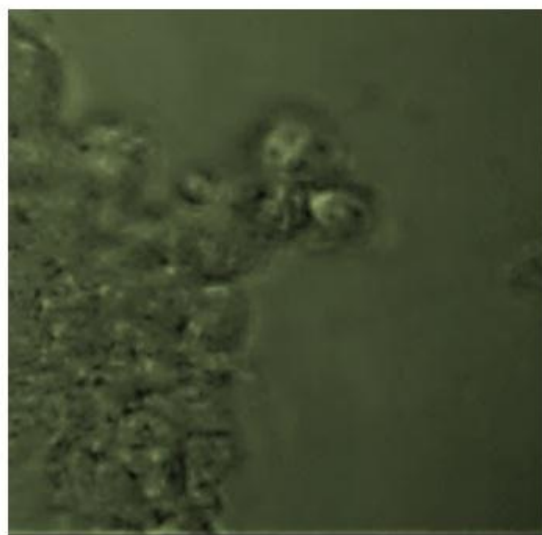


Figure 5.3 The effect of different PTX concentrations on SVGp12 cell line. The error bars represent the standard deviation (SD) of three samples

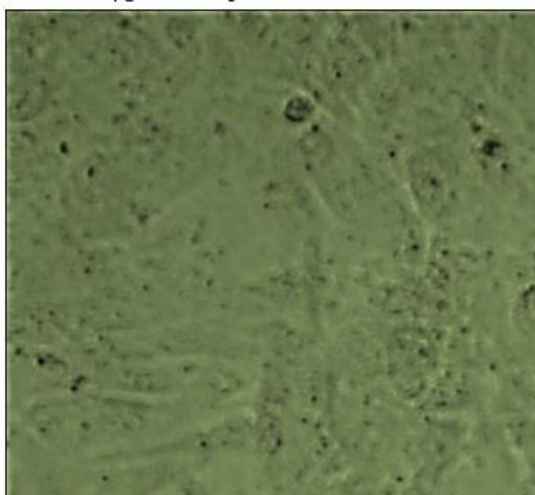
Higher rate of cell death was observed with increased concentrations of paclitaxel. Significant toxicity was observed for all concentrations and their respective cell viabilities. However, cell viability for concentration of 100 $\mu\text{g/ml}$ was $54\% \pm 2.0$ at 24 hours and $45\% \pm 2.6$ at 48 hours, moreover 250 $\mu\text{g/ml}$ showed cell viabilities of $21\% \pm 1.4$ at 24 hours and $16\% \pm 1.6$ at 48 hours ($p < 0.05$). This was confirmed with microscopic pictures shown in Figure 5.4 that were treated for 24 hours and 48 hours (Figure 5.5). Minimal viable cells were observed for the highest concentrations of PTX (250 $\mu\text{g/ml}$).



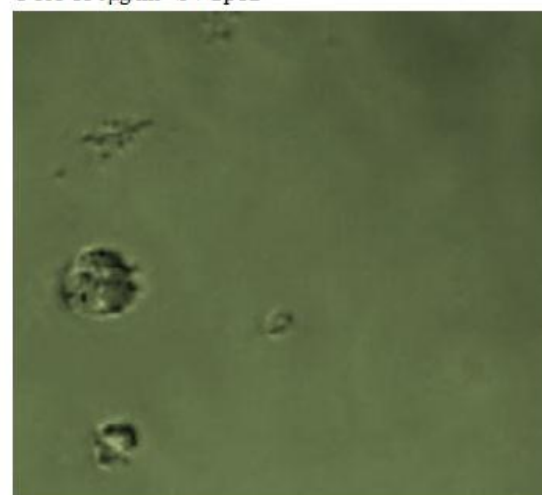
PTX 100µg/ml SVGp12



PTX 150µg/ml SVGp12



PTX 200µg/ml SVGp12



PTX 250µg/ml SVGp12

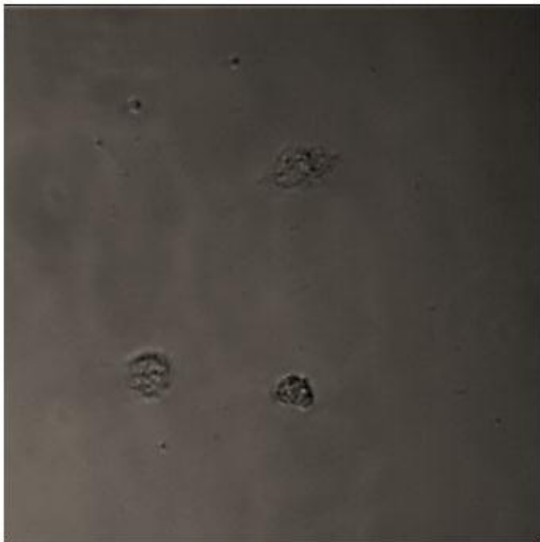
Figure 5.4 Microscopic pictures of SVGP12 treated with Paclitaxel for 24 hours (x100)



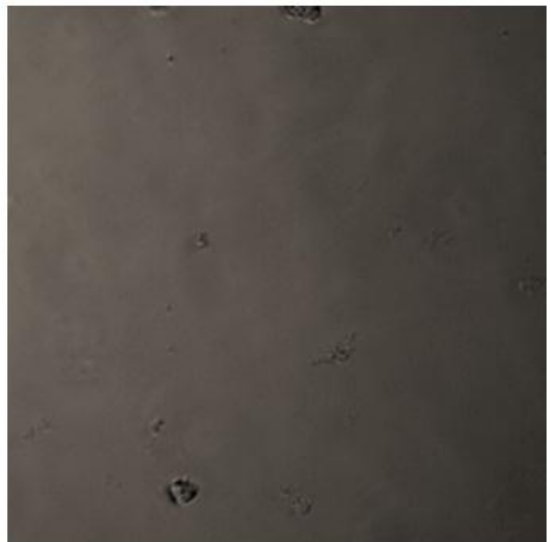
PTX 100 µg/ml SVGp12



PTX 150 µg/ml SVGp12



PTX 200 µg/ml SVGp12



PTX 250 µg/ml SVGp12

Figure 5.5 Microscopic pictures of SVGP12 treated with Paclitaxel for 48 hours (x100)

5.3.2 Effects of PTX concentration on U87-MG

Dose dependent effect of Paclitaxel on U87-MG cells, showed the influence of different Paclitaxel concentrations at 24 hours and 48 hours.

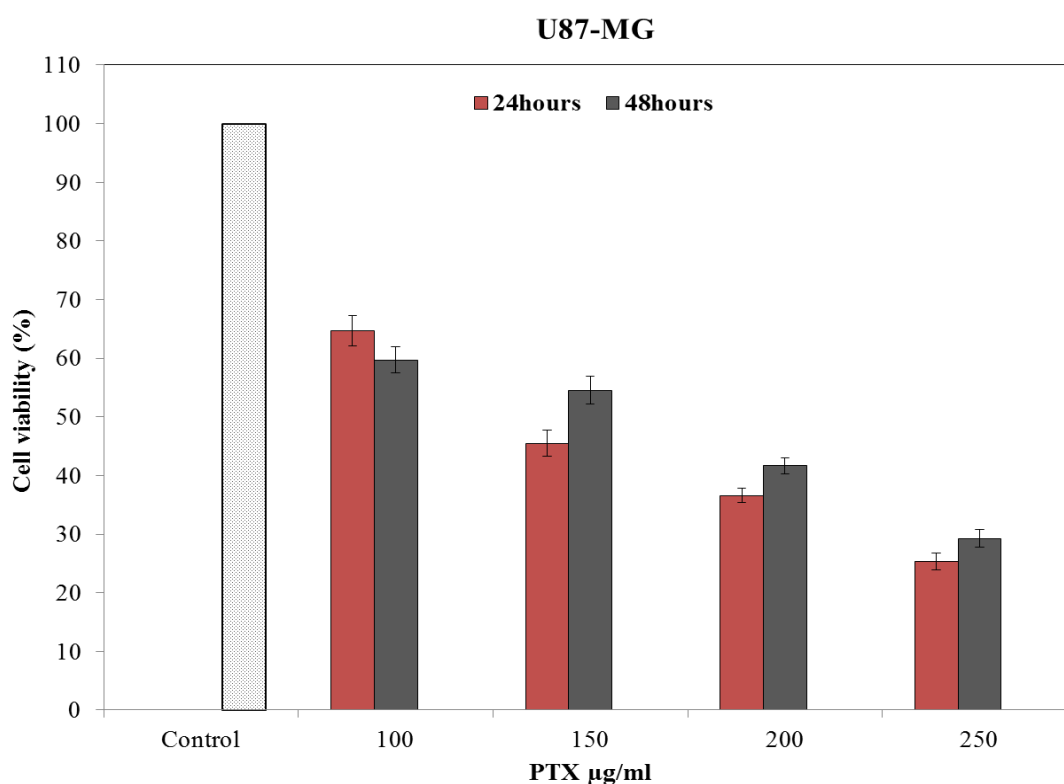
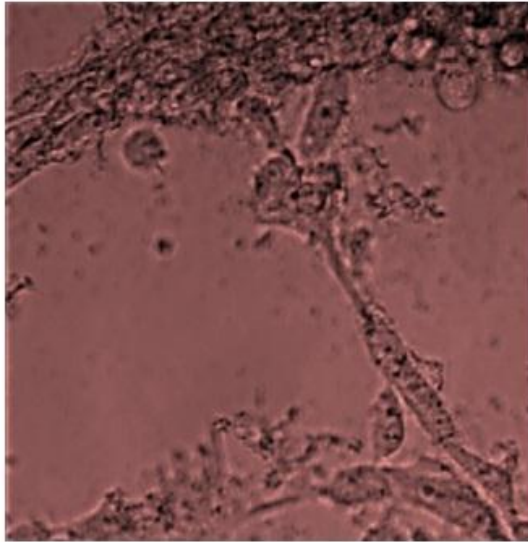
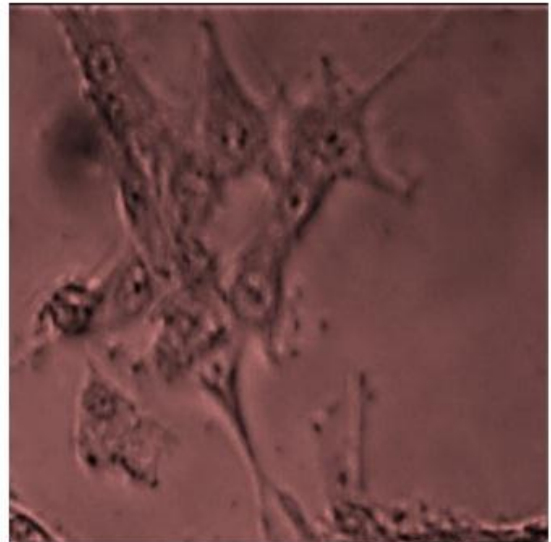


Figure 5.6 The effect of different PTX concentrations on U87-MG cell lines. The error bars represent the standard deviation (SD) of three samples

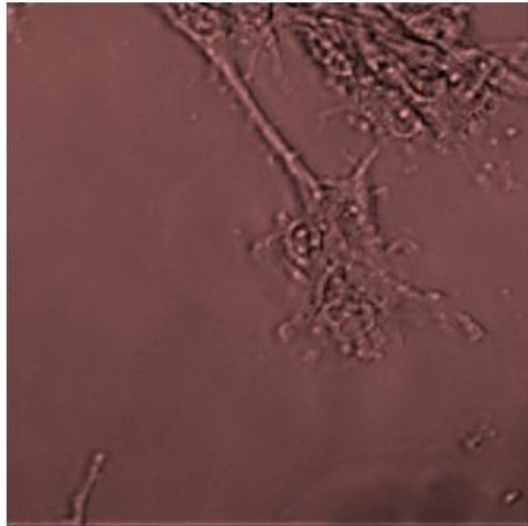
As can be observed from Figure 5.6, an addition of 100 $\mu\text{g/ml}$ of Paclitaxel treated cells for 24 hours, cell viability was found to be $64\% \pm 2.2$. Thereafter, the cell viability significantly decreased with higher concentrations of Paclitaxel ranging from 150 $\mu\text{g/ml}$ with cell viabilities of $42\% \pm 2.2$ and $36\% \pm 1.2$ for 200 $\mu\text{g/ml}$ and for 250 $\mu\text{g/ml}$ viability found to be $25\% \pm 1.4$, respectively ($p < 0.05$). No significant difference was observed for concentrations in between 200 $\mu\text{g/ml}$ and 250 $\mu\text{g/ml}$; confirmation was established with microscopic pictures shown in Figure 5.7.



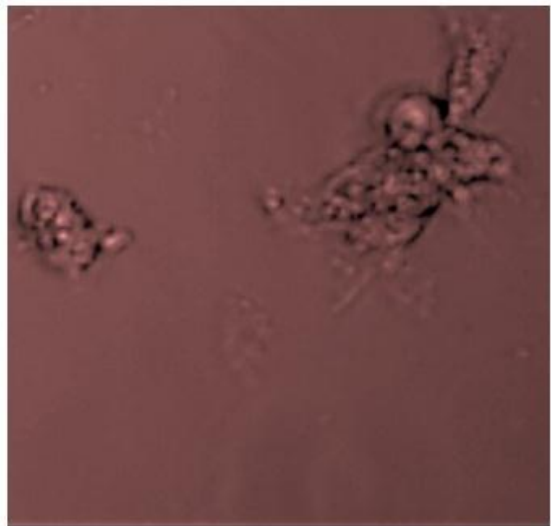
PTX 100µg/ml U87-MG



PTX 150µg/ml U87-MG



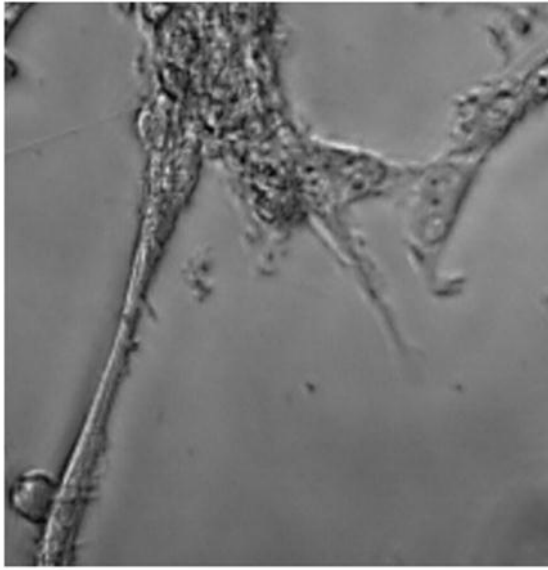
PTX 200µg/ml U87-MG



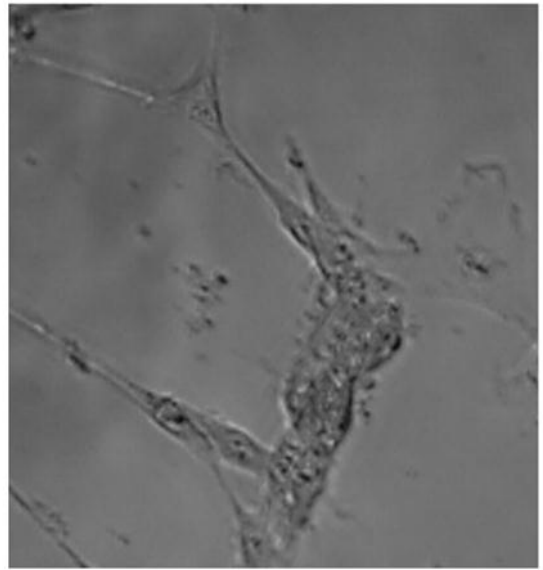
PTX 250µg/ml U87-MG

Figure 5.7 Microscopic pictures of U87-MG different treated with four different concentrations for 24 hours (x100)

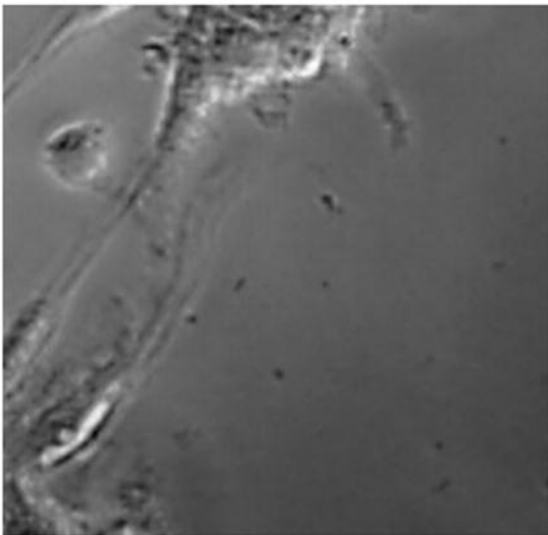
Cells that were treated for 48 hours also showed significant differences in cell viabilities for all concentrations, their percentage values were $59\% \pm 2.2$ for $100 \mu\text{g/ml}$, $54\% \pm 2.3$ for $150\mu\text{g/ml}$, $41\% \pm 1.3$ for $200 \mu\text{g/ml}$ and for $250 \mu\text{g/ml}$ observed cell viability was $29\% \pm 1.5$, respectively ($p < 0.05$). Significantly higher values were achieved for both concentrations $200 \mu\text{g/ml}$ and $250 \mu\text{g/ml}$ for comparative strengths that were treated for 24 hours ($p < 0.05$). This may be attributed to the fast multiplication of cancer cells and thus a higher concentration of drug is prudent. Furthermore, there is an extremely significant difference for untreated cells and paclitaxel treated cells ($p < 0.001$). Moreover, this is also in agreement with the microscopic picture in Figure 5.8.



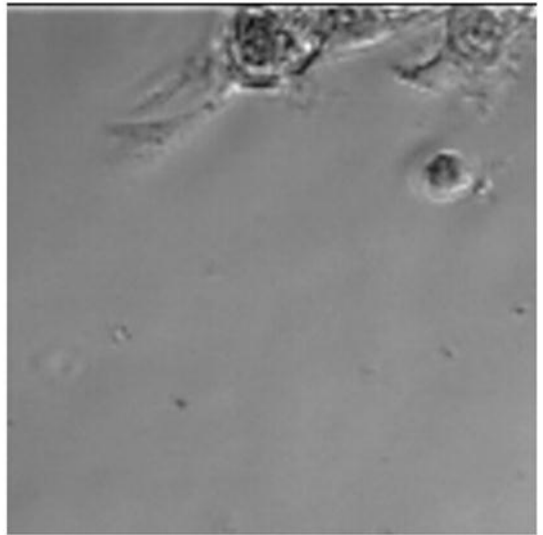
PTX 100µg/ml U87-MG



PTX 150µg/ml U87-MG



PTX 200µg/ml U87-MG



PTX 250µg/ml U87-MG

Figure 5.8 Microscopic pictures of U87-MG treated with four different concentrations for period of 48 hours (x100)

5.4 Effect of pristine CNTs on SVGp12 and U87-MG

Assessment of pristine (p) CNTs cytotoxicity, including SWNTs and MWNTs were examined on both SVGp12 and U87-MG cell lines. Four different concentrations of CNTs mg/ml of media were investigated and cells were treated for 24 and 48 hours. Data obtained are expressed as mean% \pm S.D, n = 3, p<0.05 for untreated (control) compared to treated cells.

5.4.1 Effect of p-CNTs on SVGp12

Cell viability observations from Figure 5.9 concluded no significant difference between p-CNTs and SVGp12. Even at high concentrations of 15 mg/ml, both p-SWNTs and p-MWNTs cells retained their viability. Although, no significant difference was observed, cells treated with p-SWNTs (1mg/ml) for 24 hours, showed minimal increase in cell viability (105% \pm 2.5).

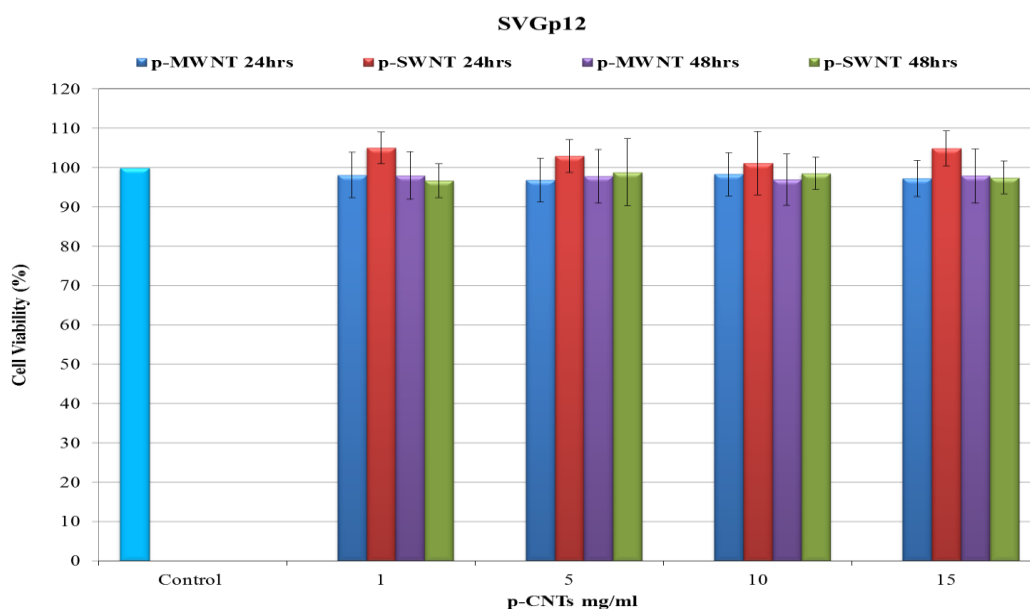


Figure 5.9 SVGp12 cell lines treated with pristine CNTs for 24 and 48hours. The error bars represent the standard deviation (SD) of three samples

Moreover, as expected, various concentrations of p-SWNTs and p-MWNTs showed no significant toxicity on SVGp12 cell line. Figure 5.10 shows SVGp12 cells treated with p-SWNT and p-MWNT (1 mg/ml) for 24 hours.

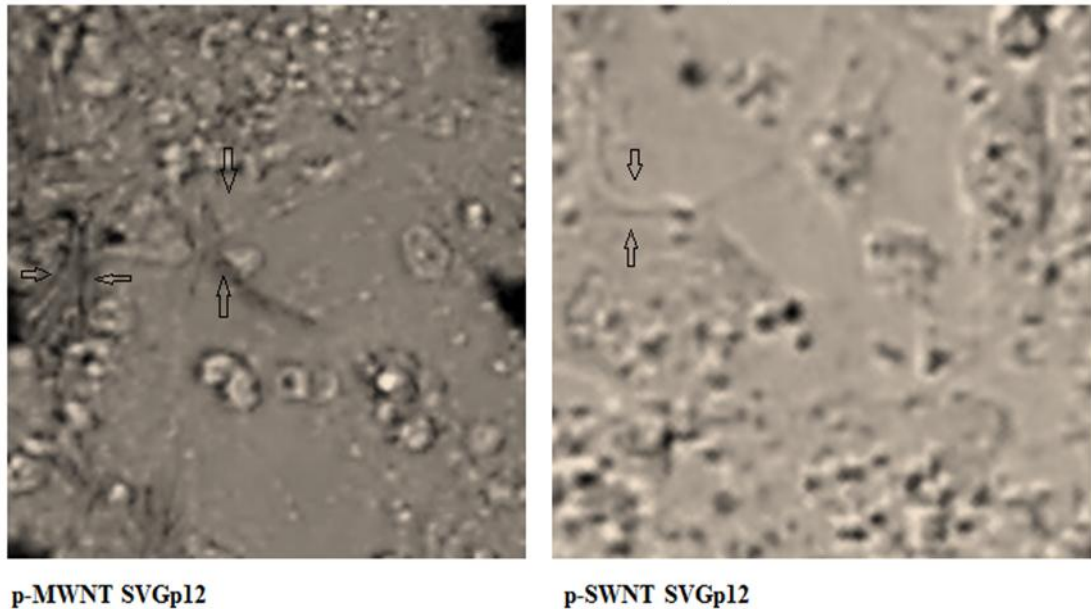


Figure 5.10 Microscope pictures of p-MWNT and p-SWNT of SVGp12 treated for 24 hours (x200)

5.4.2 Effect of p-CNTs on U87-MG

Viability of cell lines U87-MG are shown in Figure 5.11. No significant differences were determined for any concentrations when compared to untreated cells. Concluding that even at high concentration of 15 mg/ml, p-SWNTs and p-MWNTs showed no effect. Nevertheless, p-CNTs presence in cells treated for 24-48 hours were confirmed from the microscopic pictures (Figure 5.12).

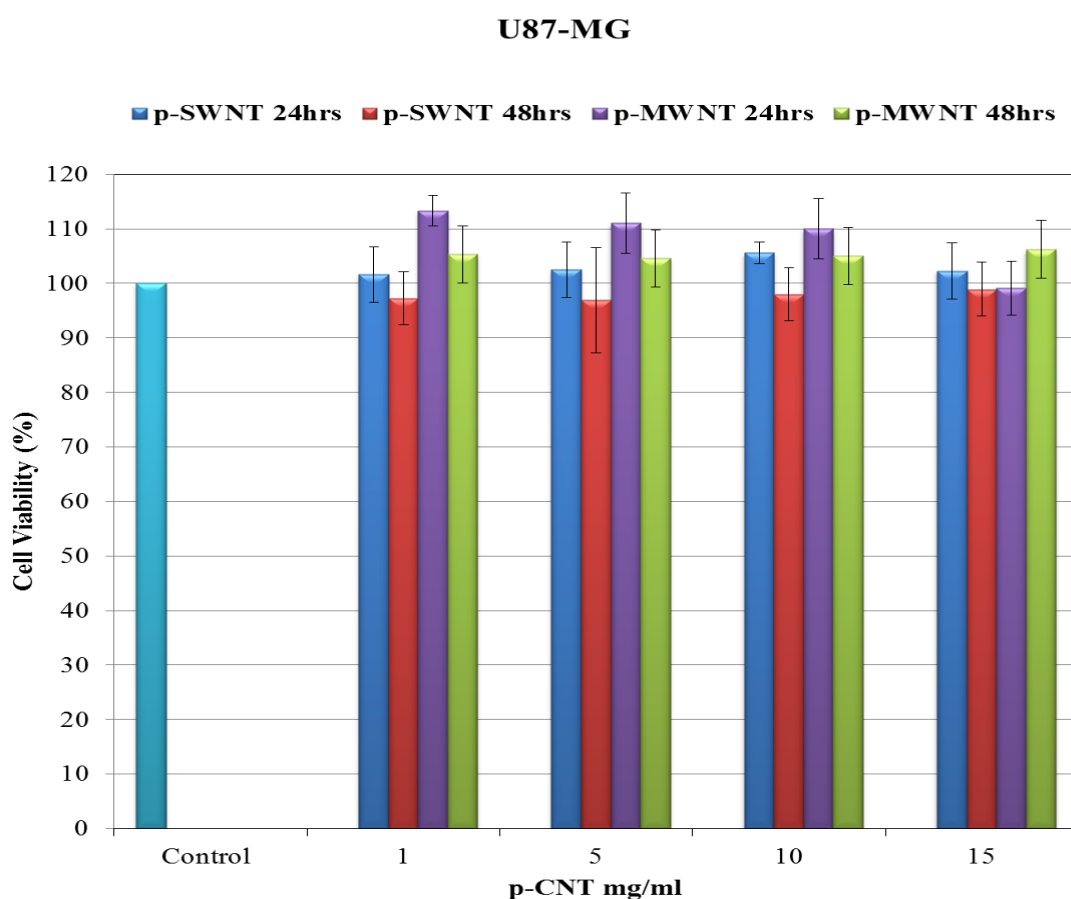
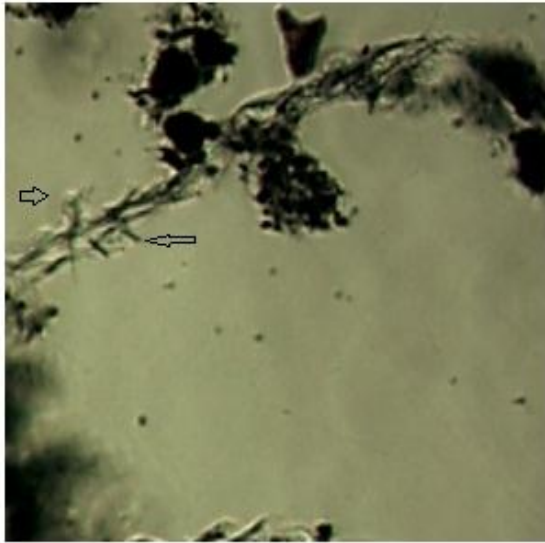


Figure 5.11 Different concentrations of pristine (p) CNTs (CNTs) on U87-MG cell line. The error bars represent the standard deviation (SD) of three samples



p-SWNT U87-MG



p-MWNT U87-MG

Figure 5.12 Microscope pictures of p-MWNT and p-SWNT of U87-MG (x200)

5.5 PTX and p-CNTs cytotoxic effect on SVGp12 and U87-MG

Comparison between PTX and p-CNTs was carried out on SVGp12 and U87-MG for a period of 24 and 48 hours. For this experiment, four different concentrations of PTX were utilized. The results are given in mean i.e. $\text{mg} \pm \text{SD}$, while IC_{50} represents the concentrations of a drug that is required for 50% inhibition *in vitro*.

5.5.1 Effect of PTX and p-CNTs on SVGp12

No significant difference was observed for PTX-p-CNTs in comparison with PTX alone for any given concentration (Figure 5.13). However, as expected there is a significant difference between PTX concentrations ($p < 0.05$).

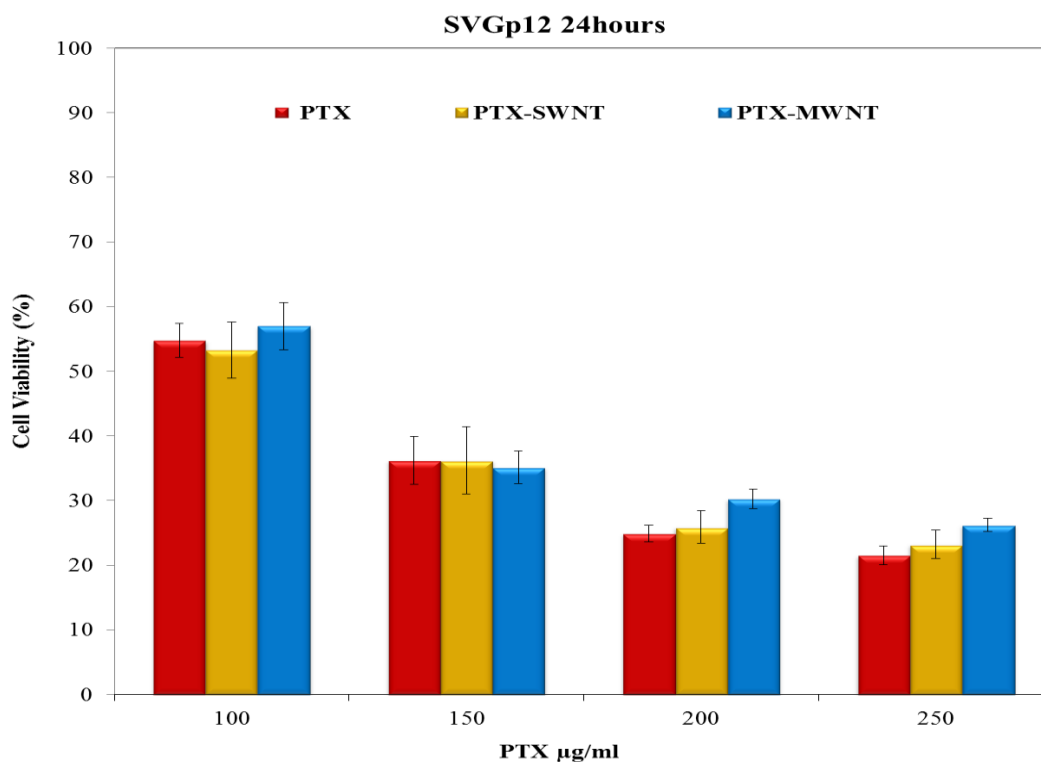


Figure 5.13 Cell viability of SVGP12 treated with PTX alone and p-CNT-PTX for 24 hours. The error bars represent the standard deviation (SD) of three samples

On comparison of the effect of p-CNT-PTX and PTX alone, the results show that CNTs do not have an effect on PTX concentrations. Even when cells were treated for longer period (48 hours), showed no significant difference (Figure 5.14).

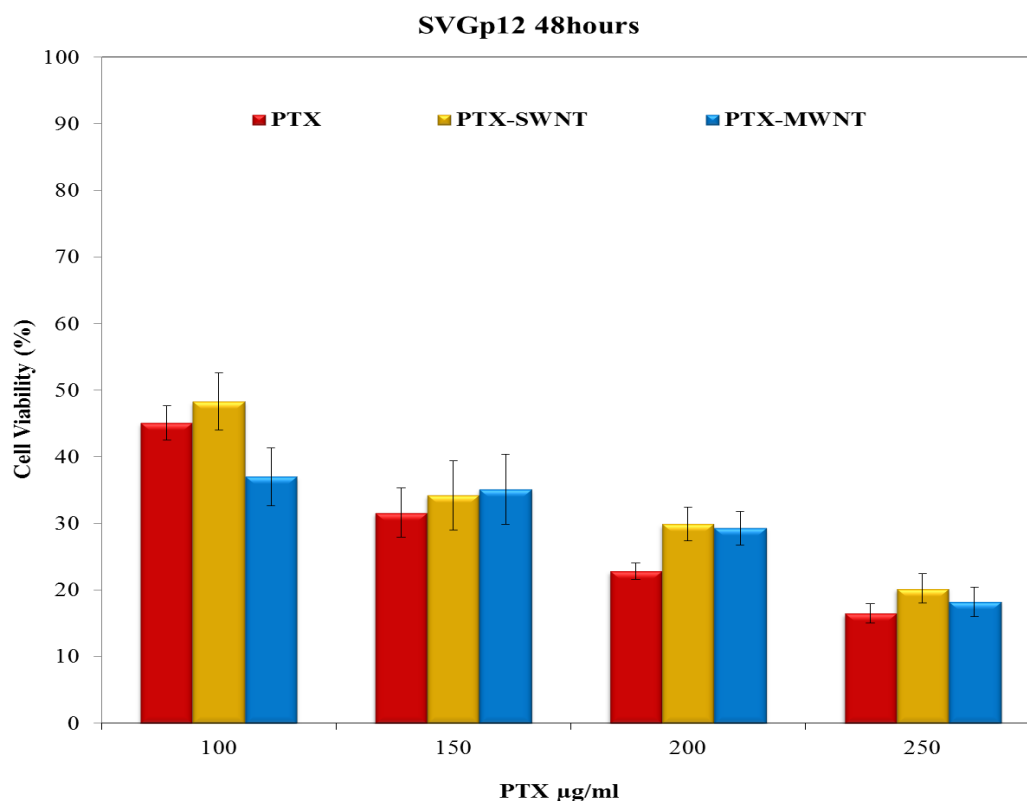


Figure 5.14 Cell viability of SVGp12 treated with PTX alone and p-CNT-PTX for 48 hours. The error bars represent the standard deviation (SD) of three samples

The presented values in Table 5.1 shows IC_{50} of all formulations and it can be seen that 6.2 mg (PTX) was required to inhibit 50% of SVGp12. Similar IC_{50} values were observed for PTX-SWNTs (6.4 mg), however 7.3 mg of PTX-MWNTs was necessary to inhibit 50% of cells. No significant difference can be observed in between IC_{50} values when compared to one another.

Table 5.1 IC₅₀ Values of the formulations in mg for SVGp12 cells

Formulations	IC ₅₀ mg ± SD	IC ₅₀ mg ± SD
	SVGp12 (24 hours)	SVGp12 (48 hours)
PTX	6.2 ± 1.1	5.7 ± 1.2
PTX-SWNT	6.4 ± 1.0	6.0 ± 1.0
PTX-MWNT	7.3 ± 0.8	5.1 ± 1.0

5.5.2 Effect of PTX and p-CNTs on U87-MG

U87-MG cell lines were treated with PTX alone (control) and PTX-SWNTs and PTX-MWNTs for 48 hours. According to Figure 5.15 cell viability values for concentrations 150 µg/ml, 200 µg/ml and 250 µg/ml showed no significant difference.

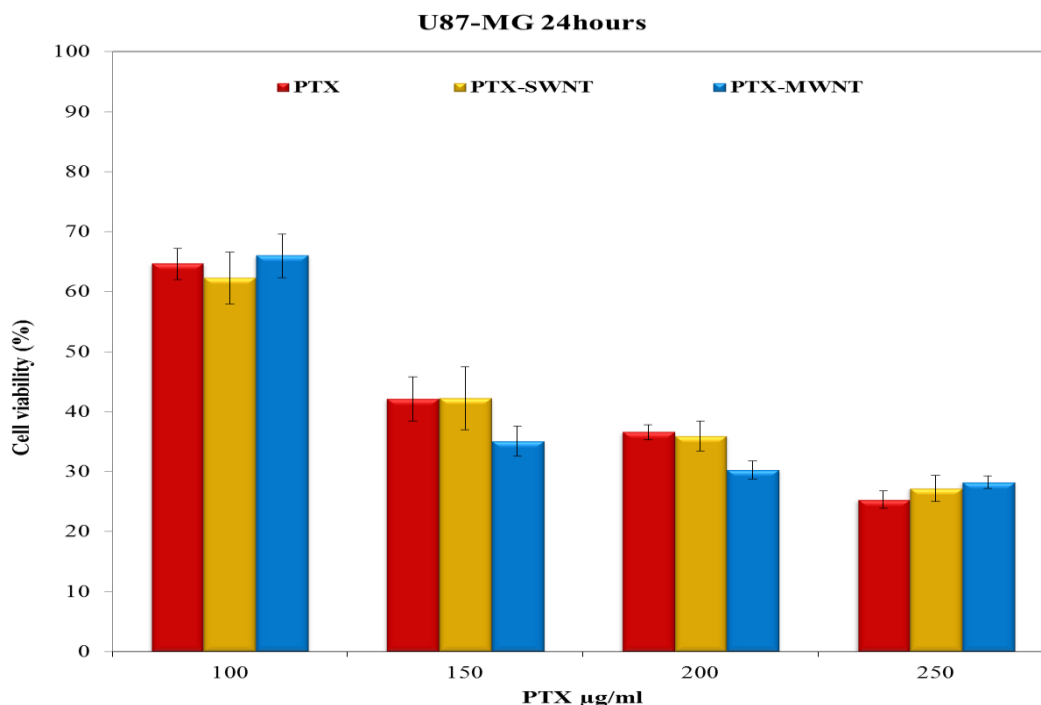


Figure 5.15 Cell viability of U87-MG treated with PTX alone and p-CNT-PTX for 24 hours The error bars represent the standard deviation (SD) of three samples

Cells treated for 48 hours elicited similar cell viabilities when compared in concentrations of PTX alone and in comparison to PTX-SWNTs and PTX-MWNTs (Figure 5.16). Moreover, no significant difference was demonstrated in IC₅₀ values no.

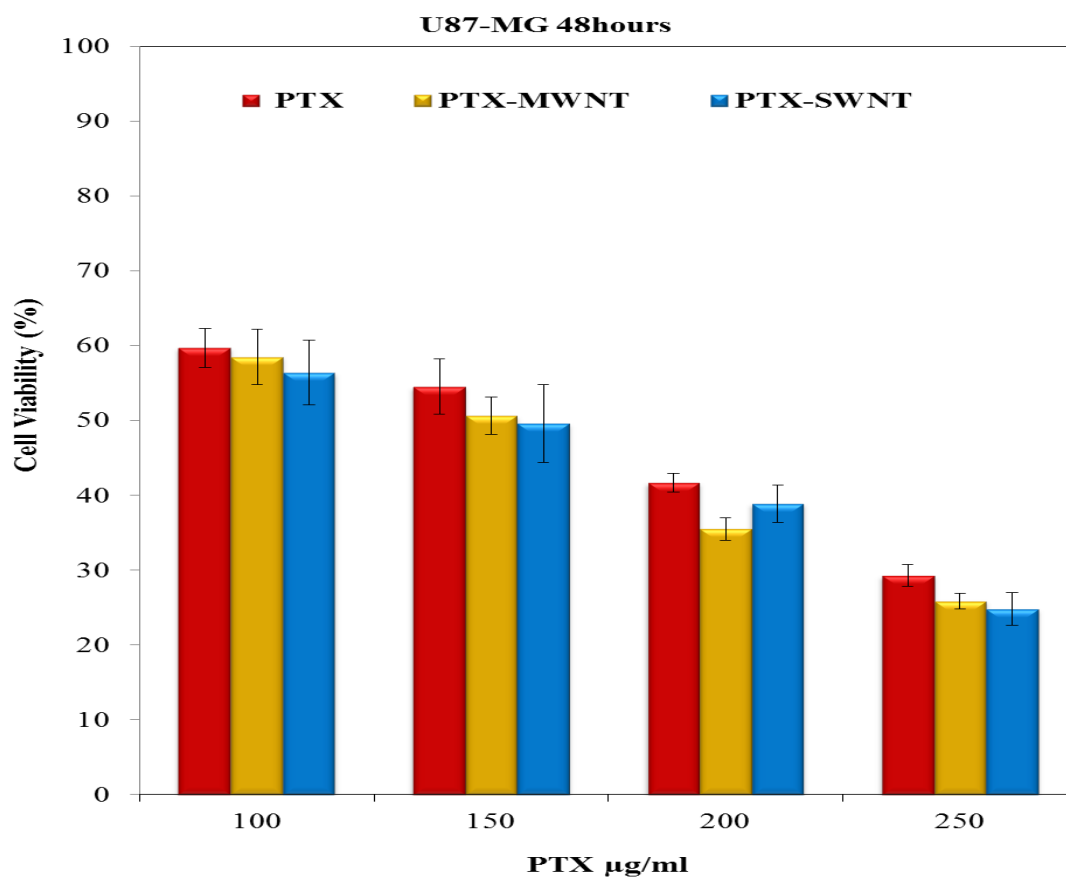


Figure 5.16 Cell viability of U87-MG treated with PTX alone and p-CNT-PTX for 48 hours. The error bars represent the standard deviation (SD) of three samples

Table 5.2 IC₅₀ Values of the formulations in mg for U87-MG cells

Formulations	IC ₅₀ mg ± SD	IC ₅₀ mg ± SD
	U87-MG (24 hours)	U87-MG (48 hours)
PTX	9.0 ± 1.5	11.0 ± 2.0
PTX-SWNT	8.8 ± 1.5	7.0 ± 1.5
PTX- MWNT	5.9 ± 0.5	7.6 ± 1.6

5.6 Effect of PTX-*f*-CNT in comparison with PTX alone and PTX-CNT on SVGp12 and U87-MG

Utilization of *f*-CNTs, including SWNTs and MWNTs were achieved with two different surfactants, namely PEG400 and PF127. Each *f*-CNTs was conjugated with four different concentrations of PTX. As controls, individually PTX, PF127 and PEG400 were compared with *f*-CNTs-PTX complexes. Data were expressed using Two-way ANOVA, followed by Bonferroni's multiple comparison test to demonstrate the significance ($p < 0.05$) of the formulations. Furthermore, the IC_{50} for each formulation was carried out to show the concentration of PTX that was required for 50% inhibition on each cell line.

5.6.1 Cytotoxic effect of CNT-PTX conjugate functionalized with PF127 and PEG400 on SVGp12

Data shown in Figure 5.17 demonstrated the effect of all formulations utilized on human astrocytes cell line (SVGp12). Respective cell lines were treated for 24 and 48 hours. Observed data showed significant differences ($p < 0.001$) for all formulations once compared to untreated. As expected PEG400, PF127, MWNTs and SWNTs showed no significant difference. PTX alone had a very significant effect at both time intervals ($p < 0.0001$). Although, formulations of PTX conjugated with *f*-CNTs demonstrated to be less toxic. Moreover, SWNT-PF127-PTX was confirmed to have significantly lower toxicity effects, maintaining cell viability of $66.10\% \pm 2.1$ at 24 hours ($p < 0.005$). Nevertheless, same formulations showed similar cell viability when treated for longer period (48 hours) and no significant differences was found when compared to one another.

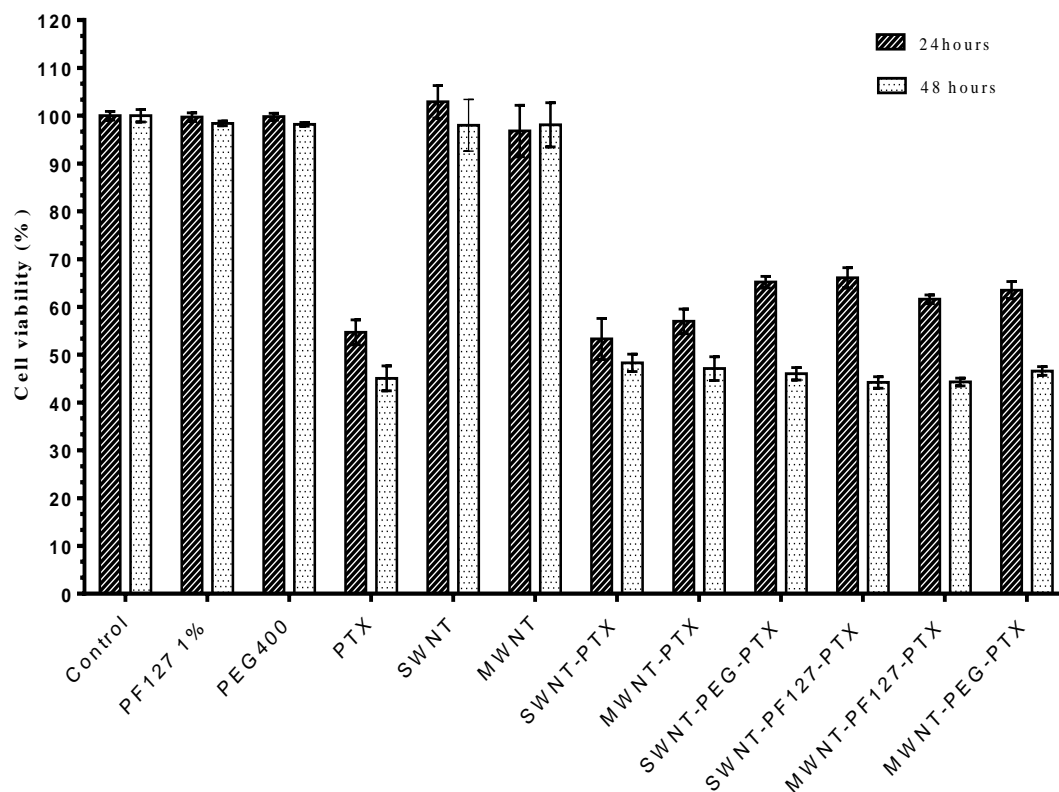


Figure 5.17 SVGp12 cell lines treated with different f-CNTs formulations. The error bars represent the standard deviation (SD) of three samples

One-way ANOVA was also performed to demonstrate the difference between the formulations and time intervals. Significant differences were observed in between 24 hours and 48 hour time frames, indicating that same formulation killed more cells in 48 hours with the same concentration ($p < 0.05$).

Cytotoxicity of all formulations investigated on SVGp12, is demonstrated in Figure 5.18 and proposed to be concentration dependent. However, positive controls, MWNTs and SWNTs showed no significant toxicity on cells.

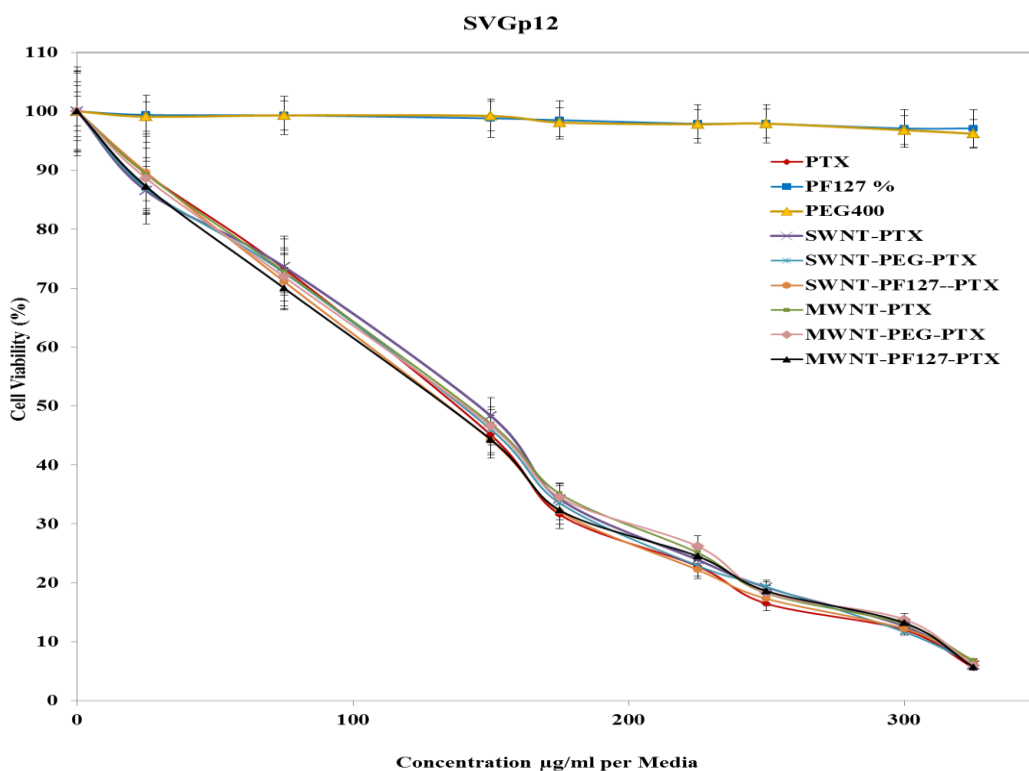


Figure 5.18 Cytotoxicity effect of formulations in viability percentage of SVGp12. The error bars represent the standard deviation (SD) of three samples

IC₅₀ values in Table 5.3, showed that PTX alone had the lowest IC₅₀ value (5.9 mg/ml), indicating that utilization of PTX used alone had more substantial toxic effect on astrocytes in comparison to PTX-*f*-CNT, followed by MWNT-PEG-PTX and MWNT-PF127-PEG with respective values of 5.99 ± 1.9 and 5.99 ± 1.7.

Lowest IC₅₀ value for *f*-CNTs was SWNT-PEG-PTX (6.85 ± 2.4) demonstrating the lowest cytotoxic effect on human cell lines. However, no significant differences could be ascertained for any of the formulations when directly compared to one another.

Table 5.3 IC₅₀ Values of the formulations in mg for SVGp12 cells

Formulations	IC₅₀ mg ± SD SVGp12
PTX	5.92 ± 1.1
SWNT-PTX	6.4 ± 1.0
SWNT-PEG-PTX	6.75 ± 1.8
SWNT-PF127-PTX	6.85 ± 2.4
MWNT-PTX	7.3 ± 0.8
MWNT-PEG-PTX	5.99 ± 1.9
MWNT-PF127-PTX	5.99 ± 1.7

5.6.2 Cytotoxic effect of PF127 and PEG400 functionalized SWNT/MWNT and PTX conjugates on U87-MG

Comparison for all formulations were carried out and only formulations of *f*-CNTs showed a significant difference on U87-MG cells ($p < 0.05$). While, PTX treated cells showed cell viability of $60\% \pm 2.1$ (Figure 5.19).

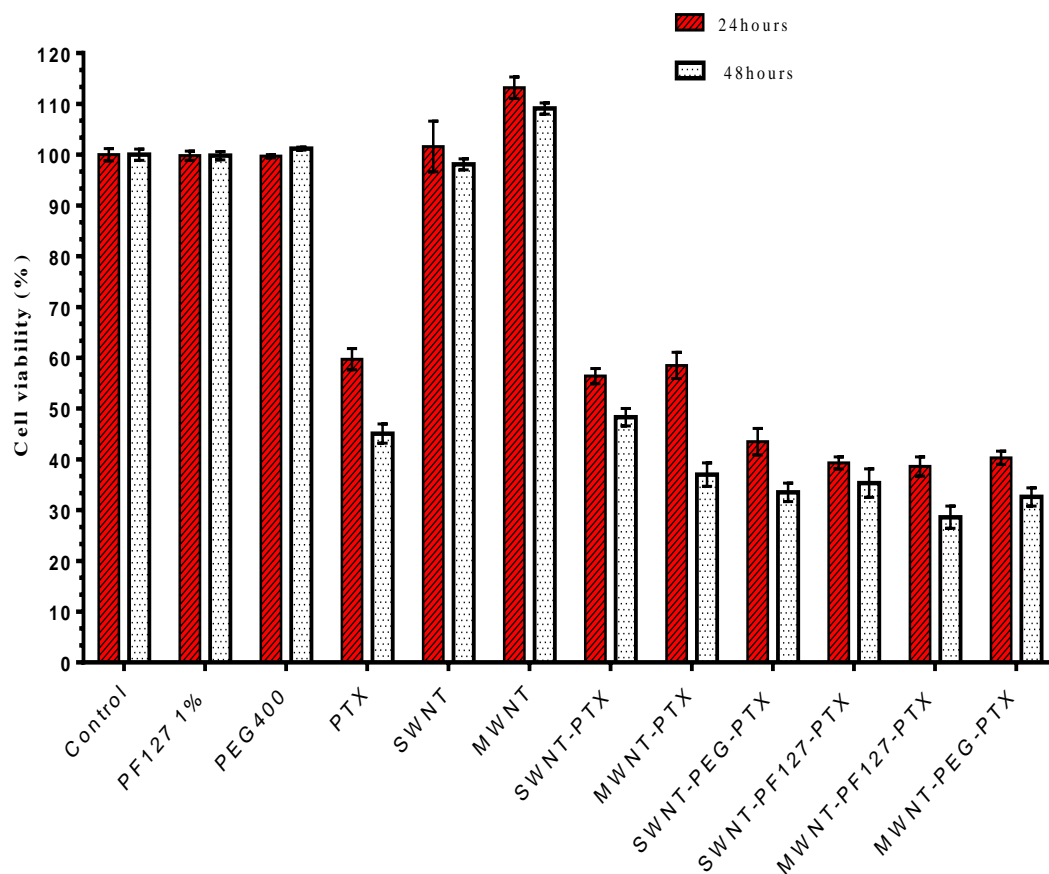


Figure 5.19 U87-MG cell lines treated with *f*-CNTs for 24 and 48 hours. The error bars represent the standard deviation (SD) of three samples

MWNT-PEG-PTX and MWNT-PF127-PTX complexes showed a significantly lower cell viability of $38\% \pm 1.9$ and $40\% \pm 1.3$, respectively ($p < 0.001$). Subsequently, from all *f*-CNTs, a significant difference between cell viabilities was detected between SWNT-PEG-PTX and MWNT-PF127-PTX with values of $44\% \pm 2.6$ and $38\% \pm 1.3$, respectively (Figure 5.20). However, significant differences were observed between 24

hours and 48 hours, indicating that same formulation killed more cells in 48 hours with the same concentration ($p < 0.05$).

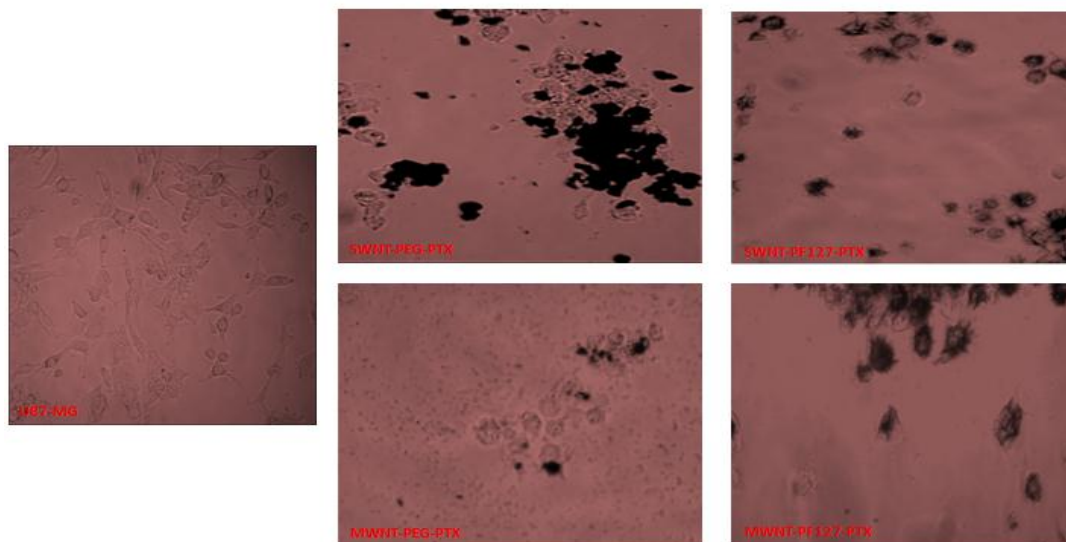


Figure 5.20 Microscopic picture of U87-MG cell lines treated with various CNTs formulations (x200)

Cytotoxicity of all formulations on U87-MG is illustrated in Figure 5.21 and elicited concentration dependency. Controls, MWNTs and SWNTs as well as PEG and PF127 examined on U87-MG, showed no significant toxicity.

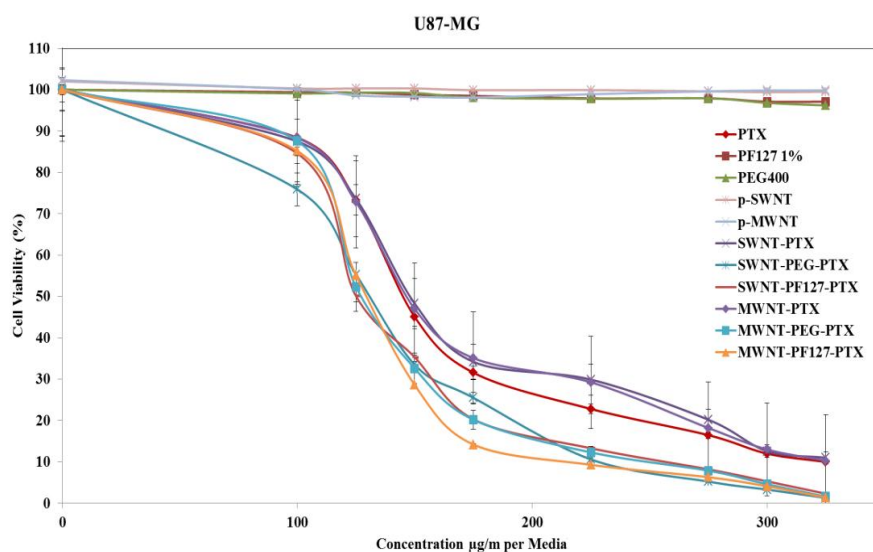


Figure 5.21 Cytotoxicity effect of formulations in viability percentage of SVGp12

The error bars represent the standard deviation (SD) of three samples

IC₅₀ values of all formulations are shown in Table 5.4. It appeared that a higher dose of PTX (11 mg) alone was required to kill 50% of cells, a significant difference is noticeable in comparison to SWNT-PEG-PTX (4.3 mg) that demonstrated the lowest IC₅₀ values (p<0.01).

Table 5.4 IC₅₀ Values of the formulations in mg for U87-MG cells

Formulations	IC ₅₀ mg ± SD U87-MG
PTX	11.0 ± 2.0
SWNT-PTX	7.70 ± 1.5
SWNT-PEG-PTX	4.3 ± 1.7
SWNT-PF127-PTX	3.5 ± 1.4
MWNT-PTX	7.6 ± 1.6
MWNT-PEG-PTX	4.5 ± 0.9
MWNT-PF127-PTX	3.9 ± 1.3

5.7 Conclusions

Cytotoxicity of CNTs and *f*-CNTs-PTX were investigated on SVGp12 and U87-MG. Growth curves concluded that the U87-MG cells grow faster compared to SVGp12 cells. No significant difference was found with treatment of PTX-CNTs on both cells line at both time intervals. It was only significantly evident that cell viability was decreased when PTX concentration was increased ($p < 0.05$). p-CNTs showed not to be toxic to normal astrocyte cell lines even at high concentrations of 15 mg/ml.

CNTs-PTX complexes demonstrated no effect on both cell lines at 24 and 48 hours. Once formulations were assessed for cytotoxic effects on U87-MG, *f*-CNTs were shown to decrease cell viability significantly in comparison to PTX alone. Moreover, *f*-CNTs may provide better targeting, reduced toxicity and enhanced decrease in glioma cell viability. Promisingly, lower PTX concentrations were required to kill equivalent numbers of cells with respect to PTX alone. Thus the utilization of carbon nanotubes has demonstrated a dynamic approach to address toxicity issues with anti- cancer agents.

CHAPTER 6
CONCLUSIONS
&
FUTURE STUDIES

‘ Finally, in conclusion, let me say just this ’

(Peter Sellers)

6.1 Conclusions and future work

CNTs have been functionalized and characterized using a wide variety of techniques. They have been shown to be of appropriate size, biocompatible and ideal for drug delivery applications. A paramount factor is their aqueous solubility and stability which has been demonstrated for a period of 10 days, showing no significant difference in the ζ -potential. Freeze drying formulations could lead to a higher stability for longer period of time. The stability over extended periods of time holds tantalising possibilities for future work.

Loading efficiency of PTX confirmed that *f*-CNTs have an enhanced ability to load more drug molecules owing to the branched functional groups acting as anchors for the drug. Interestingly, their efficiency was highly dependent on drug concentration; however when 200 $\mu\text{g/ml}$ of PTX was reached, loading efficiency dropped suddenly suggesting a stoichiometric effect due to non-covalent functionalization of the surfactant onto CNT walls. Nevertheless, this hypothesis would require verification through further experimental studies with different types CNTs, varying in diameters and lengths.

f-CNTs have demonstrated no significant toxic effect on SVGp12. In contrast, both *f*-SWNT and *f*-MWNT showed significantly lower cell viability than the individual drug alone on the glioblastoma cell lines. Moreover, a more pronounced decrease in cell viability was achieved at lower concentrations of PTX, showing an overall

improvement in lowering the cytotoxicity on normal astrocyte cell lines. It must be noted however that the shape and size of CNTs are critical factors, affecting the toxicity and efficiency of drug delivery systems. They moreover affect the cytotoxicity of CNTs which was assessed through MTT assay defining cell viability. MTT assay reagent binds to the CNTs thus creating uncertainty in the cytotoxicity assessment.

SWNTs and MWNTs have demonstrated biocompatibility, suggesting that if cultured for longer period of time, negative effects are likely due to physical rather than chemical interactions. More work is required to establish biological consequences associated with long-term interactions of SWNTs and MWNTs with brain cells. The findings of this research are encouraging to say the least however further research into the utilization of SWNTs and MWNTs for *in vivo* applications in cell systems is a necessity. Enormous interest to explore these formulations on animal models whereby the serum chemistry can be identified may be the way forward to progress this area of research.

CHAPTER 7

REFERENCES

Alberts, B. L., D. B. Raff, J. M. Roberts, K. Watson, J. D. (1994). Molecular Biology of the Cell. 3rd Edition. New York: Garland Publishing.

Arbizzani, C., S. Righi, et al. (2011). "Graphene and carbon nanotube structures supported on mesoporous xerogel carbon as catalysts for oxygen reduction reaction in proton-exchange-membrane fuel cells." International Journal of Hydrogen Energy **36**(8): 5038-5046.

Asmann, M., J. Heberlein, et al. (1999). "A review of diamond CVD utilizing halogenated precursors." Diamond and Related Materials **8**(1): 1-16.

Awasthi, K., R. Kumar, et al. (2011). "Synthesis of nano-carbon (nanotubes, nanofibres, graphene) materials." Bulletin of Materials Science **34**(4): 607-614.

Bacon, R. (1960). "Growth, Structure, and Properties of Graphite Whiskers." Journal of Applied Physics **31**(2): 283.

Becker, M. L., J. A. Fagan, et al. (2007). "Length-dependent uptake of DNA-wrapped single-walled carbon nanotubes." Advanced Materials **19**(7): 939.

Bekyarova, E., Y. Hanzawa, et al. (2002). "Cluster-mediated filling of water vapor in intratube and interstitial nanospaces of single-wall carbon nanohorns." Chemical Physics Letters **366**(5-6): 463-468.

Belin, T. and F. Epron (2005). "Characterization methods of carbon nanotubes: a review." Materials Science and Engineering B-Solid State Materials for Advanced Technology **119**(2): 105-118.

Bell, M. S., K. B. K. Teo, et al. (2006). "Carbon nanotubes by plasma-enhanced chemical vapor deposition." Pure and Applied Chemistry **78**(6): 1117-1125.

Bhirde, A. A., V. Patel, et al. (2009). "Targeted Killing of Cancer Cells in Vivo and in Vitro with EGF-Directed Carbon Nanotube-Based Drug Delivery." Acs Nano **3**(2): 307-316.

Bianco, A., K. Kostarelos, et al. (2005). "Biomedical applications of functionalised carbon nanotubes." Chem Commun (Camb)(5): 571-577.

Bianco, A., K. Kostarelos, et al. (2005). "Applications of carbon nanotubes in drug delivery." Curr Opin Chem Biol **9**(6): 674-679.

Boyle, P. and B. Levin (2008). "The World Cancer Report."

Bredel, M. (2001). "Anticancer drug resistance in primary human brain tumors." Brain Research Reviews **35**(2): 161-204.

Bredel, M. (2001). "Anticancer drug resistance in primary human brain tumors." Brain Res Brain Res Rev **35**(2): 161-204.

Bronikowski, M. J., P. A. Willis, et al. (2001). "Gas-phase production of carbon single-walled nanotubes from carbon monoxide via the HiPco process: A parametric study." Journal of Vacuum Science & Technology A **19**(4): 1800-1805.

Chen, J., S. Chen, et al. (2008). "Functionalized single-walled carbon nanotubes as rationally designed vehicles for tumor-targeted drug delivery." J Am Chem Soc **130**(49): 16778-16785.

Chen, X. and H. J. Schluesener (2010). "Multi-walled carbon nanotubes affect drug transport across cell membrane in rat astrocytes." Nanotechnology **21**(10):105104-105113

Cheng, J. P., M. J. Meziani, et al. (2011). "Poly(ethylene glycol)-conjugated multi-walled carbon nanotubes as an efficient drug carrier for overcoming multidrug resistance." Toxicology and Applied Pharmacology **250**(2): 184-193.

Chizari, K., I. Janowska, et al. (2010). "Tuning of nitrogen-doped carbon nanotubes as catalyst support for liquid-phase reaction." Applied Catalysis A: General **380**(1-2): 72-80.

Costa, S., E. Borowiak-Palen, et al. (2008). "Characterization of carbon nanotubes by Raman spectroscopy." Materials Science-Poland **26**(2): 433-441.

Cui, D., F. Tian, et al. (2005). "Effect of single wall carbon nanotubes on human HEK293 cells." Toxicol Lett **155**(1): 73-85.

Djordjevic, V., J. Djustebek, et al. (2006). "Methods of purification and characterization of carbon nanotubes." Journal of Optoelectronics and Advanced Materials **8**(4): 1631-1634.

Dresselhaus, M. S., G. Dresselhaus, et al. (2005). "Raman spectroscopy of carbon nanotubes." Physics Reports-Review Section of Physics Letters **409**(2): 47-99.

Drexler, K. E. (1981). "Molecular Engineering - an Approach to the Development of General Capabilities for Molecular Manipulation." Proceedings of the National Academy of Sciences of the United States of America-Physical Sciences **78**(9): 5275-5278.

Dulbecco, R. and G. Freeman (1959). "Plaque production by the polyoma virus." Virology **8**(3): 396-397.

Dumortier, H., S. Lacotte, et al. (2006). "Functionalized carbon nanotubes are non-cytotoxic and preserve the functionality of primary immune cells." Nano Letters **6**(7): 1522-1528.

Eagle, H. (1955). "The specific amino acid requirements of a mammalian cell (strain L) in tissue culture." Journal of Biological Chemistry **214**(2): 839-852.

Earnest, F., 3rd, J. W. Kernohan, et al. (1950). "Oligodendrogliomas; a review of 200 cases." Arch Neurol Psychiatry **63**(6): 964-976.

Endo, M. (1988). "Grow Carbon-Fibers in the Vapor-Phase." Chemtech **18**(9): 568-576.

Firme, C. P. and P. R. Bandaru (2010). "Toxicity issues in the application of carbon nanotubes to biological systems." Nanomedicine-Nanotechnology Biology and Medicine **6**(2): 245-256.

Fisher, J. L., J. A. Schwartzbaum, et al. (2007). "Epidemiology of brain tumors." Neurologic Clinics **25**(4): 867.

Flahaut, E., A. Peigney, et al. (2000). "Synthesis of single-walled carbon nanotube-Co-MgO composite powders and extraction of the nanotubes." Journal of Materials Chemistry **10**(2): 249-252.

Foldvari, M. and M. Bagonluri (2008). "Carbon nanotubes as functional excipients for nanomedicines: I. pharmaceutical properties." Nanomedicine-Nanotechnology Biology and Medicine **4**(3): 173-182.

Foldvari, M. and M. Bagonluri (2008). "Carbon nanotubes as functional excipients for nanomedicines: II. Drug delivery and biocompatibility issues." Nanomedicine **4**(3): 183-200.

Gandini, S., E. Botteri, et al. (2008). "Tobacco smoking and cancer: A meta-analysis." International Journal of Cancer **122**(1): 155-164.

Ge, M. H. and K. Sattler (1994). "Observation of Fullerene Cones." Chemical Physics Letters **220**(3-5): 192-196.

Gilbert, M. R., R. Ruda, et al. (2010). "Ependymomas in adults." Curr Neurol Neurosci Rep **10**(3): 240-247.

Glantz, M. J., H. Choy, et al. (1995). "Paclitaxel Disposition in Plasma and Central Nervous Systems of Humans and Rats with Brain-Tumors." Journal of the National Cancer Institute **87**(14): 1077-1081.

Ham, R. G. and W. L. McKeehan (1979). "Media and growth requirements." Methods Enzymol **58**: 44-93.

Hampel, S., D. Kunze, et al. (2008). "Carbon nanotubes filled with a chemotherapeutic agent: a nanocarrier mediates inhibition of tumor cell growth." Nanomedicine **3**(2): 175-182.

Hanahan, D. and R. A. Weinberg (2000). "The hallmarks of cancer." Cell **100**(1): 57-70.

Hanahan, D. and R. A. Weinberg (2011). "Hallmarks of Cancer: The Next Generation." Cell **144**(5): 646-674.

Hattangadi, J. A., M. Chen, et al. (2010). "Predictors of the Use of Supplemental Androgen Suppression Therapy (AST) and External Beam Radiation Therapy (EBRT) in Men with High-risk Prostate Cancer (PC) Undergoing Brachytherapy." International Journal of Radiation Oncology Biology Physics **78**(3): S577-S578.

Iijima, S. (1991). "Helical microtubules of graphitic carbon." Nature **354**(6348): 56-58.

Iijima, S. and T. Ichihashi (1993). "Single-Shell Carbon Nanotubes of 1-Nm Diameter." Nature **363**(6430): 603-605.

Iijima, S. and T. Ichihashi (1993). "Single-Shell Carbon Nanotubes of 1-Nm Diameter (Vol 363, Pg 603, 1993)." Nature **364**(6439): 737-737.

Ionescu, M. I., Y. Zhang, et al. (2012). "Nitrogen-doping effects on the growth, structure and electrical performance of carbon nanotubes obtained by spray pyrolysis method." Applied Surface Science **258**(10): 4563-4568.

Jinschek, J. R. and S. Helveg (2012). "Image resolution and sensitivity in an environmental transmission electron microscope." Micron **43**(11): 1156-1168.

Jorio, A., M. A. Pimenta, et al. (2003). "Resonance Raman spectra of carbon nanotubes by cross-polarized light." Phys Rev Lett **90**(10): 107403.

Karnofsky, D. A. (1968). "Mechanism of action of anticancer drugs at a cellular level." CA Cancer J Clin **18**(4): 232-234.

Kaye, A. and E. J. Laws (2001). Brain Tumors: An Encyclopedic Approach. New York, NY, Churchill Livingstone.

Kleihues, P. and L. H. Sobin (2000). "World health organization classification of tumors." Cancer **88**(12): 2887-2887.

Klumpp, C., K. Kostarelos, et al. (2006). "Functionalized carbon nanotubes as emerging nanovectors for the delivery of therapeutics." Biochimica Et Biophysica Acta-Biomembranes **1758**(3): 404-412.

Kostarelos, K. (2008). "The long and short of carbon nanotube toxicity." Nat Biotechnol **26**(7): 774-776.

Kostarelos, K., L. Lacerda, et al. (2007). "Cellular uptake of functionalized carbon nanotubes is independent of functional group and cell type." Nature Nanotechnology **2**(2): 108-113.

Kroto, H. W., J. R. Heath, et al. (1985). "C₆₀: Buckminsterfullerene." Nature **318**(6042): 162-163.

Kroto, H. W., J. R. Heath, et al. (1985). "C-60 - Buckminsterfullerene." Nature **318**(6042): 162-163.

Kumar, M. and Y. Ando (2010). "Chemical Vapor Deposition of Carbon Nanotubes: A Review on Growth Mechanism and Mass Production." Journal of Nanoscience and Nanotechnology **10**(6): 3739-3758.

Lacerda, L., A. Bianco, et al. (2006). "Carbon nanotubes as nanomedicines: From toxicology to pharmacology." Adv Drug Deliv Rev **58**(14): 1460-1470.

Lam, C. W., J. T. James, et al. (2004). "Pulmonary toxicity of single-wall carbon nanotubes in mice 7 and 90 days after intratracheal instillation." Toxicol Sci **77**(1): 126-134.

Lay, C. L., J. Liu, et al. (2011). "Functionalized carbon nanotubes for anticancer drug delivery." Expert Rev Med Devices **8**(5): 561-566.

Lee, C. J., D. W. Kim, et al. (1999). "Synthesis of uniformly distributed carbon nanotubes on a large area of Si substrates by thermal chemical vapor deposition." Applied Physics Letters **75**(12): 1721-1723.

Li, W. Z., J. G. Wen, et al. (2003). "Clean double-walled carbon nanotubes synthesized by CVD." Chemical Physics Letters **368**(3-4): 299-306.

Liu, X. W., H. Q. Tao, et al. (2011). "Optimization of surface chemistry on single-walled carbon nanotubes for in vivo photothermal ablation of tumors." Biomaterials **32**(1): 144-151.

Liu, Z., W. Cai, et al. (2007). "In vivo biodistribution and highly efficient tumour targeting of carbon nanotubes in mice." Nature Nanotechnology **2**(1): 47-52.

Liu, Z., K. Chen, et al. (2008). "Drug delivery with carbon nanotubes for in vivo cancer treatment." Cancer Res **68**(16): 6652-6660.

Liu, Z., K. Chen, et al. (2008). "Drug delivery with carbon nanotubes for in vivo cancer treatment." Cancer Res **68**(16): 6652-6660.

Louis, D. N., H. Ohgaki, et al. (2007). "The 2007 WHO Classification of Tumours of the Central Nervous System." Acta Neuropathologica **114**(2): 97-109.

Marassi, R. and F. Nobili (2009). Measurement methods | Structural and Chemical Properties: Transmission Electron Microscopy. Encyclopedia of Electrochemical Power Sources. G. Editor-in-Chief: Jürgen. Amsterdam, Elsevier: 769-789.

Mather, J. P. and P. E. Roberts (1998). "Introduction to cell and tissue culture; Theory and Techniques ". Texas: Baylor College of Medicine.

Maurer-Jones, M. A., K. C. Bantz, et al. (2009). "Toxicity of therapeutic nanoparticles." Nanomedicine **4**(2): 219-241.

Milnera, M., J. Kurti, et al. (2000). "Periodic resonance excitation and intertube interaction from quasicontinuous distributed helicities in single-wall carbon nanotubes." Phys Rev Lett **84**(6): 1324-1327.

Misra, R., S. Acharya, et al. (2010). "Cancer nanotechnology: application of nanotechnology in cancer therapy." Drug Discovery Today **15**(19-20): 842-850.

Nagahara, L. A., M. Ferrari, et al. (2009). "Nanofunctional Materials in Cancer Research: Challenges, Novel Methods, and Emerging Applications." Mrs Bulletin **34**(6): 406-408.

Nagasawa, D. T., Z. A. Smith, et al. (2011). "Complications associated with the treatment for spinal ependymomas." Neurosurgical Focus **31**(4): E13.

Nasibulin, A. G., P. V. Pikhitsa, et al. (2007). "A novel hybrid carbon material." Nature Nanotechnology **2**(3): 156-161.

Odom, T. W., J. L. Huang, et al. (2000). "Structure and electronic properties of carbon nanotubes." Journal of Physical Chemistry B **104**(13): 2794-2809.

Ohgaki, H. and P. Kleihues (2005). "Epidemiology and etiology of gliomas." Acta Neuropathologica **109**(1): 93-108.

Peng, B., M. Locascio, et al. (2008). "Measurements of near-ultimate strength for multiwalled carbon nanotubes and irradiation-induced crosslinking improvements." Nat Nano **3**(10): 626-631.

Popov, V. N. (2004). "Carbon nanotubes: properties and application." Materials Science & Engineering R-Reports **43**(3): 61-102.

Portney, N. G. and M. Ozkan (2006). "Nano-oncology: drug delivery, imaging, and sensing." Analytical and Bioanalytical Chemistry **384**(3): 620-630.

Qian, D., G. Wagner, et al. (2002). "Mechanics of carbon nanotubes." Applied Mechanics Reviews **55**(06): 495-533.

Radushkevich, L. V. and V. M. Lukyanovich (1952). "O strukture ugleroda, obrazujucesgja pri termiceskom razlozenii okisi ugleroda na zeleznom kontakte." Zurn. Fisic. Chim., **26**: 88-95.

Rajalakshmi, N., H. Ryu, et al. (2005). "Performance of polymer electrolyte membrane fuel cells with carbon nanotubes as oxygen reduction catalyst support material." Journal of Power Sources **140**(2): 250-257.

Reddy, S. T., A. Rehor, et al. (2006). "In vivo targeting of dendritic cells in lymph nodes with poly(propylene sulfide) nanoparticles." Journal of Controlled Release **112**(1): 26-34.

Sanchez, V. C., A. Jachak, et al. (2012). "Biological Interactions of Graphene-Family Nanomaterials: An Interdisciplinary Review." Chemical Research in Toxicology **25**(1): 15-34.

Sengupta, R., M. Bhattacharya, et al. (2011). "A review on the mechanical and electrical properties of graphite and modified graphite reinforced polymer composites." Progress in Polymer Science **36**(5): 638-670.

Serp, P., M. Corrias, et al. (2003). "Carbon nanotubes and nanofibers in catalysis." Applied Catalysis A: General **253**(2): 337-358.

Shen, H., L. M. Zhang, et al. (2012). "Biomedical Applications of Graphene." Theranostics **2**(3): 283-294.

Shvedova, A. A., E. R. Kisin, et al. (2005). "Unusual inflammatory and fibrogenic pulmonary responses to single-walled carbon nanotubes in mice." Am J Physiol Lung Cell Mol Physiol **289**(5): L698-708.

Srinivasan, C. (2007). "Do Damascus swords reveal India's mastery of nanotechnology?" Current Science **92**(3): 279-280.

Strobel, R., J. Garche, et al. (2006). "Hydrogen storage by carbon materials." Journal of Power Sources **159**(2): 781-801.

Tagmatarchis, N. and M. Prato (2004). "Functionalization of carbon nanotubes via 1,3-dipolar cycloadditions." Journal of Materials Chemistry **14**(4): 437-439.

Taniguchi, N. (1974). "On the basic concept of Nano-technology." Japan Society of Precision Engineering ICP(Part II): 18-23.

Walker, D. G. and A. H. Kaye (2001). "Diagnosis and management of astrocytomas, oligodendrogliomas and mixed gliomas: a review." Australas Radiol **45**(4): 472-482.

Wang, X., Q. Li, et al. (2009). "Fabrication of Ultralong and Electrically Uniform Single-Walled Carbon Nanotubes on Clean Substrates." Nano Letters **9**(9): 3137-3141.

Xie, X. F., T. Gan, et al. (2008). "Application of multi-walled carbon nanotubes/Nafion composite film in electrochemical determination of Pb²⁺." Fullerenes Nanotubes and Carbon Nanostructures **16**(2): 103-113.

Xu, H. Y., J. Meng, et al. (2010). "What are carbon nanotubes' roles in anti-tumor therapies?" Science China-Chemistry **53**(11): 2250-2256.

Yang, K., S. A. Zhang, et al. (2010). "Graphene in Mice: Ultrahigh In Vivo Tumor Uptake and Efficient Photothermal Therapy." Nano Letters **10**(9): 3318-3323.

Yang, Q.-h. (2011). "Dreams may come: From fullerene, carbon nanotubes to graphene." Carbon **49**(8): 2878.

Yang, W. R., P. Thordarson, et al. (2007). "Carbon nanotubes for biological and biomedical applications." Nanotechnology **18**(41): 412001

You, X. Y., J. G. Chen, et al. (1990). "Studies on the Relation between Bladder-Cancer and Benzidine or Its Derived Dyes in Shanghai." British Journal of Industrial Medicine **47**(8): 544-552.

Zhang, H., B. Wu, et al. (2011). "Separation and/or selective enrichment of single-walled carbon nanotubes based on their electronic properties." Chemical Society Reviews **40**(3): 1324-1336.

Zhao, M., C. Liang, et al. (2010). "Magnetic Paclitaxel Nanoparticles Inhibit Glioma Growth and Improve the Survival of Rats Bearing Glioma Xenografts." Anticancer Research **30**(6): 2217-2223.